Coordinated Science Laboratory

UNIVERSITY OF ILLINOIS - URBANA, ILLINOIS

602 090

CROSSED FIELD CHARGED PARTICLE DELAY LINES

176p — $3.00

H.G. Slottow

REPORT R-214 JUNE, 1964

COORDINATED SCIENCE LABORATORY
UNIVERSITY OF ILLINOIS
URBANA, ILLINOIS

Contract DA-28-043-AMC-00073(E)

The research reported in this document was made possible by support extended to the University of Illinois, Coordinated Science Laboratory, jointly by the Department of the Army, Department of the Navy (Office of Naval Research), and the Department of the Air Force (Office of Scientific Research) under Department of Army Contract DA-28-043-AMC-00073(E).

CROSSED FIELD CHARGED PARTICLE DELAY LINES

ABSTRACT

Crossed electric and magnetic fields are used to focus a beam of charged particles and to control the drift velocity of these particles. The novel and useful properties are: (1) the time delay can be varied continuously and rapidly; (2) the frequency band is potentially very wide.

A discussion of the effects that limit bandwidth is presented and several means for reducing the limitations are described. In particular, a hyperboloidal structure is described that can maintain equal flight times in circular delay lines; the use of plasmas is discussed, and the field averaging properties of high energy electrons is analyzed.

Experiments are described in which electrons or ions drifting at speeds less than 10^4 meters/second delay signals by as much as 50 microseconds. Results, usually in the form of oscillograms, show the effects of space charge, and in the case of tenuous plasmas, the effects of pressure on the shapes of video pulses.

ACKNOWLEDGMENTS

The author is deeply indebted to Dr. Arnold Nordsieck for his guidance, for his encouragement, and for the intellectual stimulation he has provided during the course of this and other research. Special thanks go to Dr. Peter Ponzo both for programming assistance and for a series of valuable discussions on the mathematics of electron dynamics. The author also acknowledges the importance of several conversations with Dr. Robert Adler. In particular, his observations on focussing problems led the author to realize the advantages inherent in the use of high energy electrons. Discussions with Mr. B. Voth and D. Skaperdas, and with Professors H. Knoebel, M. Raether, L. Lavatelli, A. Kupperman, and C. Chen, were also helpful.

Many members of the CSL staff contributed to the experiments. G. Burr, N. Powers, and N. Vassos not only fabricated the tube elements, but also assisted in solving constructional problems. W. Lawrence, T. Popeny, and D. Coad assisted in the assembly of the tubes; and, members of the high vacuum research group, D. Lee, W. Schuemann, and H. Tomaschke, taught the author some of their technique.

For assistance in the preparation of this report, the author is grateful to R. McFarlane, A. Tewes, W. Fillman, J. Cummings, M. Barnard, J. McClerren, and L. Morgan.

Finally, the author wishes to thank Professors Daniel Alpert and Richard Brown for their support of this work and for their encouragement.

TABLE OF CONTENTS

		Page
CHAPTER I.	INTRODUCTION	1
1.1	General Description	1
1.2	Delay Lines and Their Uses	5
1.3	History	7
CHAPTER II.	THE ELECTRON DELAY LINE	9
2.1	Particle Motion in Static Electric and Magnetic Fields	9
2.2	Field Structures	15
2.3	Space Charge Effects	19
2.3.1	Beam Spreading	21
2.3.2	Velocity Slip	22
2.3.3	Instabilities	38
2.4	Coupling Problems	41
2.5	Effects of Circular Motion	52
CHAPTER III.	THE PLASMA DELAY LINE	57
3.1	Description	58
3.2	Confinement	60
3.3	Choice of Gas	63
3.4	Transverse Effects	64
CHAPTER IV.	EXPERIMENTAL PROCEDURES	73
4.1	Experimental Tubes	73
4.2	The Vacuum System	90
4.3	The Magnet	92
4.4	Circuits and Procedures	93
CHAPTER V.	EXPERIMENTAL RESULTS	101
5.1	Measurements in the Electron Mode	101
5.1.1	Sharp Pulses	102
5.1.2	Broad Electron Pulses	120
5.2	Results in the Plasma Mode	128

CHAPTER VI. CONCLUSIONS 146

6.1 Summary of Results 146
6.2 Suggestions for Further Research 150

BIBLIOGRAPHY 153

APPENDIX A. MOTION OF ELECTRONS IN UNIFORM MAGNETIC FIELD AND NONUNIFORM ELECTRIC FIELD 155

APPENDIX B. PROPERTIES OF HIGH ENERGY ELECTRONS IN CROSSED ELECTRIC AND MAGNETIC FIELDS 160

APPENDIX C. COMPUTER CALCULATION 169

VITA 172

CHAPTER I

INTRODUCTION

The times of flight of electrons in crossed electric and magnetic fields can provide useful delays of information in modern communication systems. Furthermore, because the drift velocity is directly proportional to the electric field, continuous and rapid control of delays is easily achieved. Finally, the frequency band can, in principle, be very wide. For these reasons the study of the crossed field delay line is interesting, and to the extent that it leads to engineering development, it will be important.

In practice, it may be difficult to achieve wide bandwidth. The presence of narrow band couplers, the dispersive effects of space charge forces and of collisions, the variation of flight times through transition regions, all tend to degrade bandwidth. One purpose of this report is to assess the extent of these influences. More generally the goals are to develop an understanding of crossed field delay lines which will be useful as a basis for design, and to describe a series of experiments which have contributed to this understanding.

1.1 General Description

Figure 1.1 shows a schematic diagram of the delay line. A signal, impressed on an electron beam in the injection region, propagates through the crossed field drift region and couples to the external circuits in the extraction region. The components need not be physically distinct. The gun and the input coupler may be combined, the collector and output coupler may be combined, and furthermore

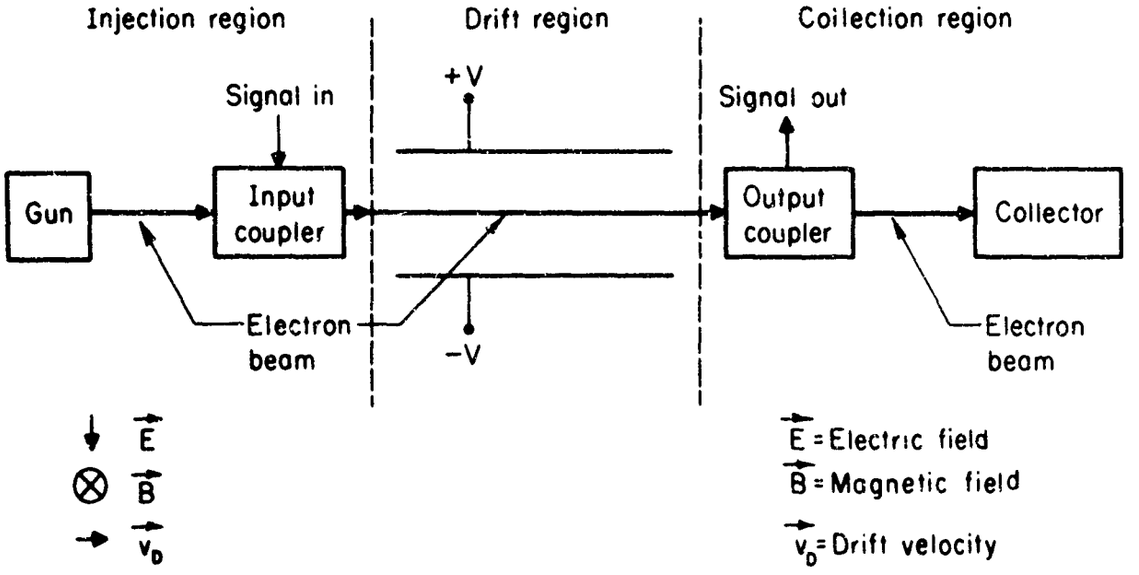

Figure 1.1

Schematic Diagram of Crossed Field Delay Line

these structures may be entirely immersed in the crossed field drift region.

The basic mechanism is the interaction of a charged particle with a uniform magnetic field and a crossed electric field. For a wide range of parameter values the resulting motion is a drift perpendicular to the fields, and a superimposed cyclotron orbit that is circular, or nearly circular. The orbital motion depends explicitly on the magnetic field, and also on the mass, charge, and kinetic energy of the particle. It also depends implicitly on the electric field which in part determines the kinetic energy. In contrast the magnitude of the drift velocity is simply the ratio of the electric and magnetic field intensities. More precisely, the orbit frequency in radians per second is

$$\omega_c = -\eta B, \tag{1.1}$$

its radius in meters is

$$1/B \sqrt{2/\eta(V-V_d)} , \tag{1.2}$$

and the drift velocity in meters per second is

$$\vec{v}_d = \frac{\vec{E} \times \vec{B}}{B^2} . \tag{1.3}$$

In these equations η is the charge to mass ratio, $\vec{E}$ is the electric field, $\vec{B}$ is the magnetic field, V is the total kinetic energy of the particle in units of electron volts, and V_d is the kinetic energy in the drift motion. Variation of either field controls the transit time of particles through the drift space.

Although the effect that provides the long time delay is thus an average motion of the electrons, the orbital motion can vary the

transit times by small amounts. For example, if the electrons couple to the external circuits while they are still in cycloidal motion, the time resolution is, at best, one period of the cyclotron frequency. Even more restrictive are energy spreads and variations in initial conditions of electrons which can limit the spatial resolution of signals to an orbit radius. In Chapter II we discuss these effects in detail.

These orbit effects are generally masked by the dispersion of electrons which drift through different fields from injector to collector. In fact, the central problem in design is to minimize this dispersion, and at the same time to provide enough electrons at the output to give useful signal levels. Unfortunately, the two aspects of the problem are usually connected. For example, additional external electric fields can restrain electrons from streaming to the walls of the device along the magnetic field lines. These fields, however, are related to the transverse electric fields which control the drift velocities, through Poisson's or La Place's equation, and therefore they cannot be specified independently. A gain in signal level may well be achieved at the cost of increased dispersion, and a consequent reduction of bandwidth. Chapter II is largely a discussion of the influence of these effects on the properties of electron delay lines.

The problems of signal level and of dispersion can, in principle, be uncoupled by the use of positive ions in the drift space. The ions not only inhibit the loss of electrons through their focussing forces, but they also neutralize the electronic space charge. Additional electric fields are therefore unnecessary, and a simple drift structure is possible. Although all the charged particles would

ultimately diffuse to the walls, the inertia of the ions inhibits this process and enough particles reach the collector to give useful signal levels with transit times in the 10 to 100 microsecond range. Since the ions drift with the electrons the signal is actually carried by a moving plasma, and we have called devices of this kind plasma delay lines. Chapter III is a discussion of the properties of these lines.

The principal part of this work is an experimental study of the crossed field delay line. Because of the apparent simplicity of the plasma delay line the first experiments were designed to study its properties. We discovered, however, that it was possible to inject sharp electron pulses that even after 12 microseconds had rise times of only 0.1 microsecond. Within the limitations imposed by the plasma tubes we therefore studied their behavior as electron delay lines also.

In Chapter IV we describe these tubes and the apparatus used in the experiments. In Chapter V we describe the measurements and interpret the results. Finally, in Chapter VI we suggest possibilities for additional research, and we indicate the lines along which engineering development might proceed.

The delay line is, of course, an engineering component, and its importance depends on the functions it can perform. These functions are, in fact, important, and in the following section we discuss them together with some standard techniques for providing time delays.

1.2 Delay Lines and Their Uses

The time delays required in different applications and the bandwidth requirements span many orders of magnitude. It is thus not

surprising that a variety of techniques have been developed. Delays in the submicrosecond region are often provided by appropriate lengths of coaxial cable, or, when the waves interact with an electron beam, by helices or other forms of slow wave guide. For microsecond delays when high frequency response is not required, special cables, or cascaded sections of series inductance, and shunt capacitance are useful. For long delays the low velocities of sonic waves are attractive. Mercury lines, once used as memory elements in special digital computers, have given way to the more stable fused quartz lines which can provide millisecond time delays with bandwidths of about 50 megacycles. Where bandwidths of 10 megacycles are adequate, magnetostrictive lines have proved useful. Both types of sonic delay lines have been intensively developed in the last two decades, and have found wide use as buffer memories, integrators, correlators, and function generators.

These techniques are most useful in the construction of delay lines with fixed time delays, or in some cases, of tapped or discretely adjustable lines. Recently, however, interest in continuously variable delay lines has grown. Cumming [1] and Wong [2] have shown how variable lines can produce frequency, phase, and serrodyne modulation, and Wong has analyzed lumped high pass and low pass lines in which semiconductor diodes function as variable capacators. Cooper [3], in his studies of tracing and tracking distortion in phonograph records, has described a compensation scheme which uses a variable delay line. In addition it seems clear that such lines would be useful in autocorrelators and cross-correlators where a range of time intervals could be swept automatically, and in systems in which the time delay must be

syncronized with another timing element.

1.3 History

In view of the sustained interest in delay lines and the extensive development of the related magnetrons and crossed field amplifiers, the work on crossed field delay lines has been surprisingly meager. To the author's knowledge, only two accounts appear in the literature: a laboratory report by Lavatelli [4] in 1956 and a short communication in 1962 by Klüver [5].

Lavatelli described a circular delay line in which a fixed axial magnetic field and the radial component of an electric field control the drift of electrons through positions of increasing angle. The electric field, which is established between an inner disk and an outer closed cylinder, has an axial component which prevents electrons from streaming along the magnetic field lines. The electrons are emmitted from a line filament aligned with the magnetic field and are injected into the drift space by the action of a curved electrode which, like a plate of a split anode magnetron, partially surrounds the filament. A metal electrode downstream collects the electrons.

In preliminary experiments Lavatelli observed that an input current pulse was always followed by a sequence of four delayed pulses at the collector instead of the expected single pulse and that furthermore the delay of the first of these pulses was independent of the electric field. He was unable to complete his investigation of this device, and although he speculated on the cause of these results, he could not explain them. Nevertheless, the work was promising. He emphasized

that electron drift in crossed fields was independent of electron energy, and he observed signals that were delayed by as much as 100 microseconds as they traversed several inches.

Klüver has described a variable delay line in which a continuous ribbon beam of electrons transports the signals through the drift space on the fast cyclotron wave. The signals are impressed on the beam and extracted from the beam by Cuccia couplers in cavities that are tuned to the cyclotron frequency. Since the electrons traverse the cavities at an appropriate fixed velocity, they must also traverse two regions of velocity transition on either side of the variable drift region. An electron gun guides the beam to the input couplers and a collector recovers the beam beyond the output coupler. Thus the problems of signal injection and extraction are separated from problems of beam injection and collection.

Klüver reported a number of measurements at different drift velocities. We note only the measurement at the lowest velocity. He observed a current of 0.015 microampere at a velocity of 4.03×10^{4} meters per second (3.4×10^{-3} volts). The total delay over 26 centimeters was 8 microseconds.

These two developments do not truly indicate the background against which the development of crossed field delay lines can proceed. The literature of magnetrons and the magnetron amplifiers contains much that is pertinent to the delay line. In addition the literature of plasma physics provides useful insights into the behavior of charged particles in the kinds of field configurations with which we are concerned. Appropriate references will be cited in the following pages.

CHAPTER II

THE ELECTRON DELAY LINE

The crossed field delay line, operating with an electron beam at high vacuum, can be realized in many ways. Certainly Lavatelli's tube, essentially a triode, differs markedly from Klüver's tube, a microwave device which resembles the beam amplifiers from which it derives. Nevertheless, the influences which limit the performance of these devices are the same. The most important of these are the space charge effects, which cause velocity slip across the beams and create instabilities in thin beams. In this chapter we relate the magnitude of these effects to the properties of the delay line, and we consider means for minimizing the effects. We also discuss the problems of injecting and extracting signals, and we estimate the effects of the electron orbital motion on performance. We describe field structures which are appropriate for use in the delay line, and in particular we describe a hyperboloidal structure, new at least in this application, which is precisely correct for a circular delay line. To discuss these topics properly we first review some additional properties of charged particles in crossed electric and magnetic fields.

2.1 Particle Motion in Static Electric and Magnetic Fields

Electric and magnetic fields govern the motion of charged particles according to the equation

$$\ddot{\vec{r}} = \eta(\vec{E} + \dot{\vec{r}} \times \vec{B}) \qquad (2.1)$$

where r, $\dot{\vec{r}}$, and $\ddot{\vec{r}}$ are the position, velocity, and acceleration of the

particle. Since in the delay line magnetic fields are large and currents small, $\vec{B}$ is influenced negligibly by the currents and is therefore a function of position only. The electric field, however, may depend on space charges as well as on external sources. If these charges are sufficiently small, or when the distribution of charge is constant, $\vec{E}$ is also a function of position only, and the motions of charged particles can be described by orbit theory.

When the fields are constant the motion of an electron is described by the equation

$$\vec{r} = R\vec{g} + (\vec{E} \times \vec{B})\ t/B^2 + \vec{r}_0 \ . \qquad (2.2)$$

The term $\vec{g}$ is a unit vector perpendicular to $\vec{B}$ (and $\vec{\omega}$), and rotating with frequency and sense of $\vec{\omega}$, as shown in Figure 2.1. The first

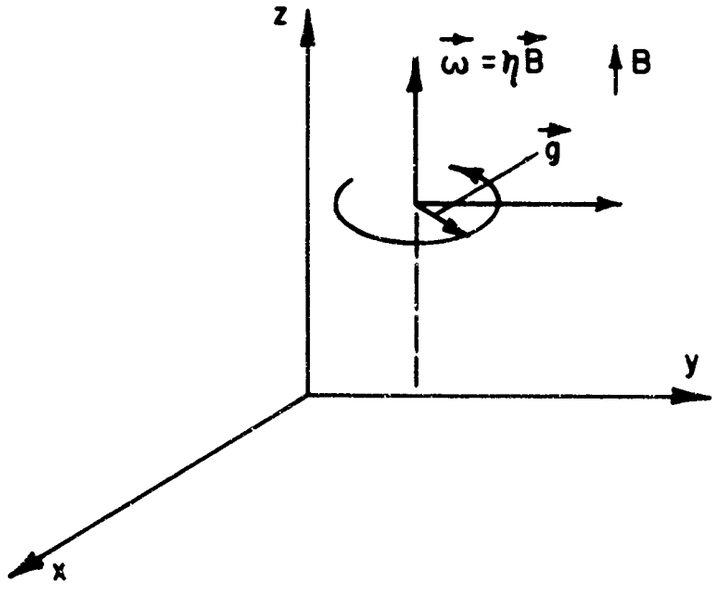

Figure 2.1

Motion of Electron in Magnetic Field

term $\vec{Rg}$ thus describes a circular motion with radius R and angular frequency $\vec{\omega}$ where R is related to the rotational energy by the equation

$$R = 1/B \sqrt{2V_r/\eta} \quad . \qquad (2.3)$$

The remaining terms represent the initial position and subsequent drift of the guiding center of this circle.

The combined motion is cycloidal, with a drift velocity $\vec{v}_d = (\vec{E} \times \vec{B})/B^2$. The exact form depends on the ratio of the rotational energy V_r to the drift energy V_d. Figure 2.2 shows the motions for

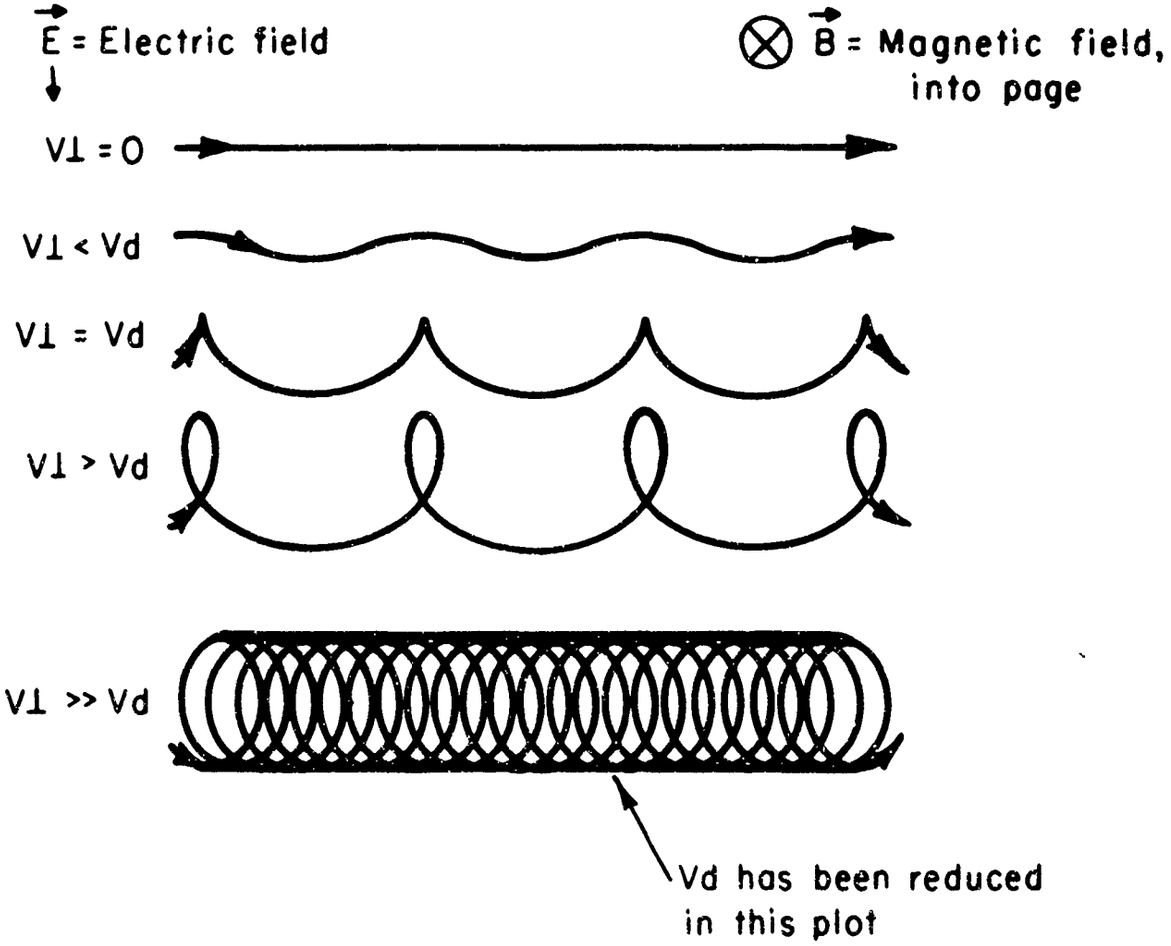

Figure 2.2

Electron Motions in Crossed Electric and Magnetic Fields

various ranges of V_r/V_d. The condition most frequently met in the electron delay line is $V_r/V_d \gg 1$.

If $\vec{E}$ or $\vec{B}$ is inhomogeneous, but if the relative change over one orbit radius is small, some new features appear. We show in Appendix A that small inhomogeneities in $\vec{E}$ distort the orbital motion into ellipses but that the equation for drift velocity is unchanged if for $\vec{E}$ we use the value at the orbit center. Inhomogeneities in $\vec{B}$, on the other hand, give rise to drifts even in the absence of an electric field, and they also affect the velocity along the magnetic field lines.

Alfvén [6] has studied these effects in a first order theory and his results have been described in various forms by a number of authors. Following Spitzer [7] we write for the drift velocity across the magnetic field

$$v_r = (1/B)(\vec{E} \times \vec{B}) + (1/\eta B^3)(\vec{B} \times \nabla B)\ \{1/2\ v_r^2 + v_\ell^2\} \qquad (2.4)$$

where v_r is the orbital velocity, v_ℓ is the velocity along the field lines, and B is the magnitude of the magnetic field. The magnetic field inhomogeneity thus contributes two terms to the transverse drift, one proportional to the transverse energy in the orbital motion, and the second proportional to the energy of motion along the field lines. The first of these, frequently called the gradient drift, arises from the variation in the orbit curvature as the particle gyrates through the varying magnetic field. Thus its detailed motion resembles the motion in constant crossed fields. The second term arises from the centrifugal forces the particle experiences as it moves along curved magnetic

lines. It is frequently called the curvature drift. Superimposed on these drifts is the approximately circular orbital motions with frequency, now to first order, equal to ηB.

Unless the electron beam in the delay line has no energy spread, these energy dependent drifts clearly contribute to the signal dispersion, and at least in the drift region we shall usually assume that the magnetic field is uniform. The one exception which we discuss later is a configuration in which the gradient drift opposes the $\vec{E} \times \vec{B}$ drift, thus allowing the use of large electric fields for given time delays. In the injection and extraction regions, however, it is sometimes convenient to use spatially varying magnetic fields. The magnetic drifts will then influence the motions, and the gradient drift, in particular, can serve as an energy filter to reduce the energy spread of the beam in the drift region. We shall discuss this effect in connection with injection and extraction problems.

In the direction of the magnetic field Spitzer gives for the acceleration

$$dv_{\ell}/dt = (\eta/B)(\vec{E} \cdot \vec{B}) - (1/2\ B^2)(v_r^2 \vec{B} \cdot \nabla B). \qquad (2.5)$$

The first term is of course just the acceleration produced by the longitudinal component of the external electric field. The second term controls the motions such that v_r/B^2 remains constant. From conservation principles, as $\vec{B}$ and $\vec{v}_r$ increase, $\vec{v}_{\ell}$ must decrease and in combination with appropriate electric fields this principle could be used as the basis for an injection scheme.

The concept of a guiding center is, of course, useful only

when the orbit diameter is less than the width d of the aperture through which the electrons drift. Since, for electrons, $\eta = 1.76 \times 10^{11}$ coul/kg, the radius, from Eq. (1.2), is

$$R = 0.337 \times 10^{-5}(V_r^{1/2}/B)\text{meters} . \qquad (2.6)$$

Figure 2.3 plots R as a function of V_r with B as a parameter. We see

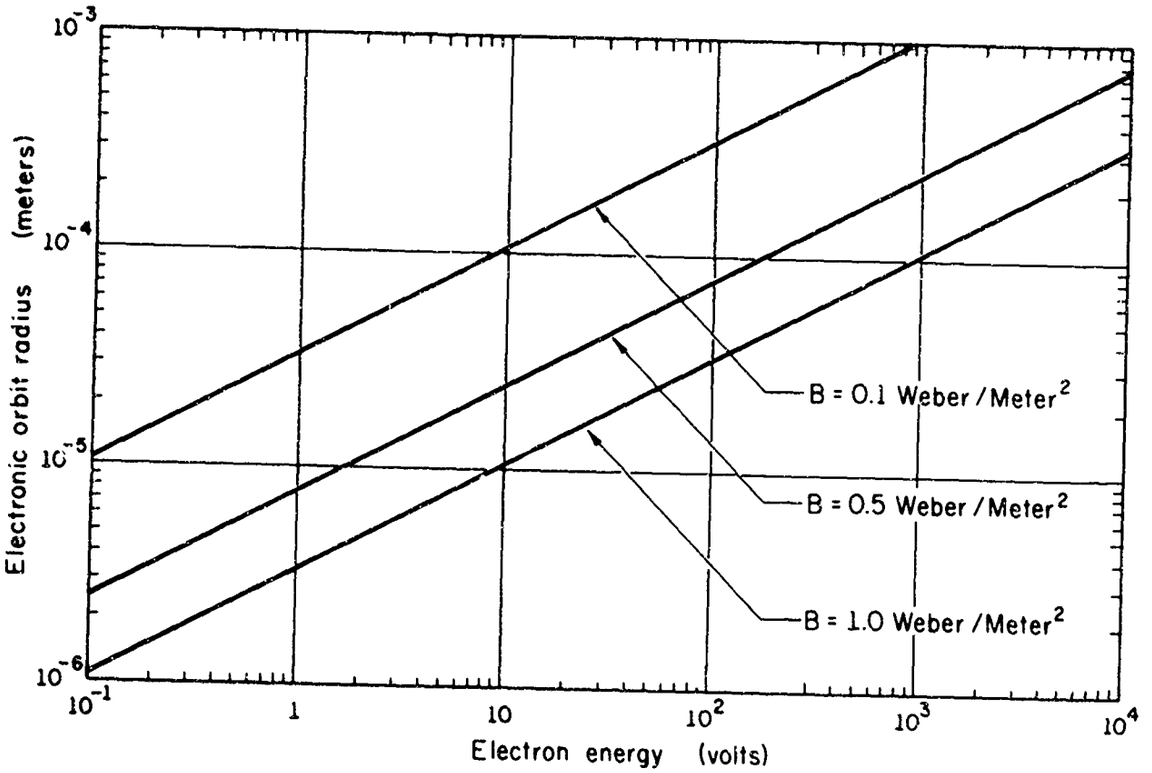

Figure 2.3

Larmor Radii in Electron Delay Line

that even with $V_r = 10^4$ volts, R is less than one millimeter. Furthermore, with electron energies in the neighborhood of a few volts, and a one centimeter aperture, the ratio R/d is so small that for many

purposes we can ignore the orbital motion altogether.

2.2 Field Structures

Uniform crossed electric and magnetic fields, although ideal for the drift motion of electrons, fail to restrain them from streaming to the walls of the container along the magnetic field lines. Because of its small mass, only an electron with less than a few microvolts of longitudinal energy will remain in a one centimeter aperture after 10 microseconds. Focusing forces in this direction are thus clearly necessary.

End hats can focus electrons here as they do in magnetrons by providing longitudinal components of electric field at the edges of the aperture. Figure 2.4 shows electric field lines and equal potential lines for both a wide aperture and a narrow aperture drift region. For a delay line this field arrangement has several disadvantages. Because electrons oscillate between the end hats, spending most of the time at the turning points, the aperture is not used efficiently. Furthermore, a spread in longitudinal energy causes a corresponding spread in the positions of the turning points, the more energetic electrons reaching closer to the end hats. Since the field distortion is greatest in this region, there is a corresponding spread of drift velocities and a dispersion of signals.

These disadvantages can be largely overcome if the fields are appropriately terminated in the center of the aperture as shown in Figure 2.5. Except for small perturbations near the conductors the transverse electric field E_y is constant everywhere in the aperture.

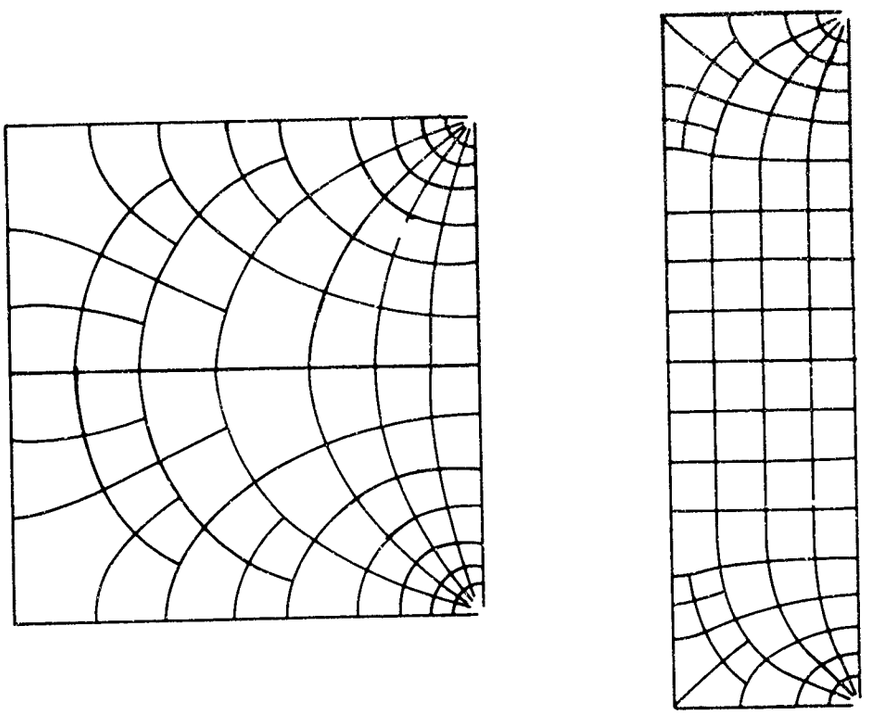

Figure 2.4

Field Lines and Equipotential Lines
in Rectangular Apertures

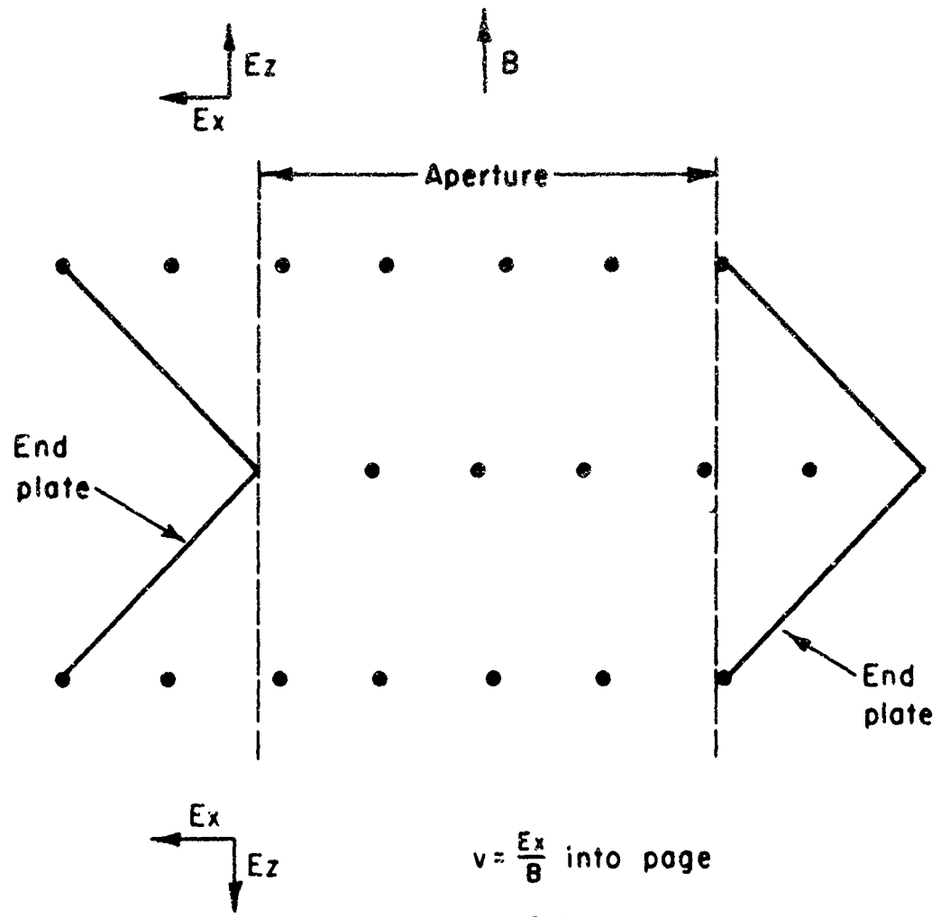

Figure 2.5

Electrode Configuration for Rectangular Delay Line

The longitudinal component of the electric field E_z, which is parallel to the magnetic field, forces electrons toward the median plane. The necessity for the center conductors arises from the nature of La Place's equation, which in terms of the fields is

$$\partial E_y/\partial y + \partial E_z/\partial z = 0 \ . \qquad (2.7)$$

Clearly, if E_y is constant, both derivatives in Eq. (2.7) are zero, and E_z must also be constant. But to focus electrons E_z must be positive

above the median plane and negative below it. These conditions imply a nonzero value of $\partial E_z/\partial z$ in the neighborhood of the median plane. The conductors make possible a transition in E_z at $z = 0$ with appropriate constant values at E_z above and below.

Although there is some distortion in the median plane, above or below the plane it falls off rapidly and at a distance equal to the distance between the conductors it is very small. Moreover, electrons travel fastest through the median plane, and thus they spend most of the time in regions of negligible distortion. A variation of this structure is used in some of the experiments to be described later.

If the drift motion of the electron is curved the requirement of equal flight times implies that the transverse electric field be nonuniform. In particular, if the drift paths are circles, the angular velocity must be a constant and the electric field must increase linearly with the radius. La Place's equation in cylindrical coordinates, when fields are independent of angle, has the form

$$\partial E_r/\partial r + E_r/r + \partial E_z/\partial z = 0 \qquad (2.8)$$

where E_r = radial component of the electric field,

E_z = longitudinal component of the electric field,

r = radial coordinate,

z = longitudinal coordinate.

The magnetic field B is assumed to be directed along the z-axis and the plane of symmetry toward which the electrons are focused by E_z is defined by $z = 0$. If we choose $E_r = -ar$, it is easy to show that $E_z = 2az$. If $a > 0$, $\vec{E}_z$ points away from the plane $z = 0$, and the electrons will be focused. The drift velocity of the electrons, $v_d = E_r/B$, thus

increases linearly with the radius. Since the electrons are tied to equipotential lines by the magnetic field, this is precisely the variation needed to maintain equal times of flight from the injector at one angle to the collector at another.

The corresponding equation for the potential is

$$V(r,z) - V(r_0,z) = (a/2)(r^2-r_0^2)-az^2 \qquad (2.9)$$

where $V(r,z)$ = the potential at the point (r,z)

r_0 = an arbitrary radius.

The equipotential surfaces are therefore hyperboloids of revolution. Unlike the rectangular structures this configuration is precisely accurate when space charge is negligible. Furthermore, we shall show that this is true for uniform space charge up to a limiting value. A suitable structure for a delay line could be formed, as shown in Figure 2.6, from sections of two hyperboloids together with field terminations in the planes of the section edges.

2.3 Space Charge Effects

The charge density, ρ, in the electron delay line is related to the current density, J, and the drift velocity, v_d, through the equation $\rho = J/v$. Because the drift velocities are small the space charge effects can be appreciable, even for small current densities. We consider in this section the nature of the effects and the conditions under which they become important.

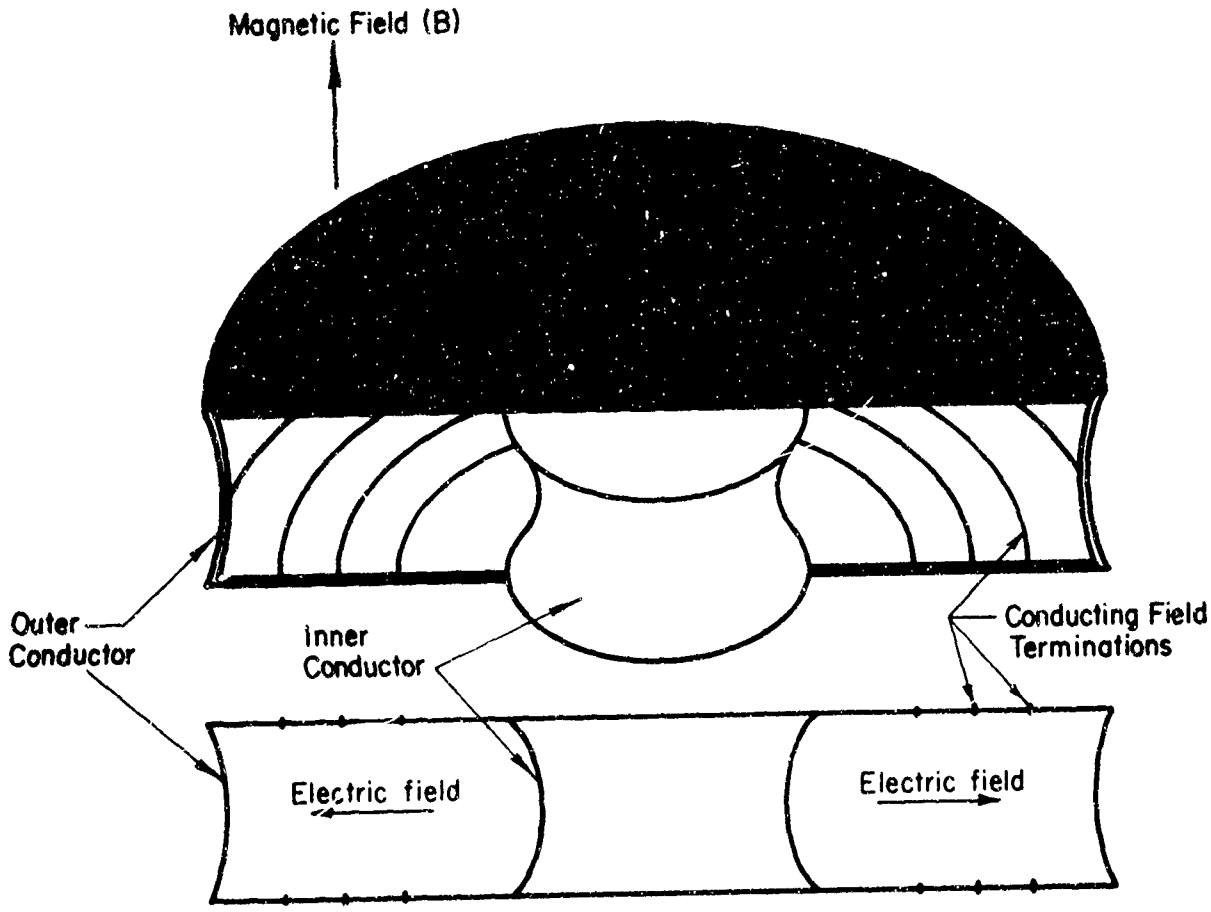

Figure 2.6

Hyperboloidal Delay Line

2.3.1 Beam Spreading

Along the magnetic field lines space charge pressure causes the beam to spread until the outward force on the edge electrons equals the inward force of the focusing fields. In the absence of focusing fields, the beam continues to spread until at sufficiently low density the behavior of the beam in this direction is controlled by the longitudinal velocities of the electrons. To estimate the size of the effect we consider a beam of electrons moving in the x direction. The extent of the beam is infinite in x and y, the beam thickness is $2z_0$, and the charge density within the beam is ρ. The convective growth of the beam with time is

$$z/z_0 = 1 + (1/2\,\epsilon)(\eta\rho t^2) \quad . \qquad (2.10)$$

The expansion with time is thus very rapid. As an example, for a beam that expands by a factor of five in 7.5 microseconds, the space charge is only $\rho = 0.7 \times 10^{-11}$ coul/m^3. For a transit distance of 0.075m, the corresponding current density is $J = 0.7 \times 10^{-7}$ amp/m^2. If the aperture for the collection of particles is the same as that for injection, the collection currents vary inversely as the expansion factor.

These figures clearly indicate that even if the electrons had no velocity components along the magnetic field lines, focusing fields would still be necessary to restrain particles from escaping. This problem, however, is not serious since the required electric fields are usually small. For example, if the density is as much as 10^{-6} coul/m^3, a figure much greater than that calculated for the case above, the electric field is only 565 volts/m.

2.3.2 Velocity Slip

A much more serious problem arises from the space charge distortion of the transverse electric field. An otherwise uniform transverse electric field is distorted in a way that enhances the electric field in regions near the positive plate and diminishes it in the regions near the negative plate. As a result there is a spread of drift velocities through the aperture and a consequent smearing of signals in the beam.

Consider the region between two infinite parallel plates perpendicular to the y-axis and separated by a distance $2y_0$. The space is uniformly filled with charge of density ρ, and the potential difference between the plates is V. In the absence of space charge the transverse electric field would be $E_{y_0} = -V/2y_0$. The charge, however depresses the potential between the plates as shown in Figure 2.7, and

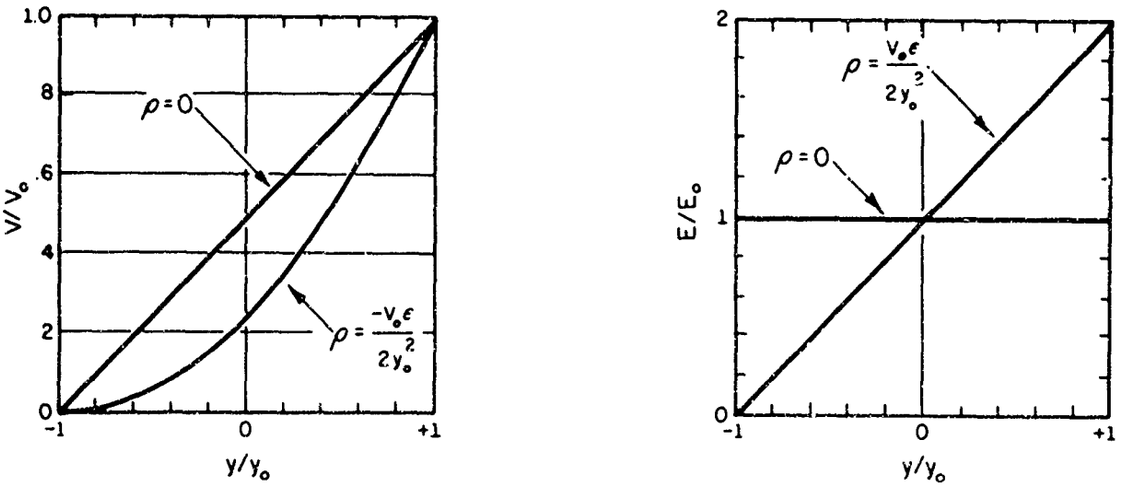

Figure 2.7

Effect of Space Charge on Field and Potential

distorts the electric field, which is now

$$E_T = E_{y_0} + (\rho/\epsilon)y. \tag{2.11}$$

The increase in the transverse electric field across the beam is therefore

$$\Delta E = (\rho/\epsilon)h \ , \tag{2.12}$$

where h is the beam thickness, and the corresponding velocity spread is

$$\Delta v = (1/B)(\rho/\epsilon)h \ . \tag{2.13}$$

In these equations the terms ρ and h appear only in the product ρh, which is proportional to the total beam current. This term, which has the dimensions of a surface charge density, is thus the natural independent variable. With $\rho h = \sigma$ we write

$$\Delta E = \sigma/\epsilon, \tag{2.14}$$

and

$$\Delta v = \sigma/B\epsilon, \tag{2.15}$$

and from these equations we find that the relative change in time delay across the beam is

$$(\Delta\tau/\tau) = (\sigma/\epsilon)/(E_{y_0} + \sigma/\epsilon). \tag{2.16}$$

The reciprocal of this quantity,

$$(\tau/\Delta\tau) = 1 + \epsilon E_{y_0}/\sigma \ , \tag{2.17}$$

is a standard figure of merit for delay lines, and its magnitude is proportional to the information capacity in the line. For a step function signal $\tau/\Delta\tau$ is physically the ratio of the time delay to the rise time at the collector.

It is useful to express $\tau/\Delta\tau$ in terms of the beam current and either the time delay or the drift velocity. Since $E_{y_0} = v_d B$, and the linear current density in z is $J' = \sigma v_d$ we can write

$$\tau/\Delta\tau = 1 + \epsilon v_d^2 \, B/J' \, . \tag{2.18}$$

If the transit distance is $\ell = v_d \tau$, we have the alternate form

$$\tau/\Delta\tau = 1 + \epsilon \ell^2 \, B/J'\tau^2 . \tag{2.19}$$

Figure 2.8 plots J' against v_d for B = 1 weber/m^2 and for several values of $\tau/\Delta\tau$. For the same parameters Figure 2.9 plots J' against τ when the transit distance is one meter. To obtain J' for any value of B, multiply J', obtained from the graph, by the correct value of B. Similarly, if the transit distance is ℓ, multiply J' from the graph by ℓ^2. As an example, if $\tau = 10^{-5}$ sec., $\ell = 0.1$ m, B = 0.5 weber/m^2, and $\tau/\Delta\tau = 100$, we find $J' = 4.45 \times 10^{-6}$ amp/m.

We see at once that both the magnetic field B and the transit distance ℓ should be large. The rapid variation of attainable current with transit length suggests that some advantage could be gained if it were possible to allow the electrons to traverse a circular path several times, using part of the aperture for each excursion.

The frequency bandwidth f_0 is inversely proportional to the rise time, $\Delta\tau$, of the distorted step function at the collector. Comparison of $\Delta\tau$ with the rise time of a single time constant linear circuit to a step function shows that

$$f_0 = 0.367(1/\Delta\tau) \tag{2.20}$$

or from the above equations

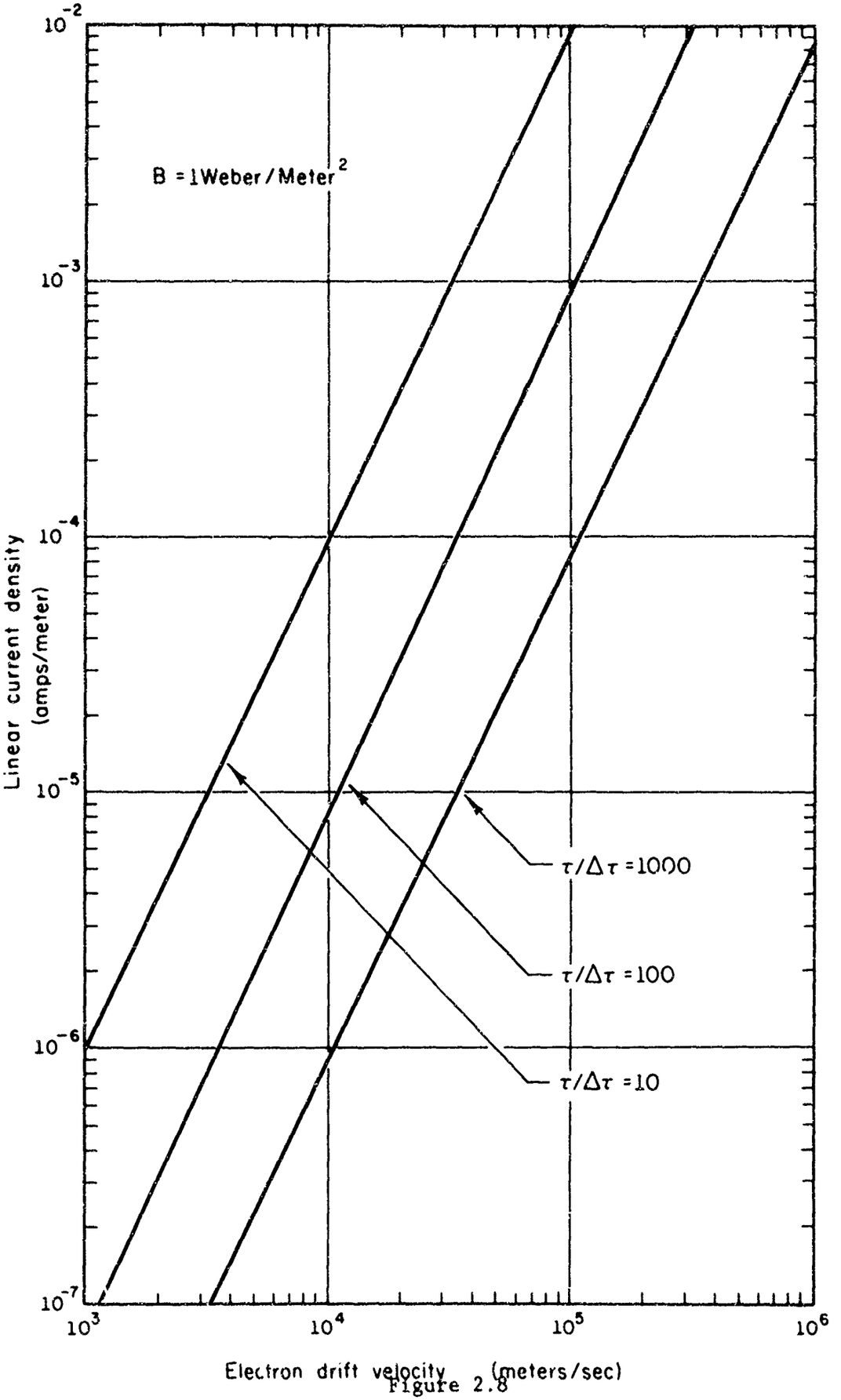

Figure 2.8

Current Density vs Drift Velocity for Several Values of $\tau/\Delta\tau$

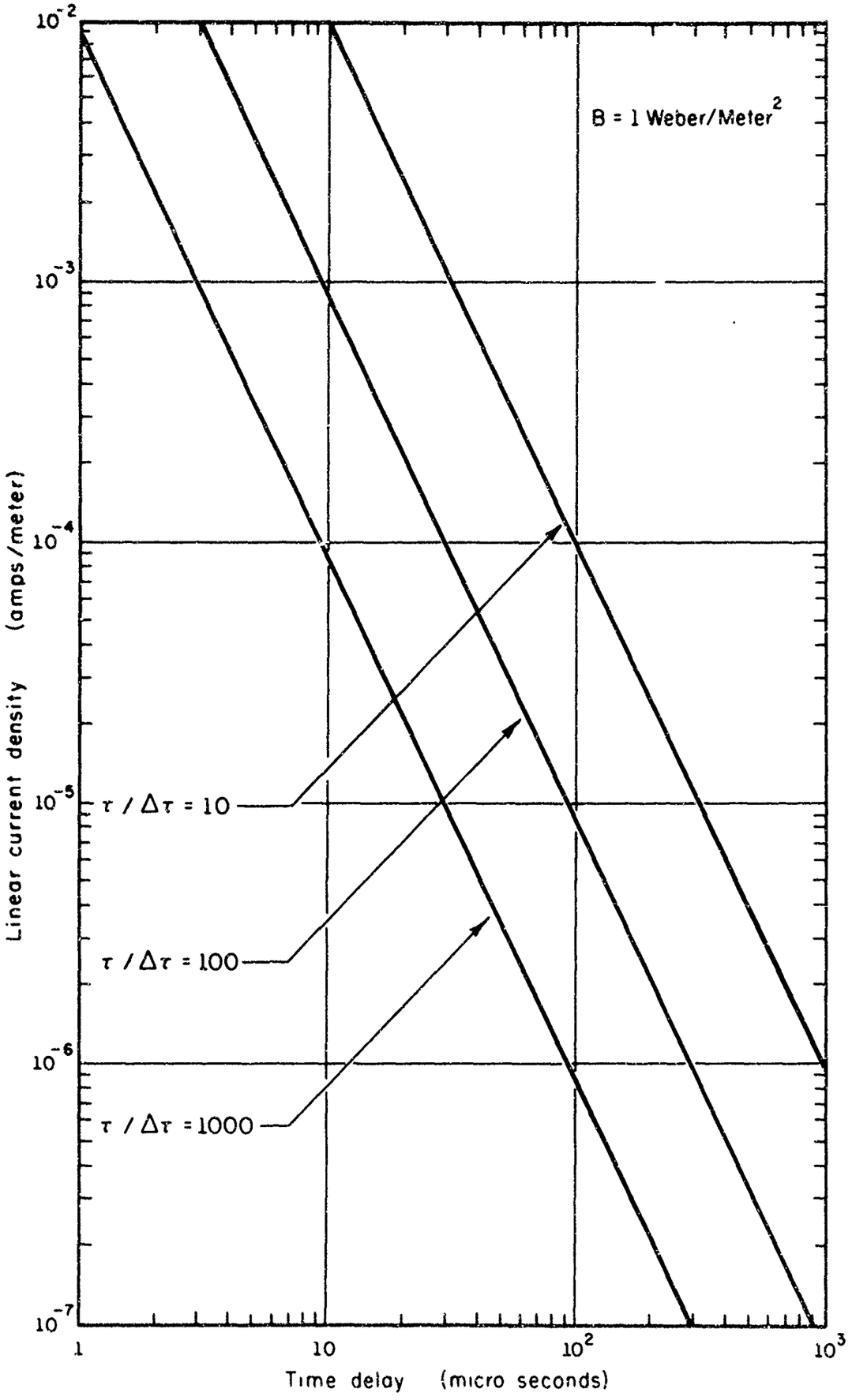

Figure 2.9

Current Density vs Time Delay for Selected Values of $\tau/\Delta\tau$

$$f_0 = 0.367\ell^2 B\epsilon/\tau^3 J' \quad . \tag{2.21}$$

Figures 2.10 and 2.11 show the influence of J' and - and ℓ on the frequency response.

In this section we have so far adopted the point of view that the electrons are effectively at the guiding centers, that the velocity slip arising from space charge degrades frequency response, and that particular performance specifications dictate relations among the parameters. Because the slip effect so seriously limits the current for long time delays, it would be desirable to reduce the slip in some way. We consider three approaches to the problem. First, compensating electric fields can be provided by external electrodes. Second, by establishing a magnetic gradient drift that opposes the normal drift it may be possible to use larger electric fields and to reduce effectively the slip. Finally, if the energy in the electron orbit is large enough so that the orbit radius is equal to the beam thickness, then all electrons in the beam would on the average sample the same field, and in principle there would be no slip. We consider first the use of hyperbolic electrodes to compensate for the disturbing electric fields.

In a circularly symmetric system Poisson's equation is satisfied if the radial and longitudinal components of the electric field have the form

$$E_r = \partial V/\partial r = -ar \tag{2.22}$$

$$E_z = -\partial V/\partial z = (2a + \rho/\epsilon)z \quad . \tag{2.23}$$

As in the case of negligible space charge the radial field E_r again has

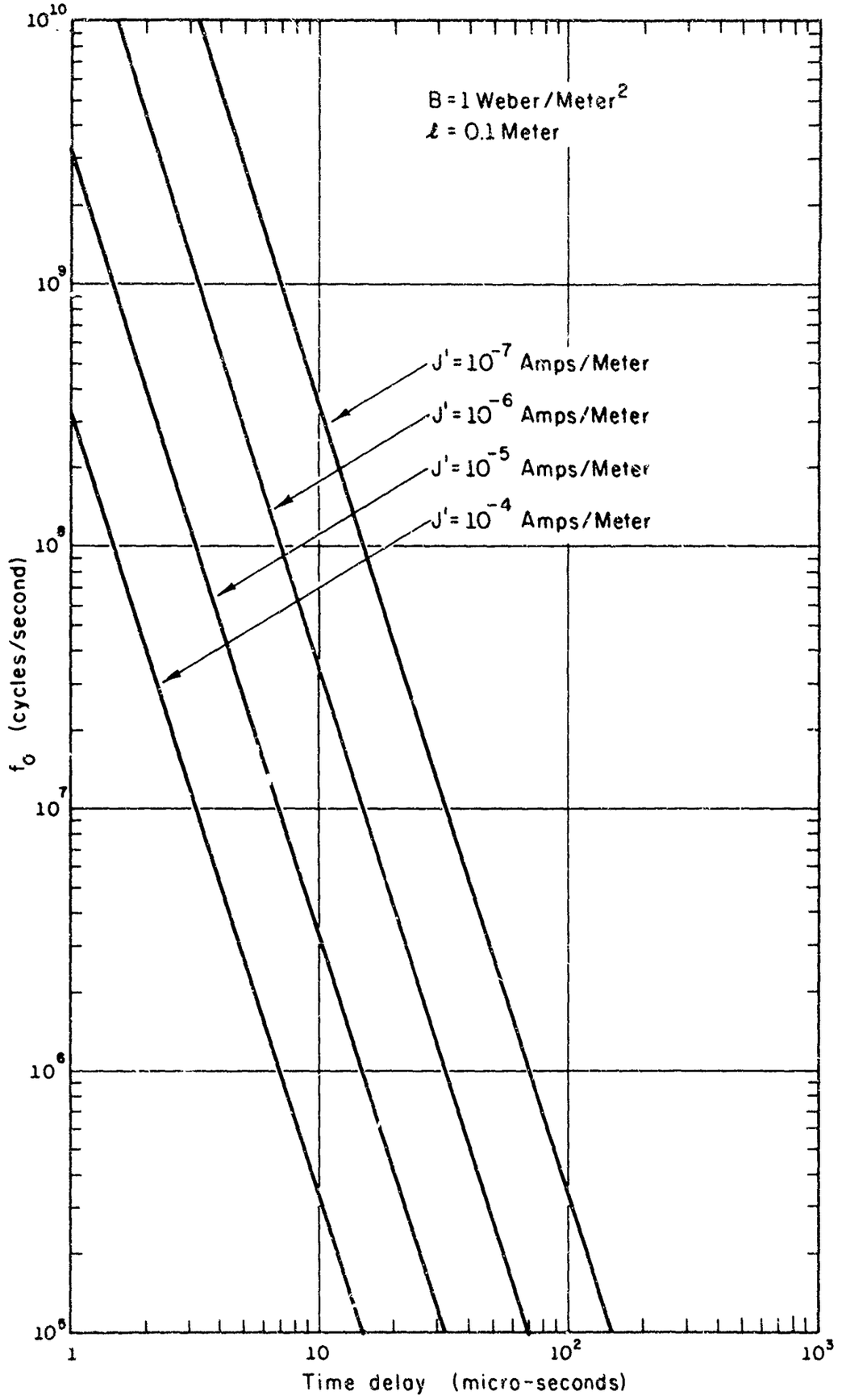

Figure 2.10

Influence of Time Delay and Linear Current Density on Frequency Response

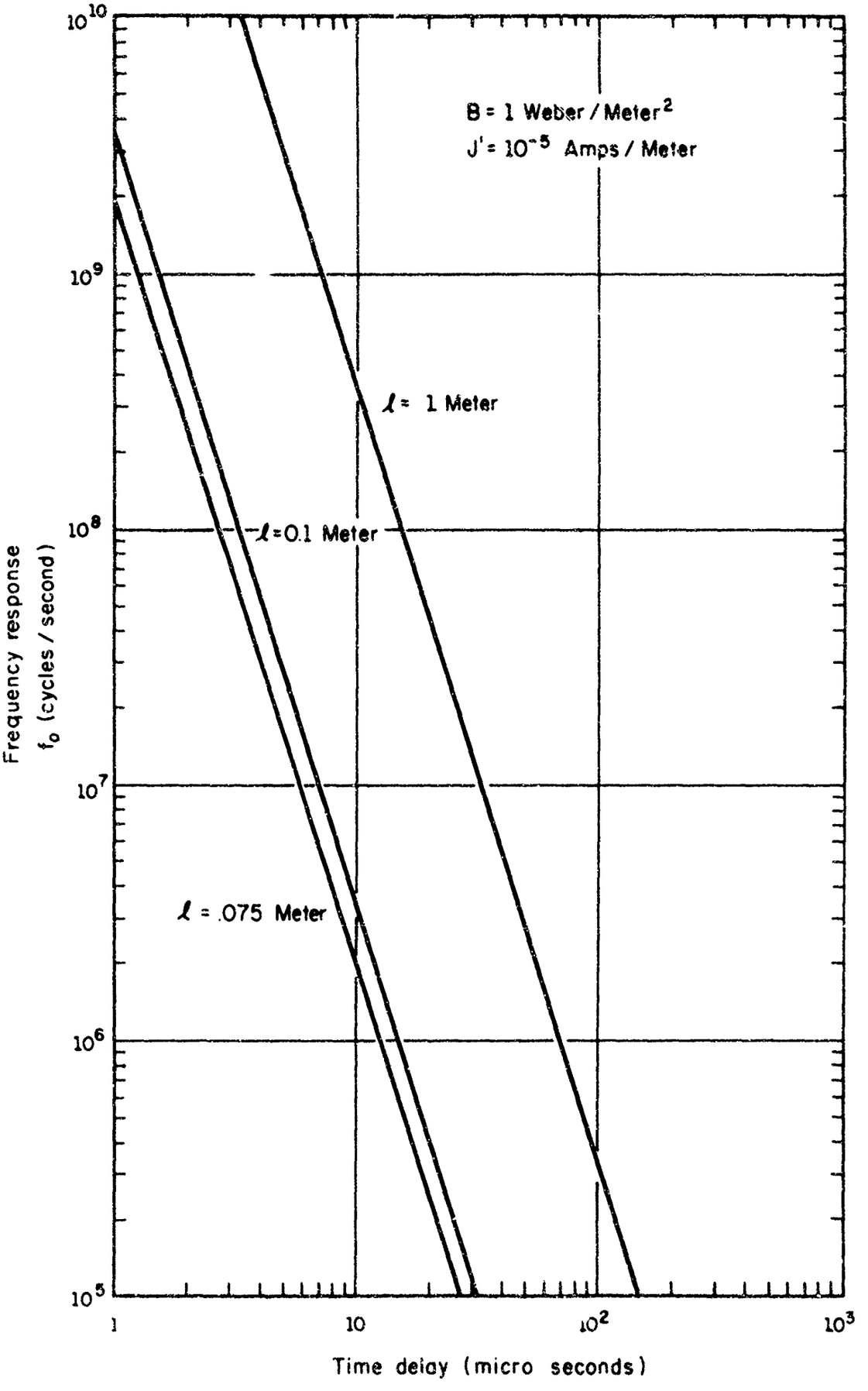

Figure 2.11

Influence of Time Delay and Transit Distance on Frequency Response

the necessary form for constant angular velocity. The focusing forces provided by E_z, however, diminish as the space charge ρ increases. The corresponding equation for the potential is

$$V(r,z) = V(r_0,0) + 1/2\ a(r^2-r_0^2) - (a + 1/2\rho/\epsilon)z. \qquad (2.24)$$

When the space charge can be neglected the angle between the cones asymtotic to the hyperboloids is $\theta = \tan^{-1}\sqrt{2}$, and the magnitude of the focusing field E_z is a maximum everywhere in the annulus. As ρ increases from 0, the angle θ increases and E_z decreases until for $\rho/2\epsilon = a$, the equipotentials are right circular cylinders and the focusing forces disappear altogether. Figure 2.12 shows cross sections of the surfaces for zero space charge, for maximum space charge, and for an intermediate value ($\rho = a\epsilon$). In the limiting case the radial field is

$$E_r = (\rho r/2\epsilon) = (\omega_p^2/2\eta)\ , \qquad (2.25)$$

where $\omega_p = \sqrt{\rho\eta/\epsilon}$ is the plasma frequency. This value for the field agrees with one given by Klüver [8] for the radial electric field in a beam that does not necessarily fill the space between the two electrodes. Klüver also gives an expression for the required voltage between the two cylinders, which, when the aperture is filled, reduces to

$$V = (\omega_p^2/4\eta)(r_1^2-r_0^2) \qquad (2.26)$$

where r_1 and r_0 are the radii of the outer and inner cylinders. This is equivalent to Eq. (2.24) in the limiting case when $a = -\rho/2\epsilon = \omega_p^2/2\eta$.

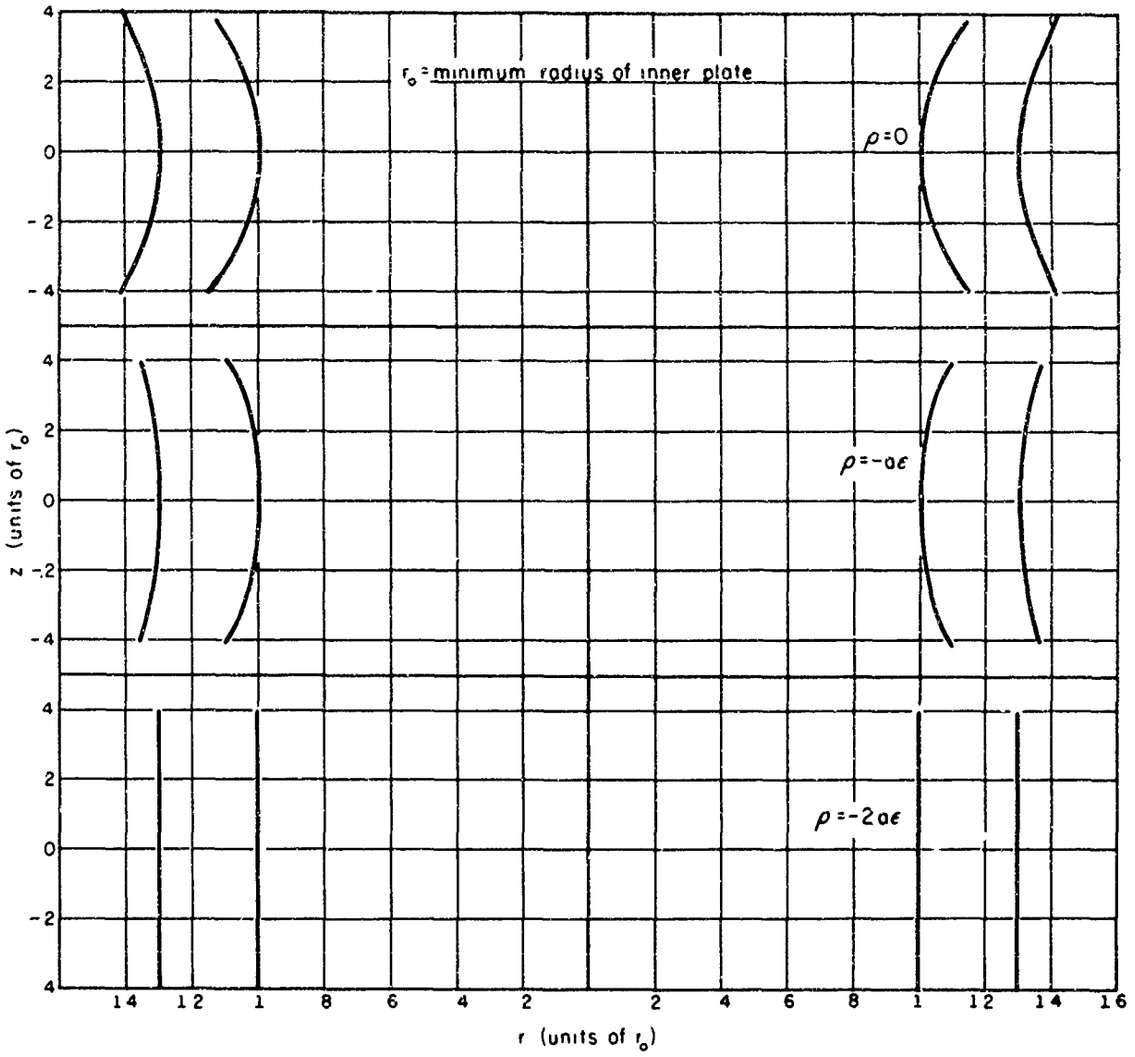

Figure 2.12

Electrode Shapes for Hyperboloidal Delay Line

In a practical case we might chose $a = -\rho/\epsilon$, which is twice the minimum value. With the transit distance equal to one revolution this choice dictates the following expressions for ρ, v_d, and J:

$$\rho = 2\pi\epsilon B/\tau \tag{2.27}$$

$$v = 2\pi r/\tau \tag{2.28}$$

$$J = 4\pi^2\epsilon Br/\tau^2 \ . \tag{2.29}$$

Figures 2.13, 2.14, and 2.15 plot ρ/B against τ, v against τ with r as a parameter, and J/B against τ with r as a parameter. We note that with B = 0.6 webers/m^2 and r = 0.05 m, the drift time τ is 31.4 $\times$ 10^{-6} sec for one revolution, and J is 1.06 $\times$ 10^{-2} amp/m^2. Since the aperture would be about one square centimeter, the total current would be about one microampere. Clearly the attainable currents are much larger than in a structure designed for zero space charge.

Even better performance could be expected if the beam made several revolutions filling part of the available aperture each time. Since part of the aperture would be used by the guiding structure the beam cross section would be reduced by a factor greater than n where n is the number of revolutions. Eq. (2.29), however, shows that the current density would increase by n^2. Thus if the electrons filled a fraction, k, of the aperture, the increase in current would be kn.

Unfortunately we have not yet achieved a complete solution to the problem. Because J varies as $1/\tau^2$, variation of τ over a wide range imposes severe requirements on an electron gun. Furthermore, for electrons already in the drift space it is impossible for ρ to follow variations in electric field. The velocity and current, of course, respond immediately, but the charge density remains the same.

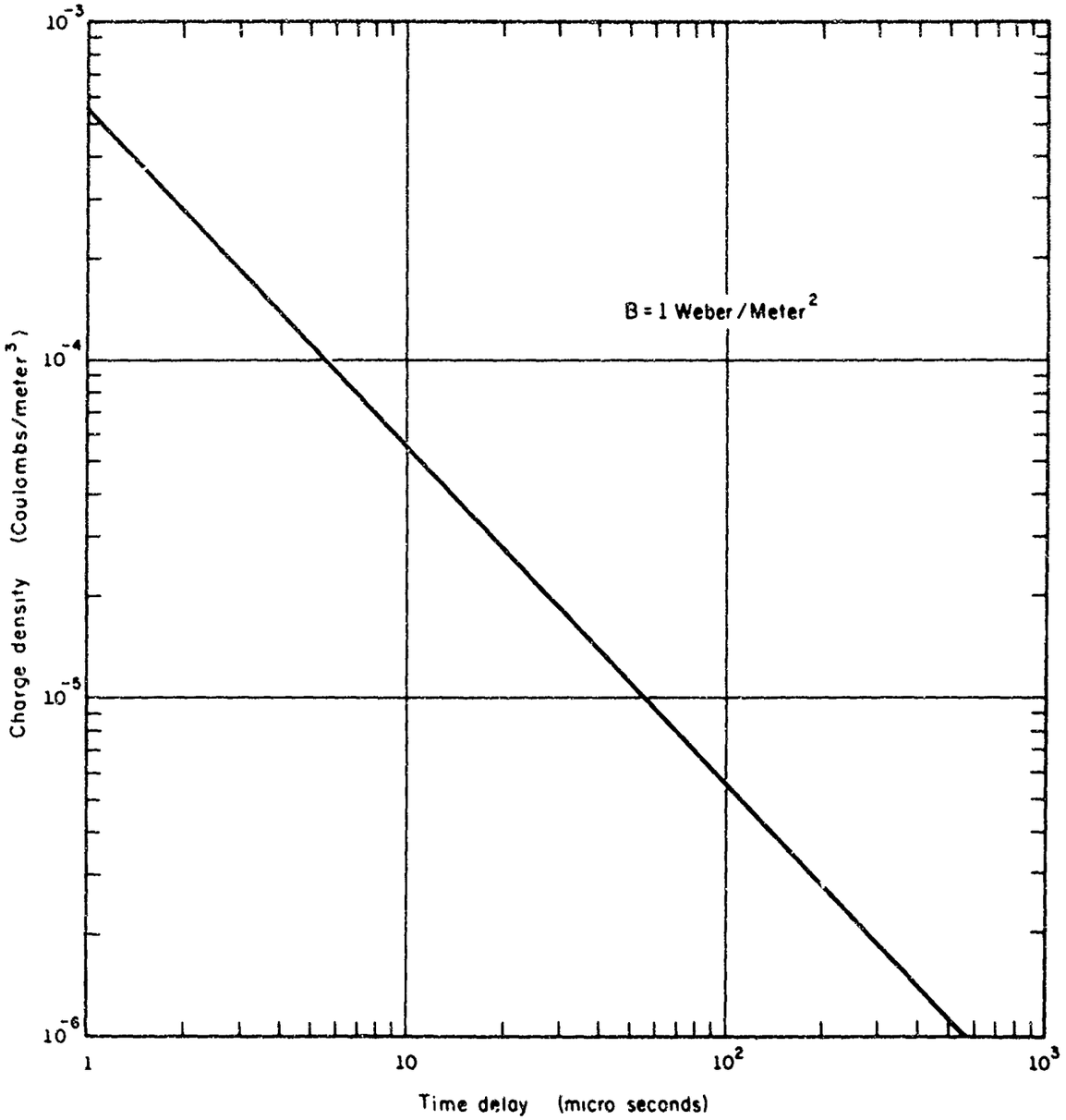

Figure 2.13

Charge Density vs Time Delay in Circular Delay Line

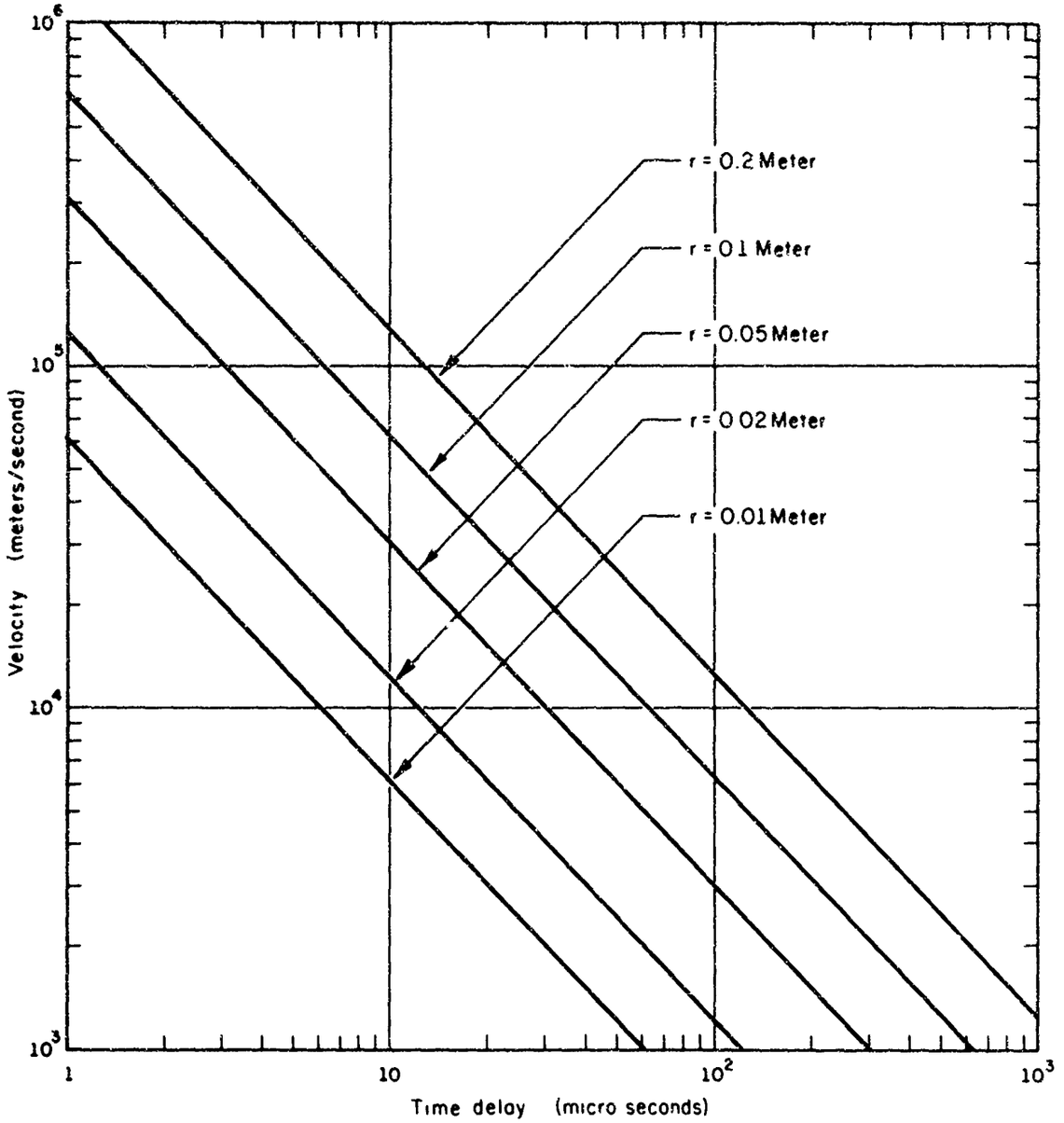

Figure 2.14

Velocity vs Time Delay in Circular Delay Line

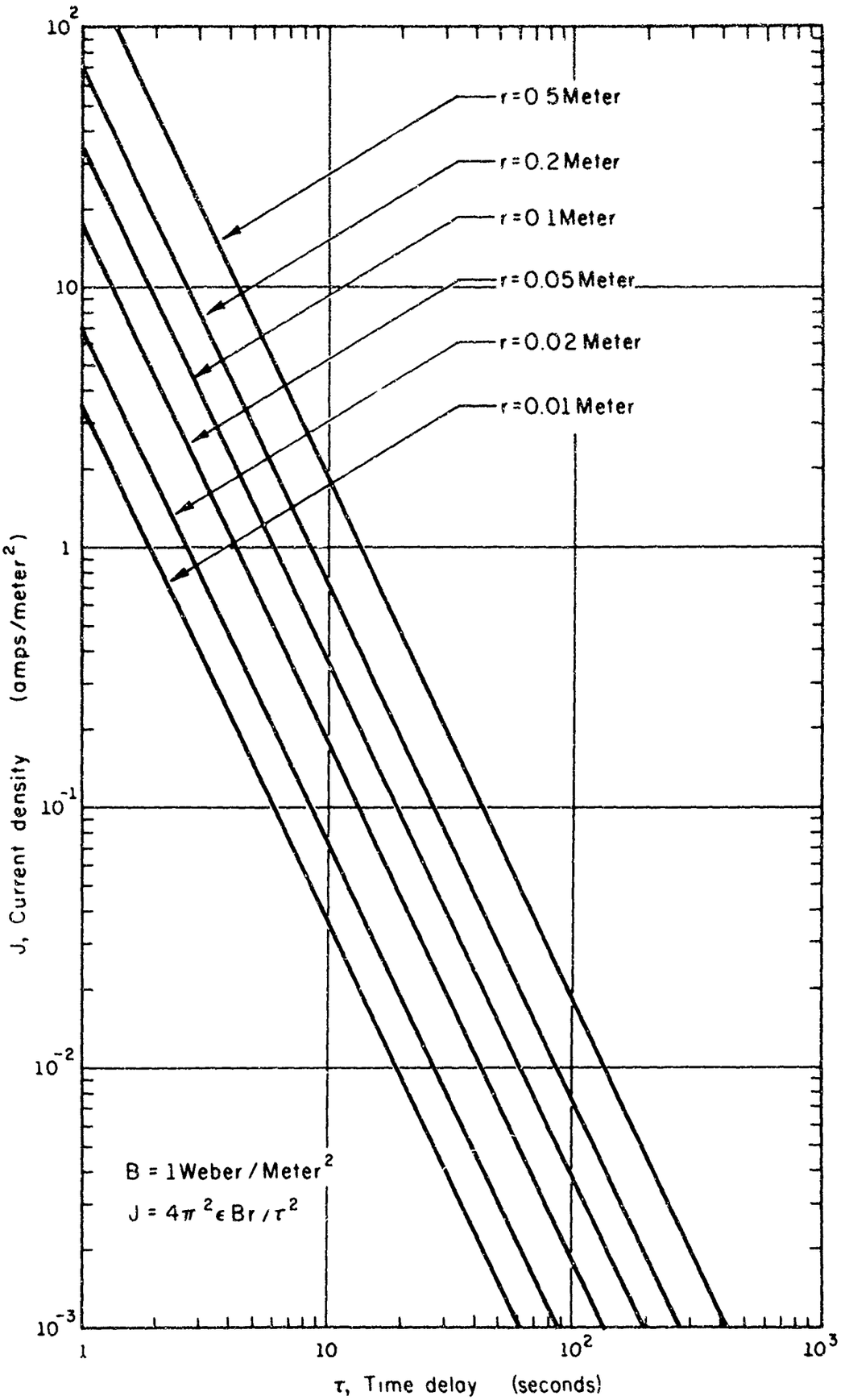

Figure 2.15

Current Density vs Time Delay in Circular Delay Line

Nevertheless, when the charge density is correct the slip effect is eliminated, and for applications where the transit time must be varied slowly over narrow ranges, balanced flow in hyperboloidal structures is appropriate.

If the magnetic field is not uniform in the drift space, but instead increases in the direction of the electric field, an opposing magnetic gradient drift is superimposed on the $\vec{E} \times \vec{B}$ drift, and the drift velocity becomes

$$v_d = E_{eff}/B = [(\mathcal{E} - v_r^2/2\eta)(|\nabla_r B|/B)]/B. \qquad (2.30)$$

In terms of the electron energy

$$v_d = [(E - V_r)(|\nabla_r B|/B)]/B. \qquad (2.31)$$

The first term in the numerator is the electric field provided by the external electrodes. The second term can be interpreted as an equivalent electric field E_m, which produces the same drift velocity as the magnetic gradient.

To be effective E_m should be large with respect to E_{eff}, and since constructional difficulties limit the magnitude of $\nabla B/B$, V_r must be large. As an example, with B = 0.5 weber/m^2, and $v_d = 10^4$ m/sec, $E_{eff} = 0.5 \times 10^4$ volts/m. To reduce the space charge effect by an order of magnitude we stipulate that $E_m = 5 \times 10^4$ volts/m, and assume that $V = 10^4$ volts. The normalized magnetic field gradient must therefore be $\nabla B/B = 5$. This means that the electrons drift in the fringing field of a magnet with the field changing with distance at a rate of 250 gauss/cm. Larger gradients and correspondingly larger reductions of the slip effect are easily achieved.

The energy dependent property of the magnetic drift is not a disadvantage in this application, because with V_r large, the relative energy spread is small.

Still another way to reduce slip is to allow the orbit diameter to equal the beam thickness. The orbit centers then lie in a plane y = 0 perpendicular to the electric field. The electric field in the beam is proportional to $\sin^{-1}(y/R)$ where R is the Larmor radius and $|y| \leq R$. The orbit itself is affected only negligibly by this field, and each electron thus averages the effects of the field in the same way. The result is that the space charge field contributes no drift and no slip.

If the orbit centers lie in a band with thickness d, the beam thickness h will be larger than the orbit diameter 2R and there will be a velocity slip Δv_1 across the beam.

The slip across a beam of the same thickness, but with electrons effectively at the guiding centers, is Δv_0 which is related to Δv_1 by the reduction factor Q

$$\Delta v_1 = Q\Delta v_0 \tag{2.32}$$

where $Q \approx d/h$. These properties are discussed in Appendix B.

The averaging effect of the high energy electrons can be combined with the magnetic gradient effect simply by using thin beams of high energy electrons in an appropriate magnetic field. Moreover, these two methods are consistent with the hyperboloidal structure, designed for zero space charge, which provides the correct transverse electric field with effective focusing fields.

2.3.3 Instabilities

The attainable current in the delay line can also be limited by still another effect of space charge, the tendency of thin beams in crossed fields to be unstable [9]. Perturbations in both space charge density and beam displacement grow as $e^{\gamma t}$ where

$$\gamma = (\rho/\epsilon B)(\alpha)$$
$$\alpha = [\beta h/2 - (\beta h/2)^2 - 1/2 \tanh \beta h/(1 + \tanh \beta h)] \tag{2.33}$$
$$\beta = 2\pi/\lambda$$

and λ = the wave length of the disturbance.

When the wavelength of the disturbance is large compared to the beam thickness, βh is small, α is approximately equal to $\beta h/2$, and

$$\gamma = \rho\beta h/2\epsilon B. \tag{2.34}$$

In terms of the surface density

$$\gamma = \sigma\beta/2\epsilon B. \tag{2.35}$$

Because these expressions have been calculated for beams with a velocity slip, the effect is sometimes called the slipping stream instability, or the diocotron effect - descriptions that refer to the velocity variation [9]. Eq. (2.35), however, has also been obtained from an analysis of an infinitely thin electron beam [10], and also from a study of an infinitely thin electron beam that in the unperturbed state is neutralized [11]. The assumption of slipping velocity is thus apparently not essential.

As βh increases, α increases less rapidly until for $\beta h = 0.8$ it reaches its maximum value, $\alpha_{max} = 0.2$. As βh increases beyond 0.8, α decreases until it vanishes when $\beta h = 1.3$. For still larger values of βh, α is imaginary and the beam is stable [9].

In terms of the surface charge density, the maximum value of γ is

$$\gamma_{max} = [(0.4)\sigma/h]/2\epsilon B. \tag{2.36}$$

Since the linear current density J' is σv_d, and the drift distance ℓ is $v_d \tau$,

$$\gamma_{max} = [(0.2)J'\tau/h\epsilon B\ell] . \tag{2.37}$$

The maximum growth in the delay time τ is then

$$e^{\gamma\tau} = e^{(0.2)J'\tau^2/h\epsilon B\ell} . \tag{2.38}$$

Since in this equation $\beta h = 0.8$, the wavelength of the disturbance is

$$\lambda = 2\pi h/0.8 = 7.86h , \tag{2.39}$$

and the frequency is

$$f = v_d/\lambda = 0.127v_d/h. \tag{2.40}$$

The importance of this mechanism to delay line performance is twofold. First, as in the travelling wave magnetron, the noise on the beam is amplified and secondly, sufficiently large growth of ripples in the beam could destroy the beam itself before it reaches the collector.

To illustrate, we plot in Figure 2.16 the dependence of J' on τ for one e-folding growth and for selected values of the remaining parameters. If the beam is not continuous but instead is just a small section with abrupt edges in the direction of propagation, the forces on the edge electrons are large, and the effects of space charge should be apparent at lower values of charge density than would be indicated by the linear theory. When the beam is thin we expect curling at the

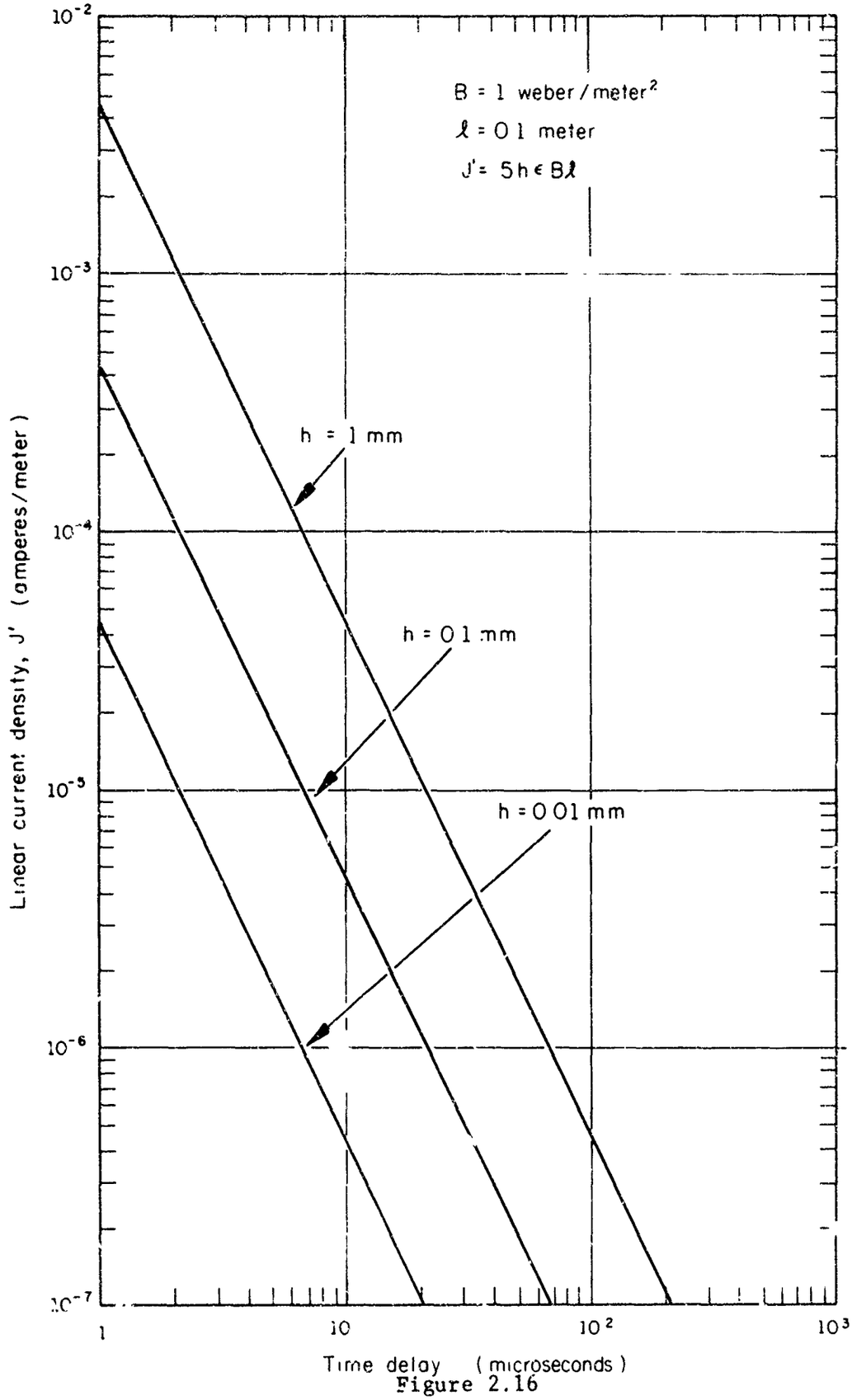

Figure 2.16

Linear Current Density vs Time Delay
for One e-folding Growth

edges and foreshortening of pulse. Similar effects have been observed in the breakup of hollow beams that are focused by a longitudinal magnetic field [12]. We discuss this effect in greater detail in connection with the experimental results.

2.4 Coupling Problems

If the dispersion of the electrons in the crossed field drift space could be entirely avoided, there would still remain the difficult problems of modulating the beam, of detecting delayed signals, and of properly launching the beam. In our discussion of these problems we distinguish between structures which do not maintain constant drift velocities and those that do. In the first class signals couple to a high velocity electron beam after it emerges from an electron gun. The beam then enters a low velocity drift space, and after entering a second high velocity region it couples to the output circuit. This arrangement has one important advantage: it allows the use of standard high frequency coupling devices – gridded gaps, helices, and, for cyclotron waves, transverse couplers. There is also a serious disadvantage: between the drift section and the couplers the beam must traverse a transition region in which the electrons can disperse. The second class of structures avoids the transition problem, but increases the difficulty of coupling and launching. We also distinguish, as we did in the discussion of the drift region, between electron motions with negligible radii and high energy trajectories in which the orbit radii equal or exceed the beam thickness. We first consider the transition problem with low energy electrons.

Figure 2.17 shows a sketch of a transition region together

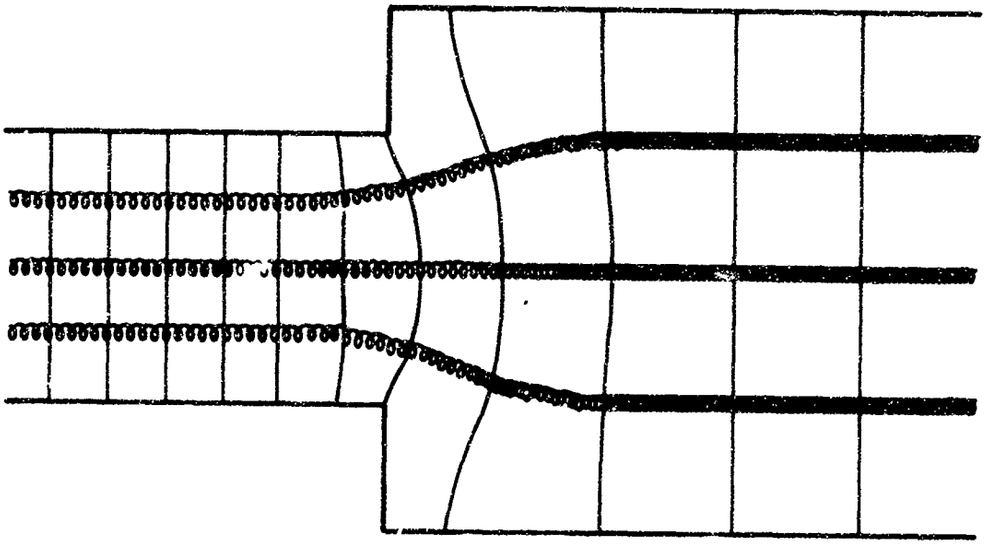

Figure 2.17

Low Energy Electrons in Transition Region

with parts of high and low velocity regions which it joins. The magnetic field is uniform. In the constant velocity regions the equipotential lines and the field lines are straight, but in the connecting regions they curve. As a result the beam expands into the low velocity regions and electrons which drift on the outer potential lines travel farther than electrons which drift along the inner lines. Moreover, the outer electric fields are less intense than the inner fields and therefore the outer electrons also travel more slowly. These effects are cumulative, and cause the outer electrons to lag behind the inner electrons. If in addition a similar coupling region is used after

the delay the effect is doubled.

The dispersion can probably be reduced by connecting the regions, as shown in Figure 2.18. Here electrons that penetrate most

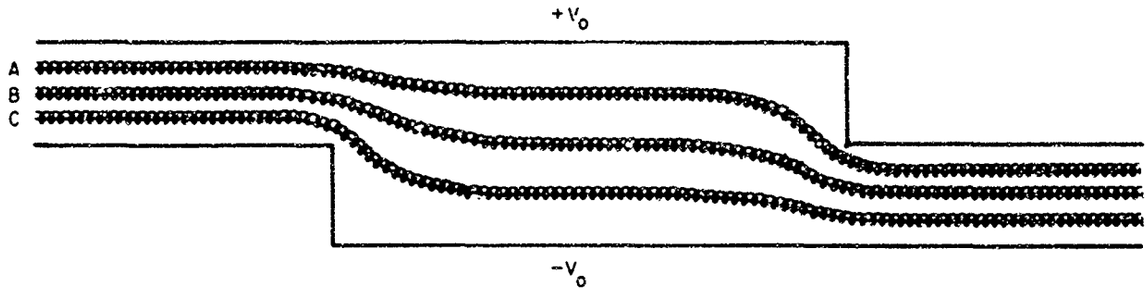

Figure 2.13

Low Energy Electrons in Compensated Transition Regions

quickly into the drift region emerge more slowly and the surface connecting all particles that represent a given sample time in a signal tends to straighten out. In the absence of space charge the compensation for the edge electrons is complete. For low current thin beams then, the compensation is effective.

A realistic model of these regions must, of course, include space charge effects, which as we have seen are important in the drift region. Although these effects could conceivably be balanced by the fields of properly shaped electrodes, this problem has not yet been solved.

Control of high energy electrons through these electric field transitions seems to present fewer difficulties. If, as in Figure 2.19, the guiding centers are confined to the median plane, the electrons average out both the space charge field and the inhomogeneities in the applied electric field. If, on the other hand, the

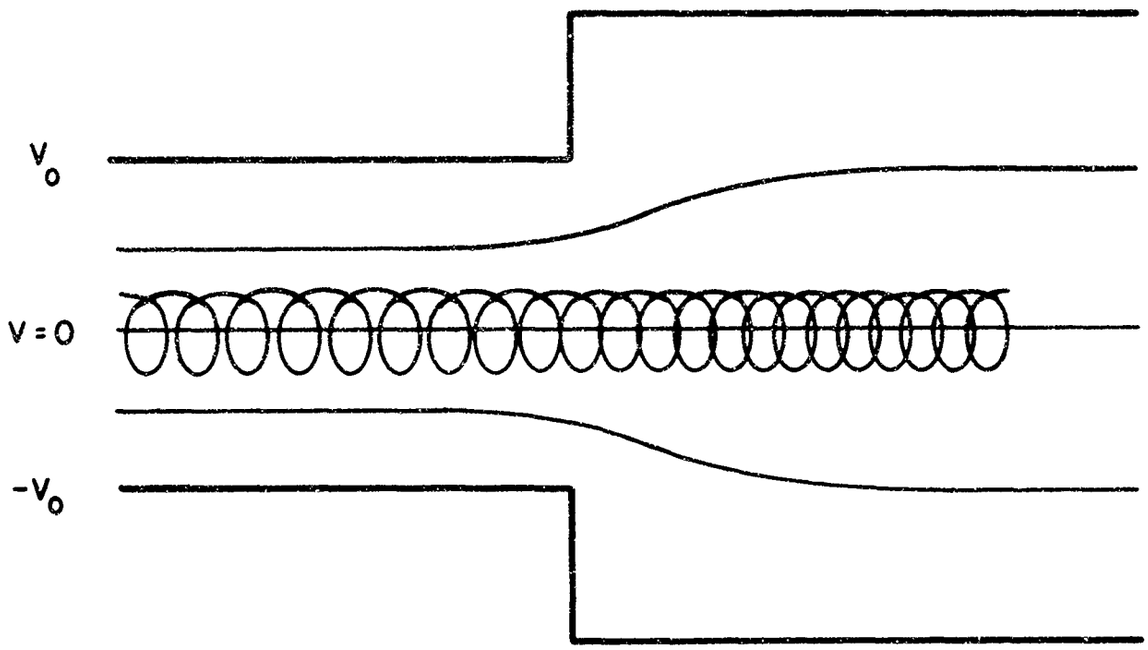

Figure 2.19

High Energy Electrons in Transition Region

guiding centers are distributed within a band of thickness d, the velocity dispersion, although not eliminated, is reduced by the factor $Q \approx d/h$. Furthermore, use of the structure of Figure 2.18 should provide additional improvement.

A transition region can also be provided by a spatially varying magnetic field in conjunction with the constant electric field. We have seen, however, that electrons have a tendency to drift at right angles to the magnetic field gradient. The beam in this kind of region is therefore more difficult to control. There still remains

one other possibility: a region in which both electric and magnetic fields vary. This kind of structure seems particularly appropriate for guiding an electron beam from a region of zero magnetic field into the drift regions of the crossed field delay line. Structures of this kind for the purpose of launching beams in travelling wave magnetrons have been studied by Hoch and Watkins [13].

The transition problem can be avoided entirely if the drift velocity remains unchanged from the point where signals are impressed on the beam to the point where they are extracted. Modulation of a slow beam, however, implies that the transit time effects may degrade the frequency response, even if the modulating structure is small. The details of the frequency response curve must depend on the structure, but we expect, in general, that the effects will be appreciable when the transit angle u approaches unity. The transit angle, as usual, is

$$u = \omega t_{\ell}, \tag{2.41}$$

where ω = the frequency of the signal in radians per second;

t_{ℓ} = the transit time of the particles through the modulator.

The frequency response falls off as

$$C = (\sin \omega t_{\ell}/2)/(\omega t_{\ell}/2) \tag{2.42}$$

or

$$C = (\sin \omega s/2v_d)/(\omega s/2v_d) \tag{2.43}$$

where s = the length of the modulation structure. When $\omega t_{\ell} = \pi$, $C = 0.636$, and since for this angle dC/du is large, this is a convenient definition of the cut-off frequency. Thus we have

$$f_0 = 0.5v_d/s, \tag{2.44}$$

which is shown in Figure 2.20 with s as a parameter.

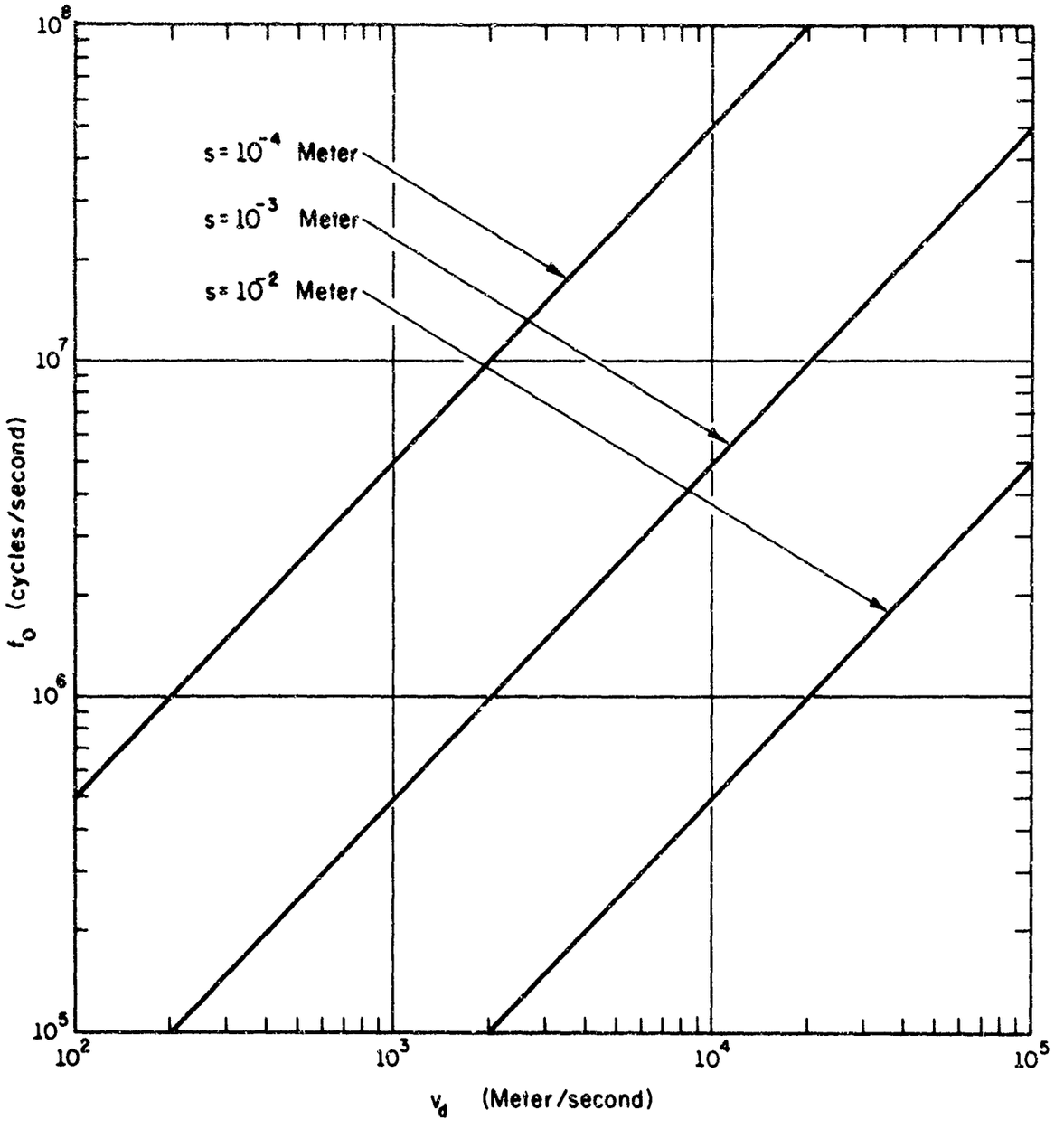

Figure 2.20

Frequency Response of Modulator

Combining the launching and modulation functions into one structure provides a way of reducing the transit time. In Figure 2.21

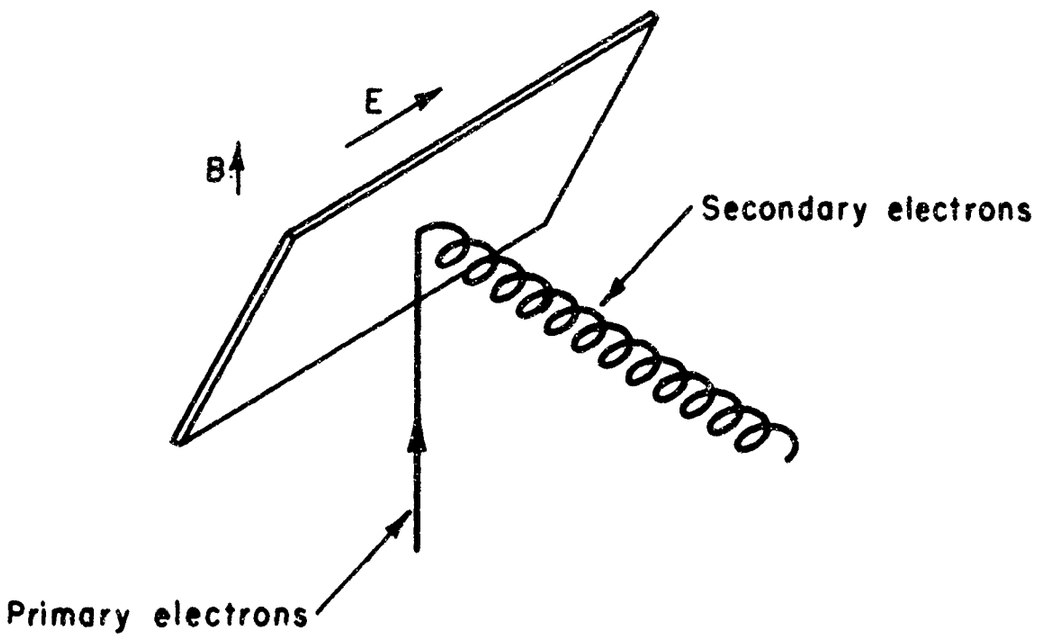

Figure 2.21

Secondary Emission of Electrons in Launching Region

primary electrons travel upward along the magnetic field lines until they strike the surface of the secondary emitter which is slightly inclined to the normal. The emitter is actually a resistor and it sustains a voltage gradient which matches the gradient in the drift space. Although some secondary electrons curve back into the surface, others escape to form the drifting beam. Variation of the current in the primary beam modulates the current in the secondary beam. The effective transit distance s for the modulator is the width of the primary beam. Since this technique was used in some of the experiments, it is appropriate to consider here the conditions under which launching is possible.

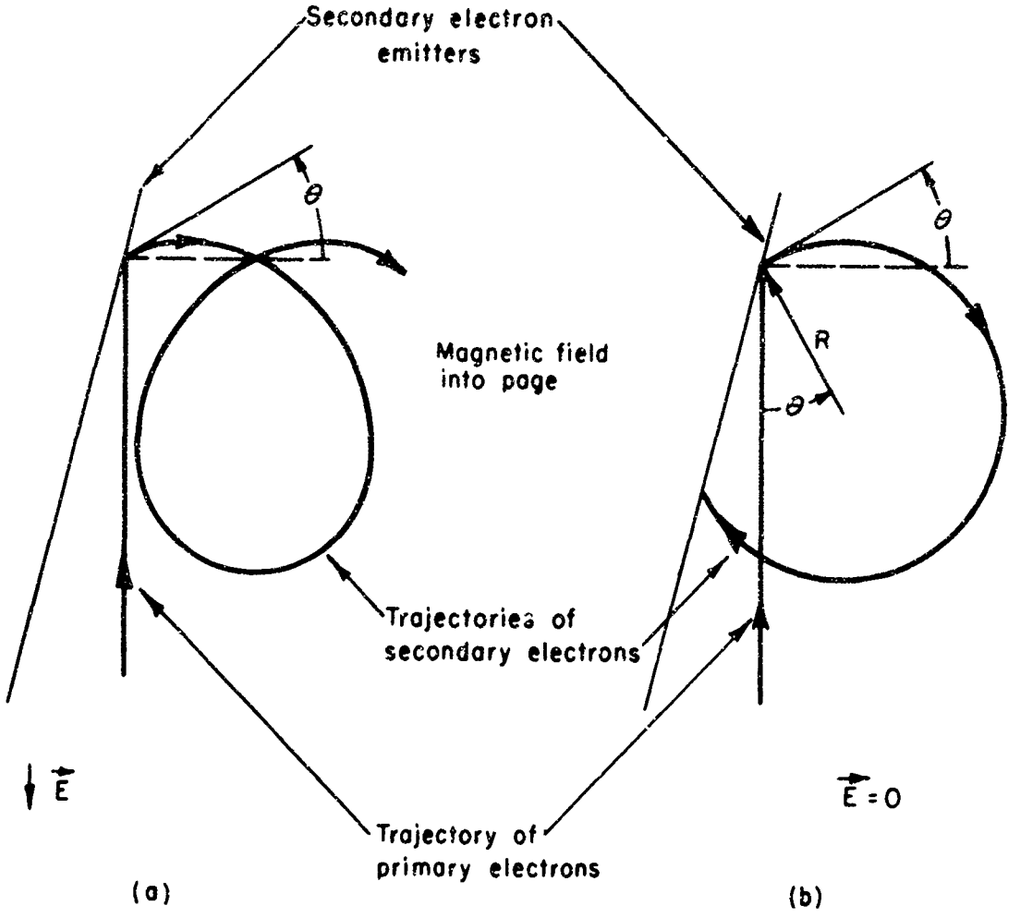

Figure 2.22

Electron Trajectories Near Secondary Emitter

Figure 2.22 shows a possible path of an electron after it emerges from the secondary emitting surface at an angle θ. In the absence of an electric field, it describes a circular arc and returns to the emitting

surface. The guiding center remains fixed at a distance R from the point of emergence and at a distance R sin θ from the surface itself. The electric field decreases the curvature of the initial arc and the guiding center moves away from the surface with the velocity $v_d = E/B$. If v_d is sufficiently large the electrons escape. The distance s of the electron from the surface is

$$s = v_d t + R[\sin(\omega t - \theta) + \sin\theta], \qquad (2.45)$$

and the condition for escape is that for $t \geq 0$, $s \geq 0$.

Figure 2.23 shows the ratio of the drift velocity v_d to the emergence velocity v_t as a function of θ. Figure 2.24 shows the actual escape value of v_d as a function of θ with the emergence energy, in electron volts, as a parameter.

The distribution of energy in emitted electrons is Gaussian with the mean value in the range of a few electron volts, and the distribution of angles at which electrons emerge is co-sinusoidal with respect to the normal [14]. Only the angular distribution in a plane perpendicular to the magnetic field is significant for this escape mechanism, but Gaddy [15] has shown that this too is co-sinusoidal. Although we expect most of the electrons that escape to emerge at large angles, there is evidently an adequate supply. For example, 17 percent of the electrons emerge from the surface at angles greater than 80 degrees. Since from our earlier discussions we expect drift beams with currents of less than one microampere, requirements on the primary beam are clearly not great.

The signals on the beam are in the form of charge density variation. If at the collection end a similar resistor between the end plates

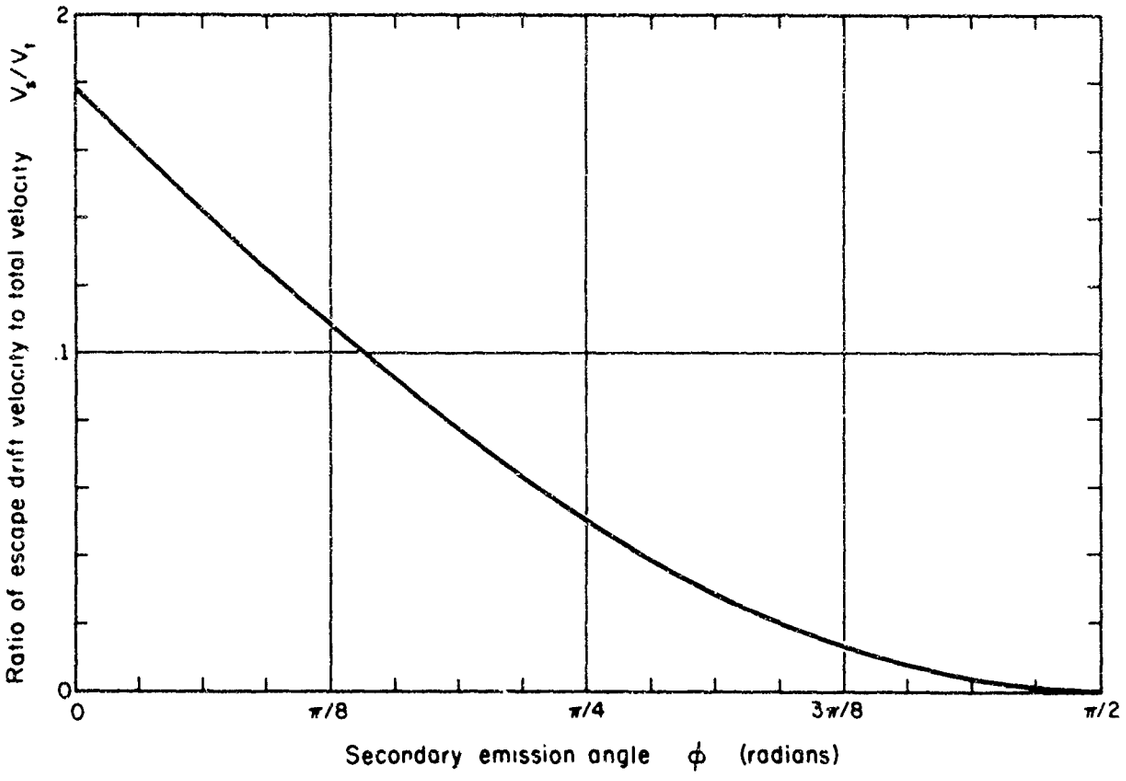

Figure 2.23

Dependence of Emission Angle on the Ratio
of Escape Drift Velocity to Total Velocity

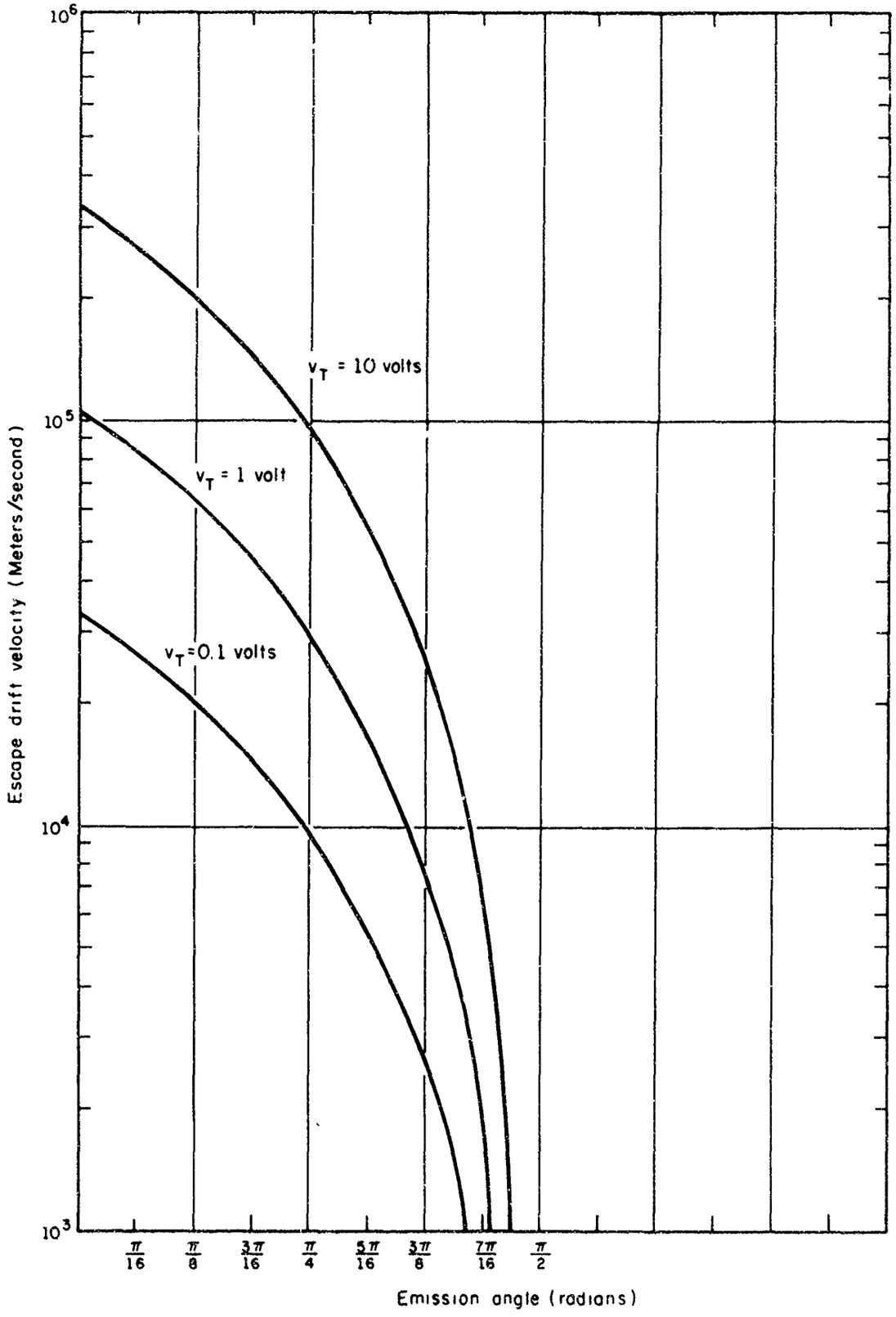

Figure 2.24

Dependence of Escape Drift Velocity
on Total Velocity and Emission Angle

is used as a collector, these variations appear in the output circuit of the delay line.

2.5 Effects of Circular Motion

If space charge effects can be neglected and if E and B are constant, any degrading influence of the beam itself on bandwidth must come from the properties of the orbital motion. In this section we examine the effects of the cyclotron frequency, the energy spread among electrons, and the spatial spread of the guiding centers.

We first consider two electrons approaching a collector, as shown in Figure 2.25. The electrons represent the same time samples of the signal; they have the same energy but the orbits do not superimpose precisely. To the left of the collector, but at a distance less than the average flight time during one cyclotron period, is a permeable shield. When the first electron enters the shield, it induces a charge on the collector and when it strikes it is, of course, abruptly removed from the process. The second electron still has one more loop to go, and as a result, the influence of these electrons spreads over the cyclotron period. This sets the upper frequency limit at the cyclotron frequency.

This limit, however, is not implicit in the properties of the beam before collection, but is rather a quantization effect that arises from collecting electrons while they are in cycloidal motion. If, in fact, the electrons could be guided without dispersion from a high field drift region to a zero field collection region, the effect would not exist at all.

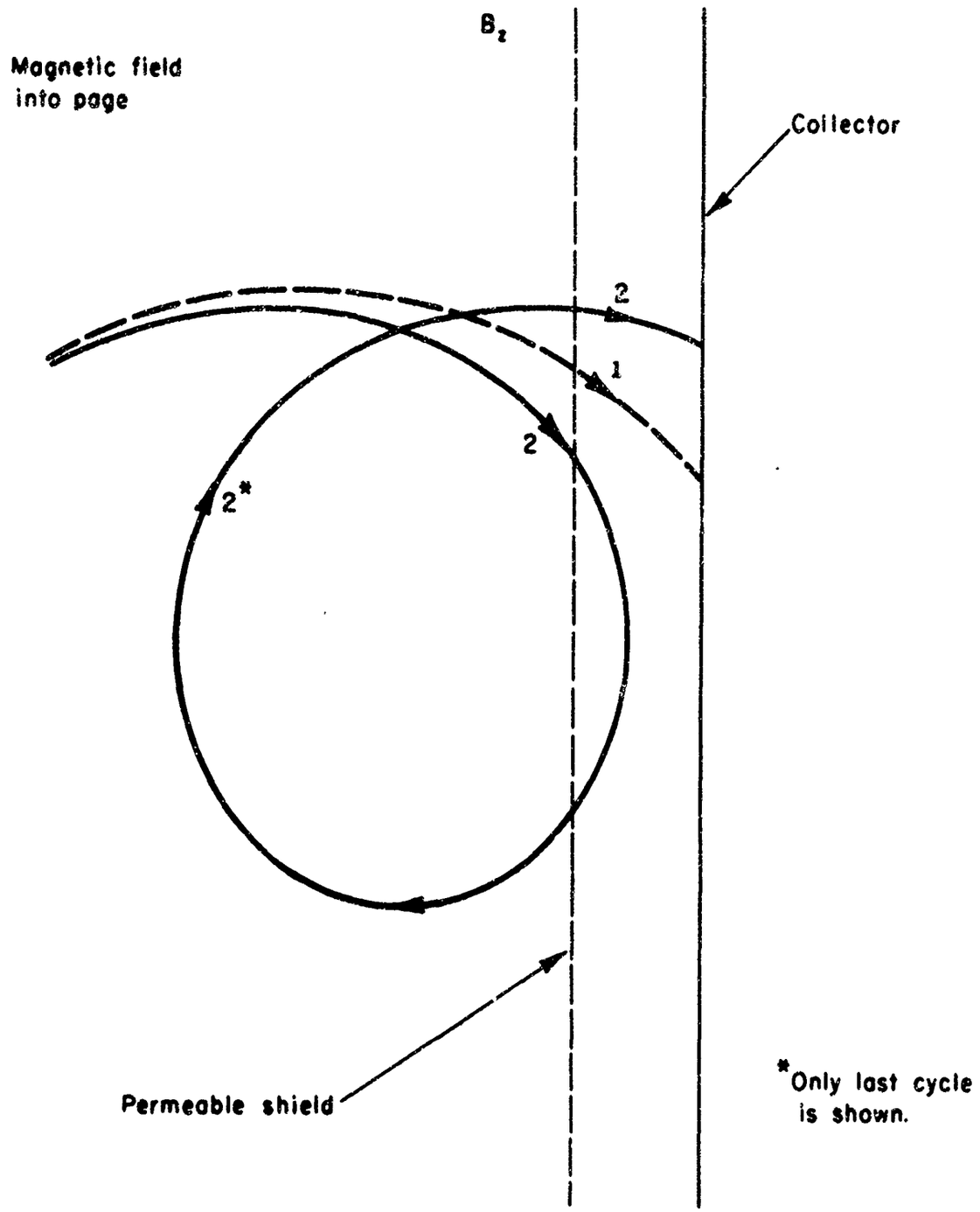

Figure 2.25

Time Uncertainty in Collection of Electrons

The difference between two orbits can be expressed in terms of small differences in the guiding centers. We have seen in our discussion of the launching of electrons from secondary emitters that the guiding centers for all electrons emerging from the same point can differ by as much as one radius. This difference is maintained as the particles traverse the drift space, and it sets an upper frequency limit far below the cyclotron frequency. Electrons from the same time samples could be collected over a time interval

$$\Delta\tau = R/v_d \tag{2.46}$$

or

$$\Delta\tau = v_r/\omega_c v_d \quad . \tag{2.47}$$

Since the cut-off frequency is

$$f_0 = 0.367(1/\Delta\tau) \tag{2.48}$$

from Eq. (2.47) we obtain

$$f_0 = (0.367)(\omega_c v_d)/v_r \tag{2.49}$$

Just as two electrons that begin at one point may have different guiding centers, two electrons with the same guiding center may be collected at different times. Ignoring phase differences which cannot contribute more than one cyclotron period of spread, the time differences arise from energy differences among the electrons. The time spread is actually proportional to the difference between the maximum and minimum radii rather than between the maximum and minimum energy. If we assume for the moment that the minimum radius is zero, the frequency limits are shown by Figure 2.26

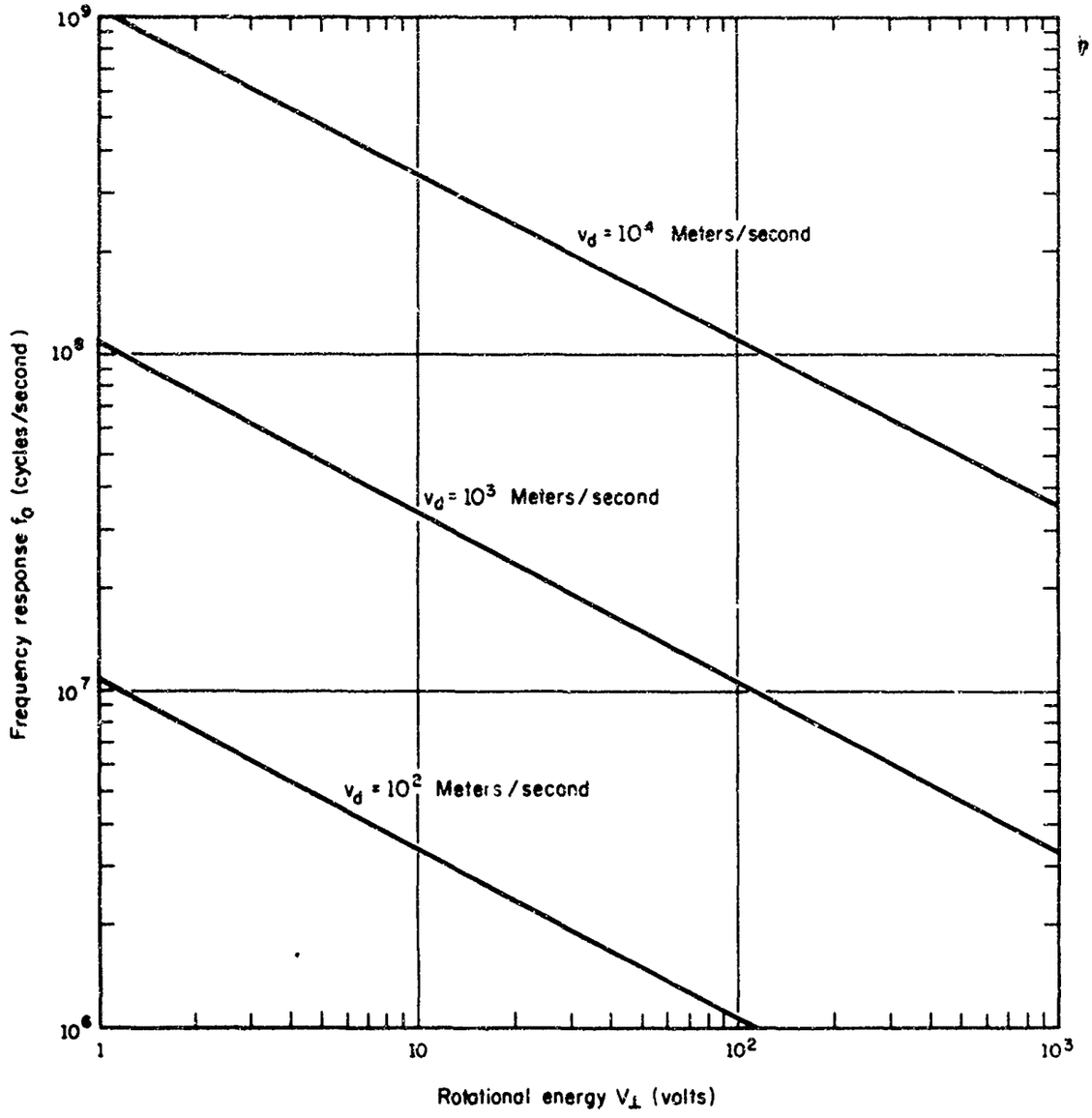

Figure 2.26

Effect of Spread in Guiding Centers on Frequency Response

These two effects – energy spread and guiding center spread – are introduced in the beam launching process, and although they are carried along by the beam, they are not magnified. This suggests that in a delay line where these limitations cannot be tolerated the solution here, as before, may lie in the generation and collection of high energy electrons in fast drift regions that are separated by a slow drift region. It is interesting to note in this connection that it is the absolute difference in radii that causes the effective dispersion when there is an energy difference. For a given energy spread the absolute spread in radius is inversely proportional to the square root of the energy. Thus the use, for example, of 10,000 volt electrons as compared to one volt electrons should, in this respect, offer an improvement of a factor of 100.

CHAPTER III

THE PLASMA DELAY LINE

In Chapter II we considered several ways of diminishing the influence of the electronic space charge. Only one of these, the use of hyperboloidal electrodes, actually compensates for the space charge in the sense that the resulting transverse electric field is the correct one over the entire beam aperture. A fourth technique which also compensates in this sense is the use of positive ions to neutralize the electronic space charge.

There are some difficulties in implementing this technique. Containment of particles may prove difficult, and collisions can degrade bandwidth. On the other hand, the potential advantages are considerable. Beam launching is simple and effective, the natural structures are rectangular, the attainable current is not charge limited, as it is in the circular structure, and theory indicates that the beam is stable. In addition the total charge can vary along the tube without destroying the compensation.

In magnetically focused recti-linear beams ions increase the maximum perveance [16,17], and they decrease the spreading of unfocused beams [18]. These effects depend on the presence of ions which accumulate over a period of time and which are trapped in the beam. In effect large numbers of electrons are neutralized by a much smaller number of essentially stationary ions. In crossed fields, however, the ions are not stationary, but instead drift with the electrons. The cyclotron frequency for ions is smaller than for electrons, the sense

of the rotation is opposite, and the radii may be larger; but the drift velocity is the same. As new electrons enter the drifting beam, therefore, new ions must be continually created. The drifting particles therefore form a plasma, and we have called devices based on this principle plasma delay lines.

3.1 Description

Figure 3.1 shows a mechanism in which the drifting electrons and ions arise in equal numbers from the ionization of the background gas by electrons in a primary beam. The primary electrons originate at a thermionic cathode and accelerate as they pass through a control grid to the slit anode from which they emerge into the drift space with energies of several hundred electron volts. Most of the electrons traverse the drift space without collision and strike the auxiliary collector above the field terminations. Some of the electrons ionize atoms of the background gas, but even after collision these primary electrons still have enough energy to reach the auxiliary collector. The ejected electrons emerge from the atoms with energies of a few volts, and together with the ions drift toward the collector. Because the magnetic focusing confines the primary electrons to a very thin sheet, the effective launching width is no greater than the slit width, and if the filament is narrow, it may be still smaller.

The ions and electrons drift toward the collector region along cycloidal paths, as shown in Figure 3.1. This drawing is, of course, not properly scaled. If the particles were equally energetic the ratio of the orbit radii would be equal to the mass ratio, which even for

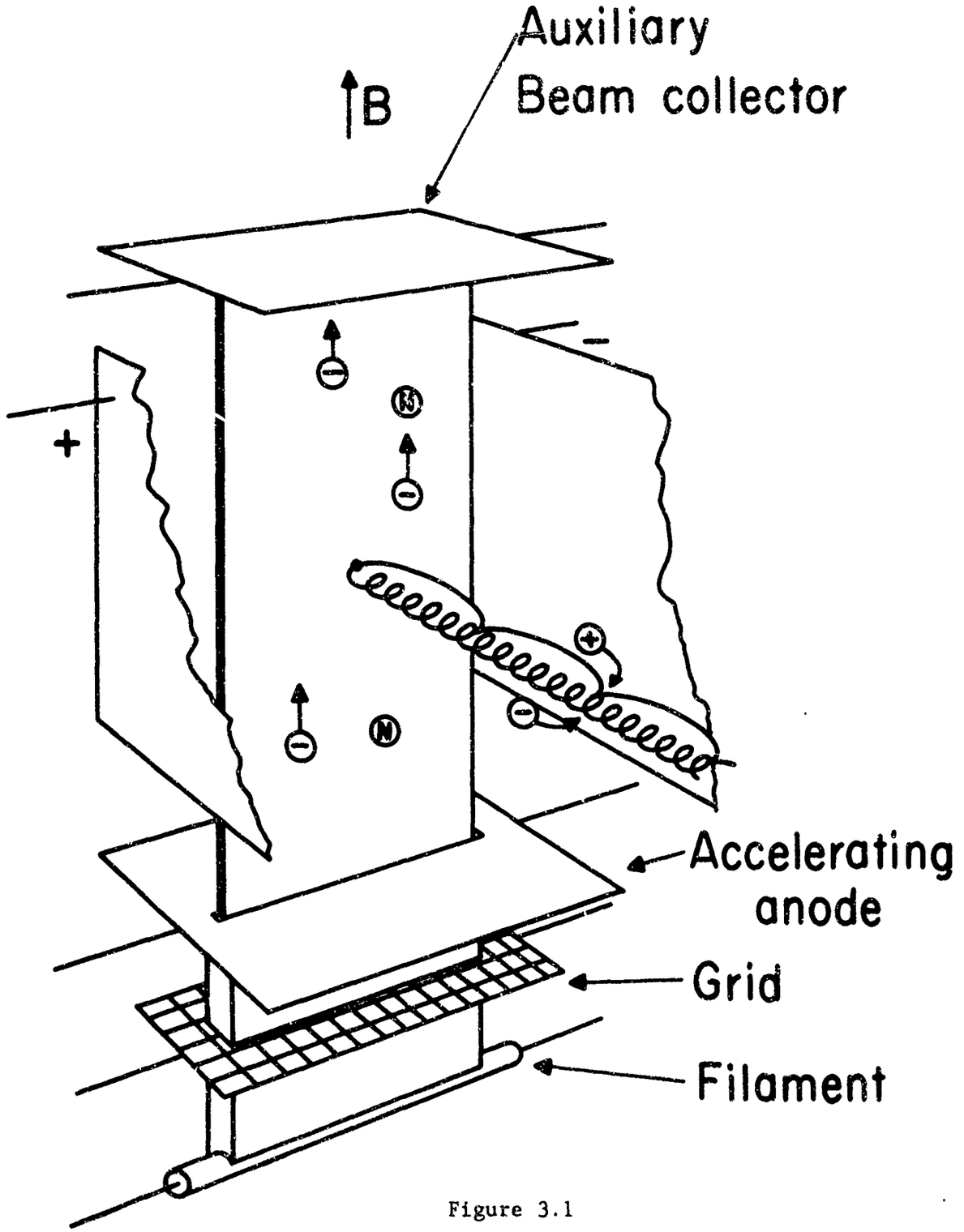

Figure 3.1

Launching of Charged Particles in the Plasma Delay Line

hydrogen ions is 1836:1. Actually, because the electrons are more energetic than the ions this ratio is considerably less, but is still in the neighborhood of several hundred. At the collector these particles pass through field terminating strips, and they are then separated by an electric field, which is parallel to the magnetic field, and collected, as shown in Figure 3.2.

Although there are no external constraints along the magnetic field to keep charged particles in the device, the electrons are in fact restrained by the focusing force of the positive ions. Of course, the ions themselves will ultimately stream to the walls and they will carry the electrons with them, but their inertia inhibits this process. In the following sections we discuss some of the properties of this device. We consider the criteria for choosing a gas, and we examine the effects of diffusion on frequency response of the device.

3.2 Confinement

The background gas in the plasma delay line is in thermal equilibrium at some tempterature which we assume to be about $290^{\circ}K$ (or about 0.025 e.V.). If we average over the transverse and the perpendicular velocity components, we find that the velocity distribution in the direction of the magnetic field is

$$f(v_z) = (M/2\pi kT)^{1/2} e^{-Mv_z^2/2kT} \qquad (3.1)$$

where M = the ion mass

$k = 1.3804 \times 10^{-23}$ joule/$^{\circ}K$, the Boltzmann constant

and T = the temperature in degrees Kelvin.

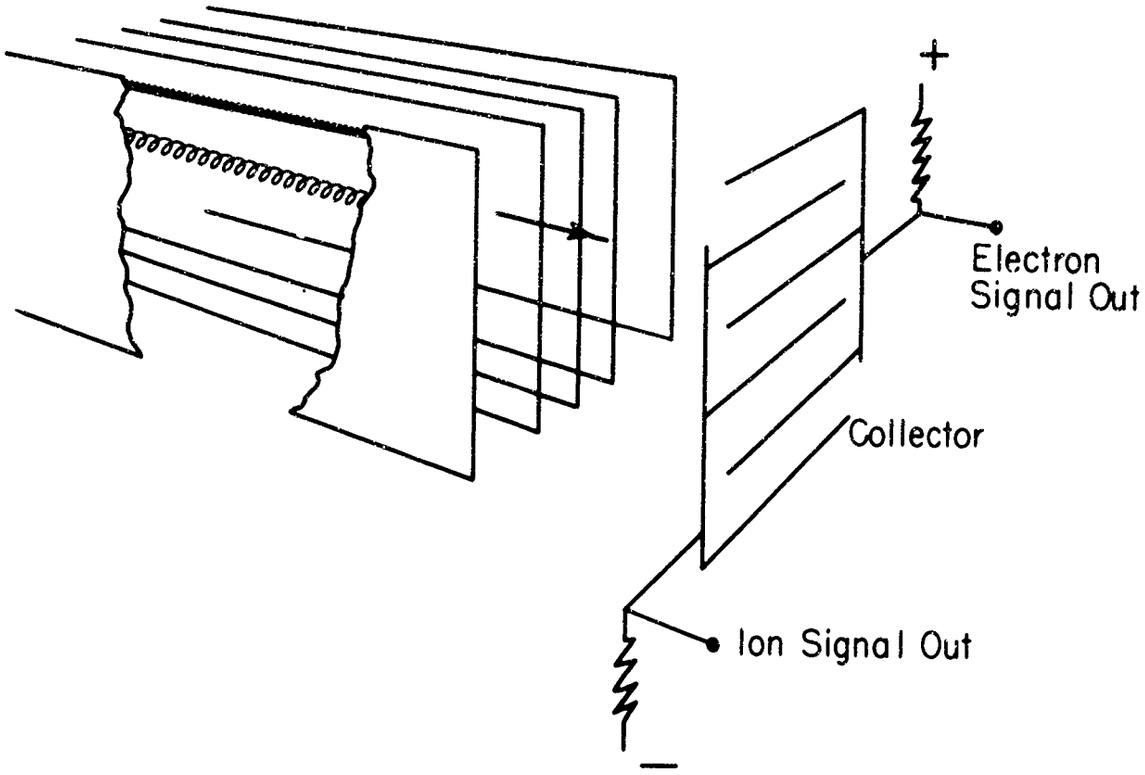

Figure 3.2

Collection Region in the Plasma Delay Line

This is a Gaussian distribution with zero mean, and a standard deviation

$$\bar{v}_z = \sqrt{kT/M} \ , \tag{3.2}$$

or in electron volts

$$\bar{V}_z = \sqrt{eV/M} \ . \tag{3.3}$$

The newly created ions have the same distribution, and since we assume that the space charge is neutralized, these ions simply stream out of the drift space along the magnetic field line. Independent of the initial charge of distribution, the ion population eventually assumes a Gaussian shape in space, and the central density falls as 1/t.

A characteristic time for confinement is the ratio of the aperture width w to the rms velocity $\bar{v}_z$,

$$t_c = w\bar{v}_z \ .$$

If the original charge density within the aperture is uniform in z, solutions of the Liouville equation show that at $t = t_c$, the normalized density has fallen to 0.68 in the center, and to 0.50 at the edges. At $t = 10t_c$ about 7 percent of the particles remain. For a one centimeter aperture we list t_c for several gases

	He	Ne	A	Hg
t_c(microseconds)	11.6	26.1	36.7	82.2

In calculating a characteristic confinement time we have in effect assumed that the electrons have a temperature of zero degrees Kelvin. This assumption does not seriously influence the result as long as the potential well created by the ions is great enough to restrain the electrons from escaping. As the density drops, however, the point is even-

tually reached where this is no longer true. This occurs at a charge density of about 10^{-6} coul/m^3 and corresponds to a potential well of about one volt. The drifting electrons that arise from the ionization process have energies of this magnitude and are therefore no longer constrained by the ions. At still lower densities the depletion of charges proceeds much more rapidly, the process being essentially the same as the beam spreading described in Chapter II.

At sufficiently high pressures the diffusion of particles along the magnetic field lines is inhibited by collisions – the higher the pressure the smaller the loss. We shall see, however, that collisions not only degrade the frequency bandwidth but also cause particle losses in the direction of the electric field. We assume, therefore, that the mean free path for ion-neutral collisions is greater than the aperture, and that the limiting process of particle streaming is chiefly responsible for particle loss.

3.3 Choice of Gas

From confinement considerations it would appear that a heavy gas such as mercury should be used in the delay line. This choice seems particularly good because the ionization efficiency is high. Nevertheless, the character of the ion orbit makes a heavy ion completely unsuitable, at least for a wide aperture beam.

The ions start their trajectories with the velocities, at the time of ionization, of the parent atoms. For heavy ions these are small compared to the drift velocities and as a result the orbits are almost simple cycloids. The Larmor radius is then

$$R = EM/eB^2 \qquad (3.4)$$

where e is the electronic charge.

Figure 3.3 shows the variation of the Larmor radius as a function of the electric fields for several ion species. For mercury we see that, for not unreasonably large electric fields, the ion will strike the end plate before it has completed one complete cycle. Even if the ion radius is smaller than the aperture it is clear that ions whose guiding centers are within one radius of the positive plate will be collected. We assume that the excess electrons, unrestrained by the attractive force of the ions, leave the drift space under the combined action of their own space charge forces and their kinetic energy. Similarly at the negative plate the ion density will be less than in the center of the drift space and the electrons for this region will be forced out of the drift region. These considerations lead us to choose a lighter ion such as helium.

3.4 Transverse Effects

In the absence of collisions, charge particles drift along lines of equal potential and there is no transverse drift. Collisions, however, shift the particles from one equal potential line to another, generally in the direction of the electric force. If the motion of a particle before collision is a simple cycloid, the collision shifts the guiding center a distance that is between zero and the diameter of the Larmor circle. A reasonable estimate of the average shift is the Larmor radius. If the motion before collision is a prolate cycloid, the circle is, of course, larger. In this case, the particle moves

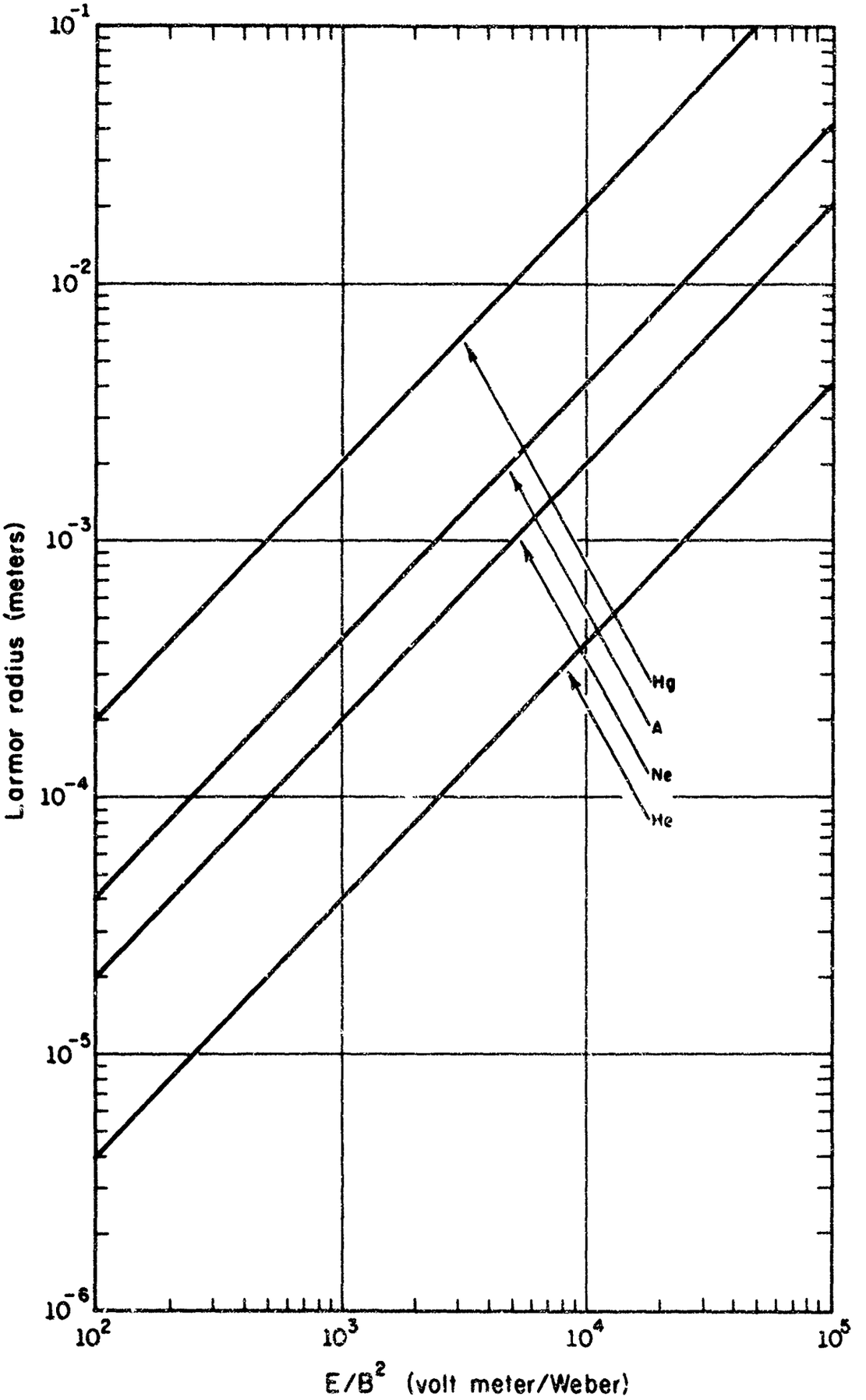

Figure 3.3

Dependence of Larmor Radius on Fields

during part of each cycle in the direction opposite to the E/B drift velocity, and collisions in this time interval shift the particles in the direction of negative electric force. Although the range of shift difference is now greater, the Larmor radius for the simple cycloid remains a good estimate for the average. The transverse drift velocity, v_t, is then the product of the radius, R, and the collision frequency, ν,

$$r_t = R\nu. \tag{3.5}$$

Since $R = EM/eB^2$, the drift velocity is therefore

$$v_t = \nu ME/(eB^2). \tag{3.6}$$

The expression for the drift agrees in the strong magnetic field case with that given by Allis [19].

As in the case of streaming the principle effect of the transverse drift on the performance of the plasma delay line is the reduction of current available at the collector. The removal of ions from parts of the beam aperture again leaves a surplus of electrons which no longer remain in the drift space. In helium the principle effect contributing to the high collision frequency is the phenomenon of charge transfer. In this process an ion which may have a high kinetic energy gives up an electron to a neutral atom at thermal energy. The kinetic energy is carried off by the old ion, now a neutral atom, and the new ion begins its cycloidal orbit at the point of collision. Its orbit center has advanced, on the average, a distance of one radius toward the negative plate.

Cramer and Simons have measured cross sections for both elas-

tic and charge transfer collisions, and for an energy of 4 volts they give 134.9 collisions/cm at a pressure of 1 Torr[20]. Although they provide no data below 4 volts, for making estimates we extrapolate their results to lower energies, and at one volt we obtain 150 collisions/cm. Of course, an ion in cycloidal motion varies its kinetic energy over a cycle. For comparison we note that a helium ion describing a simple cycloidal orbit with a drift velocity of 10^4 meters/sec varies its kinetic energy from zero to a maximum of 2.9 volts.

From Figure 3.3 we see that even a helium ion can traverse half the aperture after about 10 collisions. The mean free path λ_f for collisions should be as large as possible, but should at least be comparable to the distance travelled by the ion. For a cycloidal trajectory this is twice the transit distance. As an example, if the number of collisions per second is 150, the mean free path at a pressure p is $\lambda_f = 6.6 \times 10^{-5} p^{-1}$ meters. If we stipulate that $\lambda_f = 0.1$ meter, then at most the pressure should be 6.6×10^{-4} Torr.

In the direction of the drift velocity, collisions cause diffusion of particles which reduces the frequency bandwidth. For simplicity we consider a one dimensional problem in which at zero time a uniform particle density μ exists between $x = -b$ and $x = b$. The density outside this region is initially zero. The particles diffuse into this region with time and the central density decreases. The diffusion equation is

$$\frac{\partial \mu(x,t)}{\partial t} = D \frac{\partial^2 \mu(x,t)}{\partial x^2} \qquad (3.7)$$

where D is the diffusion coefficient. With the introduction of dimen-

sionless variables

$$U = \mu/\mu_0 \tag{3.8}$$

$$X = x/b \tag{3.9}$$

$$T = \frac{2D}{b^2}\, t \tag{3.10}$$

we obtain the dimensionless equation

$$\frac{\partial U}{\partial T} = \frac{1}{2}\,\frac{\partial^2 U}{\partial X^2} \tag{3.11}$$

which, for these initial conditions has the solution

$$U(X,T) = \int_1^1 \exp[-(X-X')^2/2T]dX' \ . \tag{3.12}$$

This is just the convolution of a rectangular pulse with a Gaussian curve whose variance is the dimensionless time. The integral can be evaluated and U(x,T) can be expressed explicitly as

$$U(X,T) = \frac{1}{2}\left[\mathrm{Erf}\,\frac{1+X}{\sqrt{2T}} + \mathrm{Erf}\,\frac{1-X}{\sqrt{2T}}\right]. \tag{3.13}$$

Although U is a function only of X and T, we note that T is actually determinated by both the diffusion coefficient D and the distance scale b as well as by the actual time t. Figure 3.4 shows the pulse shape for several values of $\sqrt{T}$.

We note that the relative distance over which the density changes by 90 percent is about

$$\Delta X = 3\sqrt{T}\ , \tag{3.14}$$

or substituting from Eq. (3.9) and Eq. (3.10)

$$\Delta x = 3\sqrt{2Dt}\ . \tag{3.15}$$

With the drift velocity v_d the corresponding rise time is

$$\Delta\tau = (3/v_d)\sqrt{2D} \tag{3.16}$$

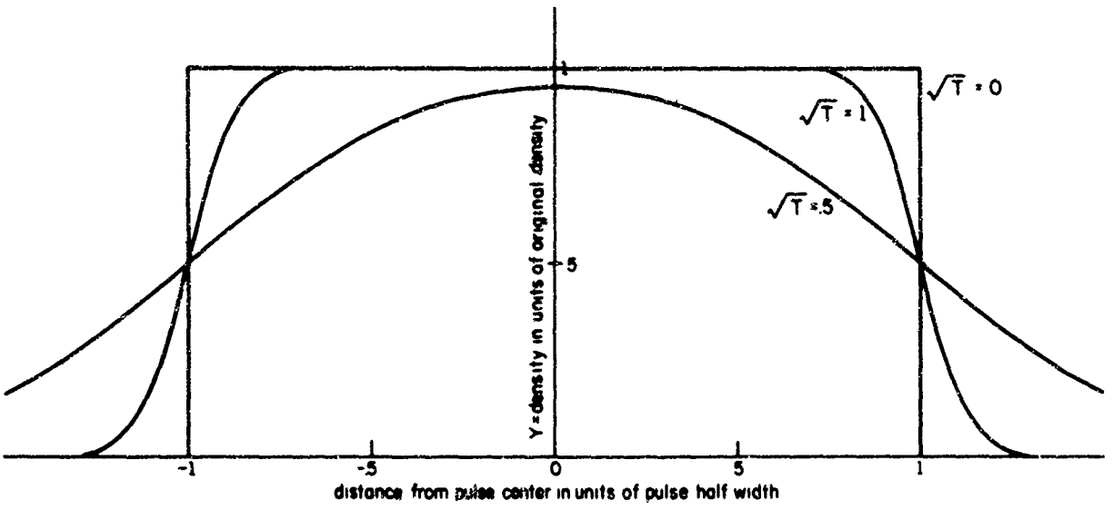

Figure 3.4

Pulse Shape as a Function of $\sqrt{T}$

where τ is the total time delay. Figure 3.5 plots diffusion coefficient against rise time.

When electrons control the diffusion the coefficient D is

$$D = \frac{2\lambda v_r/3}{1 + (\omega\lambda/v_r)^2} \tag{3.17}$$

where λ is the mean free path for electrons. When ions control the diffusion [21] the coefficient is

$$D_i = \frac{\lambda_i v_{ri}/3}{1 + (\omega_i \lambda_i/v_{ri})^2} \tag{3.18}$$

where λ_i is the mean free path for ions.

Using Eq. (3.16), Eq. (3.17), and Eq. (3.18) together with relations of λ and λ_i to pressure we can determine the influence of pressure on rise time. From data given by Brown [22] and from our extrapolation of Cramer and Simon's data, we obtain the mean free paths,

$$\lambda = 0.05p^{-1} \text{ cm.}$$

$$\lambda_i = (0.67 \times 10^{-2})\ p^{-1} \text{ cm.}$$

Figure 3.6 shows the relation between pressure and rise time for both electron and ion controlled diffusion when B = 1 weber/m^2, $v_d = 10^4$ m/sec, and τ = 10 microseconds.

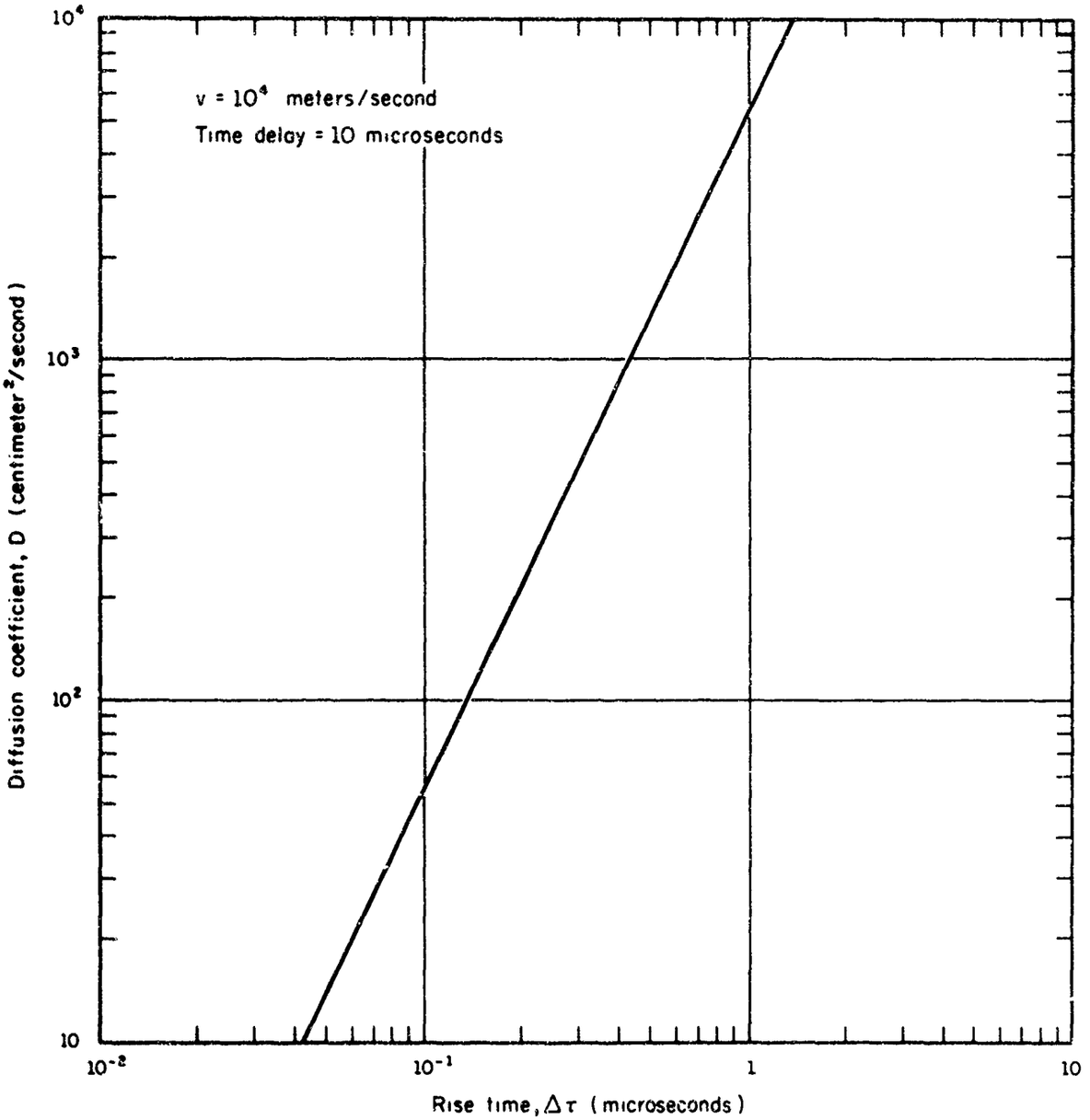

Figure 3.5

Diffusion Coefficient vs. Pulse Rise Time

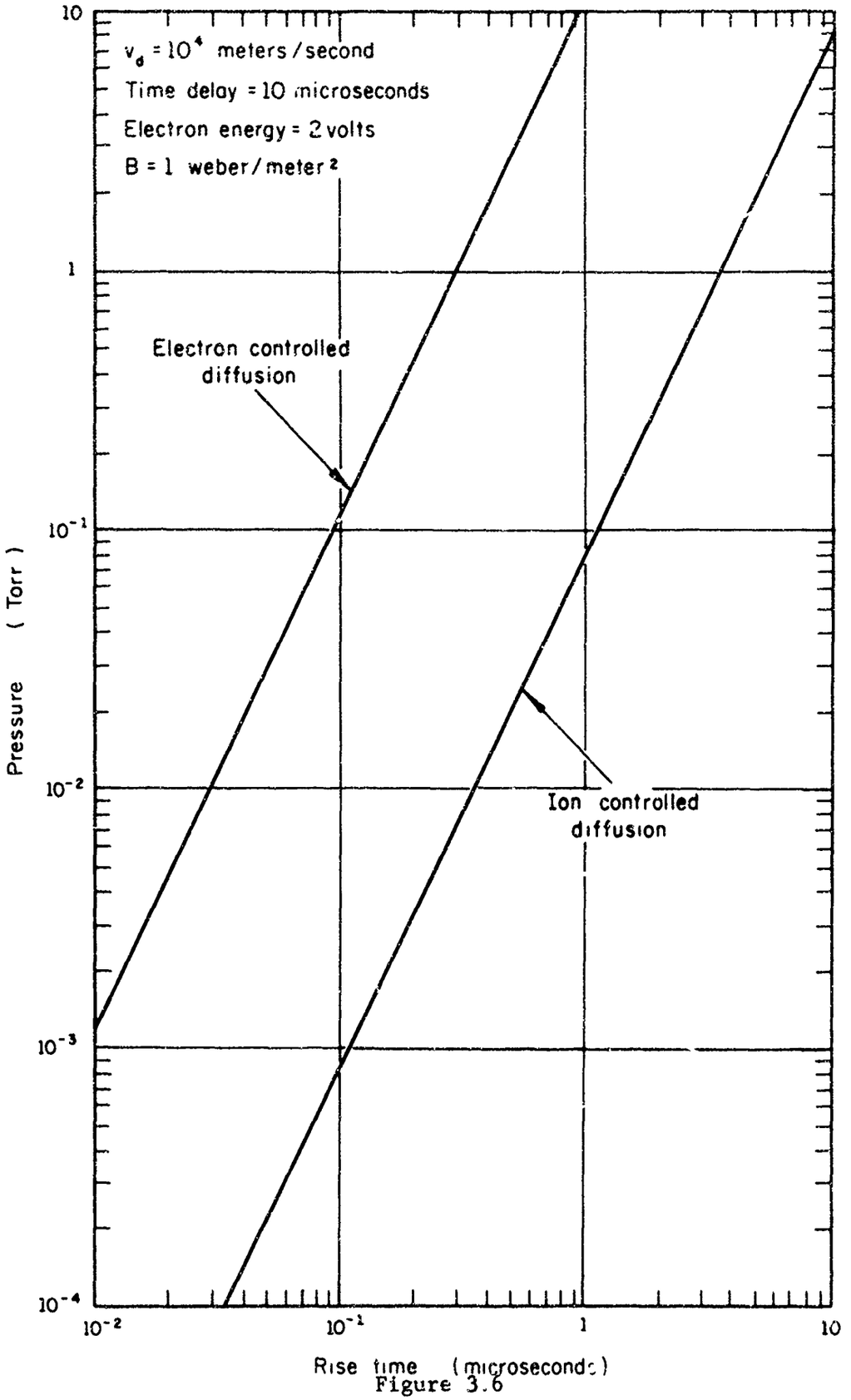

Figure 3.6

Pressure vs. Pulse Rise Time

CHAPTER IV

EXPERIMENTAL PROCEDURES

Because of its structural simplicity and its promise of high currents with little dispersion, the plasma realization of the delay line was chosen first for experimental investigation. Observations at high vacuum, however, disclosed that bursts of electron current could be produced by secondary emission and could be injected into the drift space. The electrons drifted through the tube at a velocity E/B and appeared at the collector in the form of sharp pulses. These observations stimulated interest in the properties of this structure as an electron delay line, and also indicated structural changes which would produce a more natural environment for the study of this effect. In the course of the investigation two additional experimental tubes were constructed, and measurements were made in both the electron mode and the plasma mode. In this chapter we describe these tubes, the circuit configurations in which they were tested, and the experimental procedures.

4.1 Experimental Tubes

The original tube, a realization of the structure indicated in Figure 3.1 and in Figure 3.2, is shown in the photograph of Figure 4.1 This tube couples to the external circuits through nine leads. Seven of these are brought through the glass press at the base of the tube. The remaining two connect to the beam collectors, and are brought through the sides of the glass. Figure 4.2 shows the tube, in perhaps better detail, before the glass envelope was attached to the

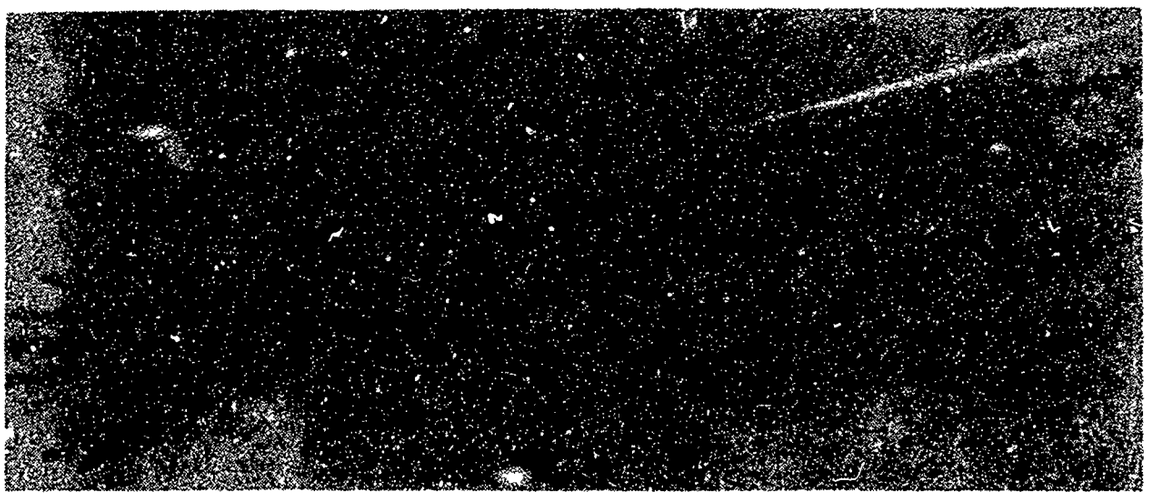

Figure 4.1

Tube I

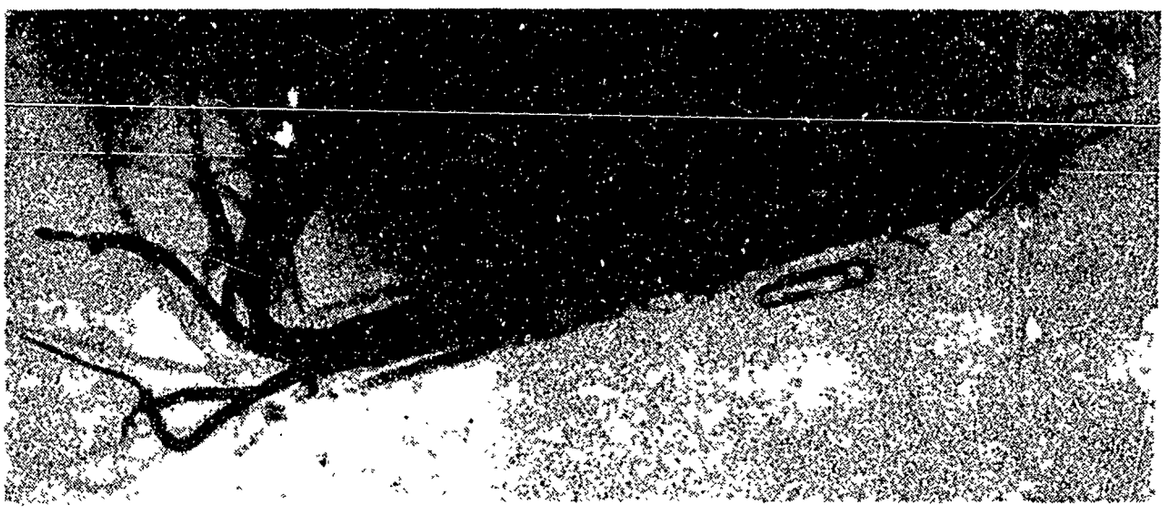

Figure 4.2

Tube I without Glass Envelope

press.

The drift section is actually a rectangular cage, bounded on two sides by the end plates, and on the ends and on the other two sides by eleven field terminating electrodes. The end plates are separated by a distance of one-half inch and a voltage V between the plates provides an electric field E = 78.7 V/m. A chain of twelve resistors, spot welded to tabs on the electrodes, maintains each electrode at the correct potential. The resistors (Texas Instruments' N60B) are spirally cut at the factory from carbon that has been deposited on a ceramic substrate, and they are compatible with a high vacuum environment.

Figure 4.3 shows the field terminating electrodes supported

Figure 4.3

Field Terminating Electrodes Partially Assembled

by part of the carbon jig used in their assembly. With the end plates in place the assembly is lowered on to molten glass strips which harden quickly to form the mechanical bonds for the structure. Figure 4.4

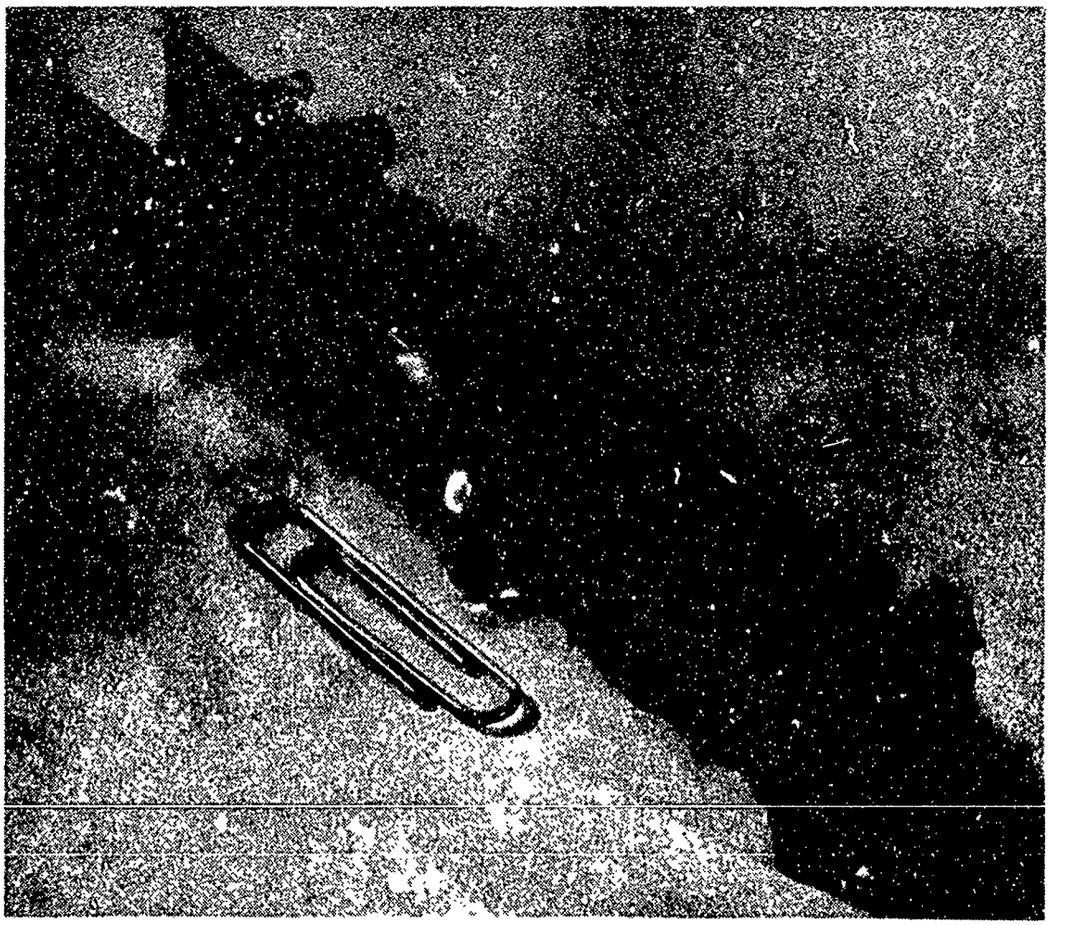

Figure 4.4
Assembled Cage

shows the assembled cage together with the auxiliary collector (top left) and the beam collector (front right). Except for their electrical tabs, which are cut in a pattern to provide space for the spot

welding electrodes, the field terminating electrodes are identical and are machined together.

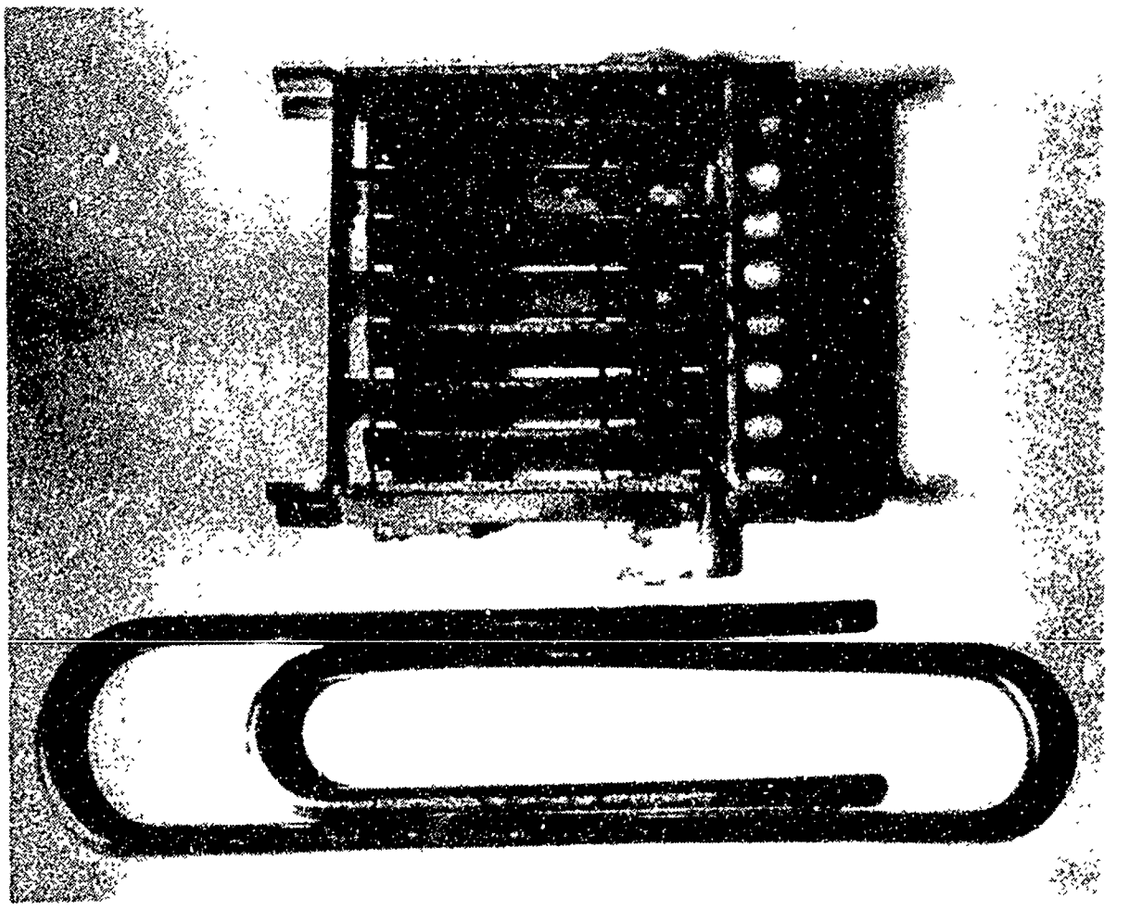

Figure 4.5

Beam Collector Assembly

Figure 4.5 shows the beam collector assembly. It consists of two electrically insulated sets of parallel plates brazed to metal supports. The two parts are glassed together and to the cage. The collector is 0.015 inch from the cage edge.

The triode electron gun is shown in Figure 4.6. A tungsten filament, 0.004 inch in diameter, is spot welded to two tungsten rods 0.03 inch in diameter. The rods are brazed to a ceramic block which is fastened by a single machine screw to a metal support. Reflected light from the slit anode shows the position of the slit with respect to the filament. The distance from the slit to the collector is approximately 3 inches.

It became clear in the course of experiments with this tube, which we shall call Tube I, that its dependence on external jigging and on glass bonds created two problems. It was difficult to make repairs and it was also difficult to make changes. For these reasons Tubes II and III were designed to be self-jigging, and the constructional principles made assembly and disassembly a straightforward process.

The basic structural technique is illustrated in Figure 4.7. The spacing between metallic pieces is maintained by cylindrical ceramic spacers cut on a lathe to appropriate lengths. A thinner ceramic tube fits through the ceramic spacers and through holes in the metallic members, and a threaded metal rod fits in the inner ceramic tube. The inner tube is cut so that its length is several thousandths of an inch less than the total length of the structures through which it fits. When these pieces are clamped together from the ends the whole structure becomes rigid, and the metal members are insulated from one another.

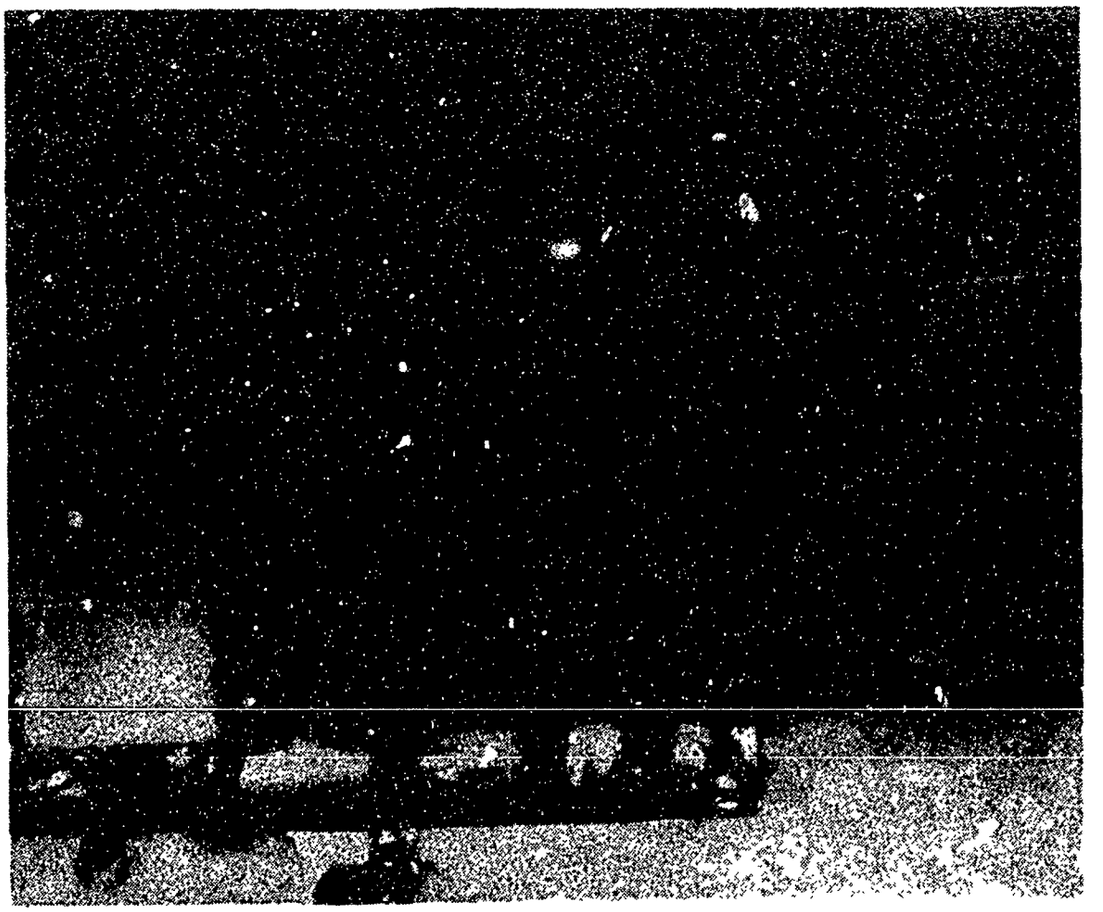

Figure 4.6

Triode Gun in Launching Region

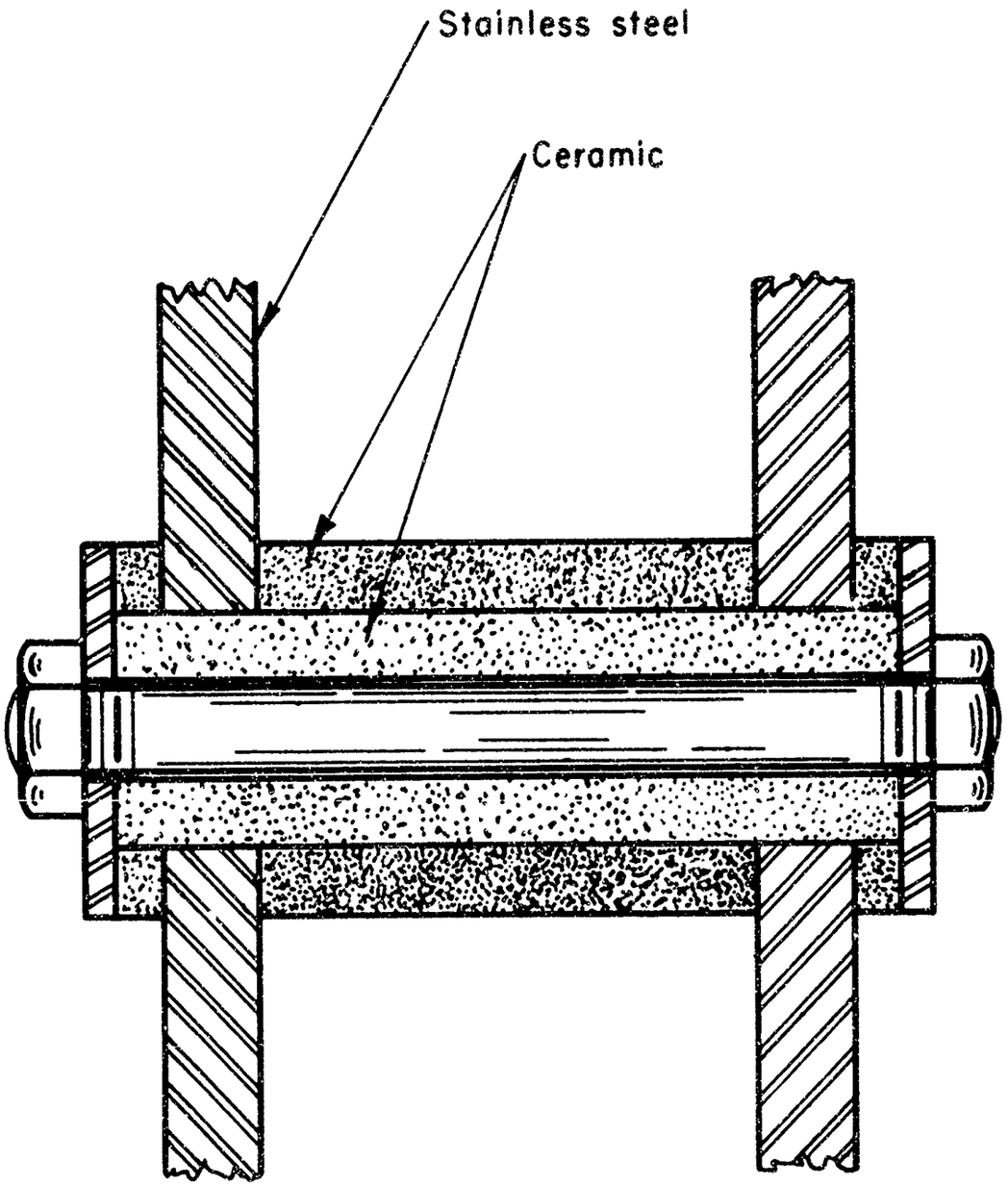

Figure 4.7

Structural Technique in Tube II and Tube III

The clamping is provided either by ordinary machine nuts which fit on the threaded ends of the rod, or by a specially made combination screw-clamp that is shown in Figure 4.8. This device has Allen heads at the

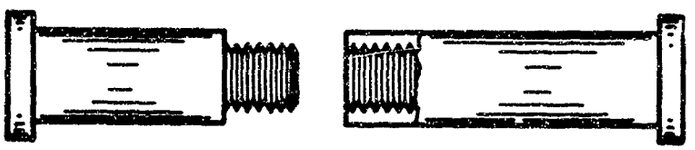

Figure 4.8

Screw Clamp Used in Assembly of Tube II and Tube III

end of each piece; the actual thickness of the clamping head can be made very small; and because it is tightened by an Allen head wrench it is easy to assemble.

A photograph of the tube, taken before it was enclosed in glass, is shown in Figure 4.9. Like Tube I it also has a triode gun section, visible at the left of the photograph. The filament is more than twice as long as in Tube I to provide more uniform heating of the filament within the aperture. The grid also differs from the grid in Tube I in that it was constructed from commercially available tungsten mesh whereas the grid in Tube I was wound by hand from tungsten wire. Figure 4.10 shows the gun and the launching region in more detail.

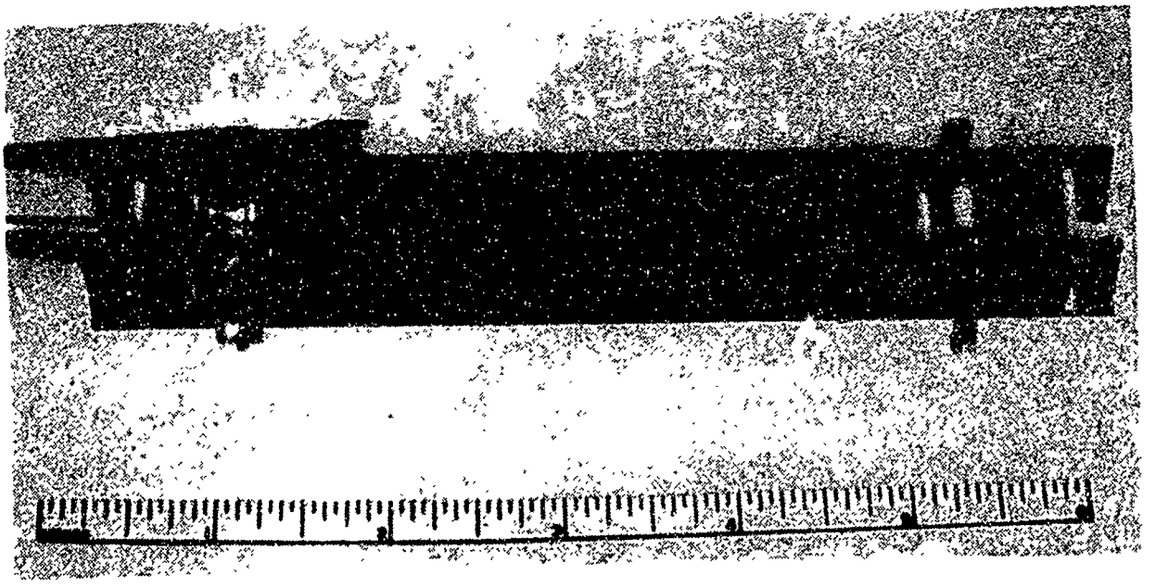

Figure 4.9

Tube II without Glass Envelope

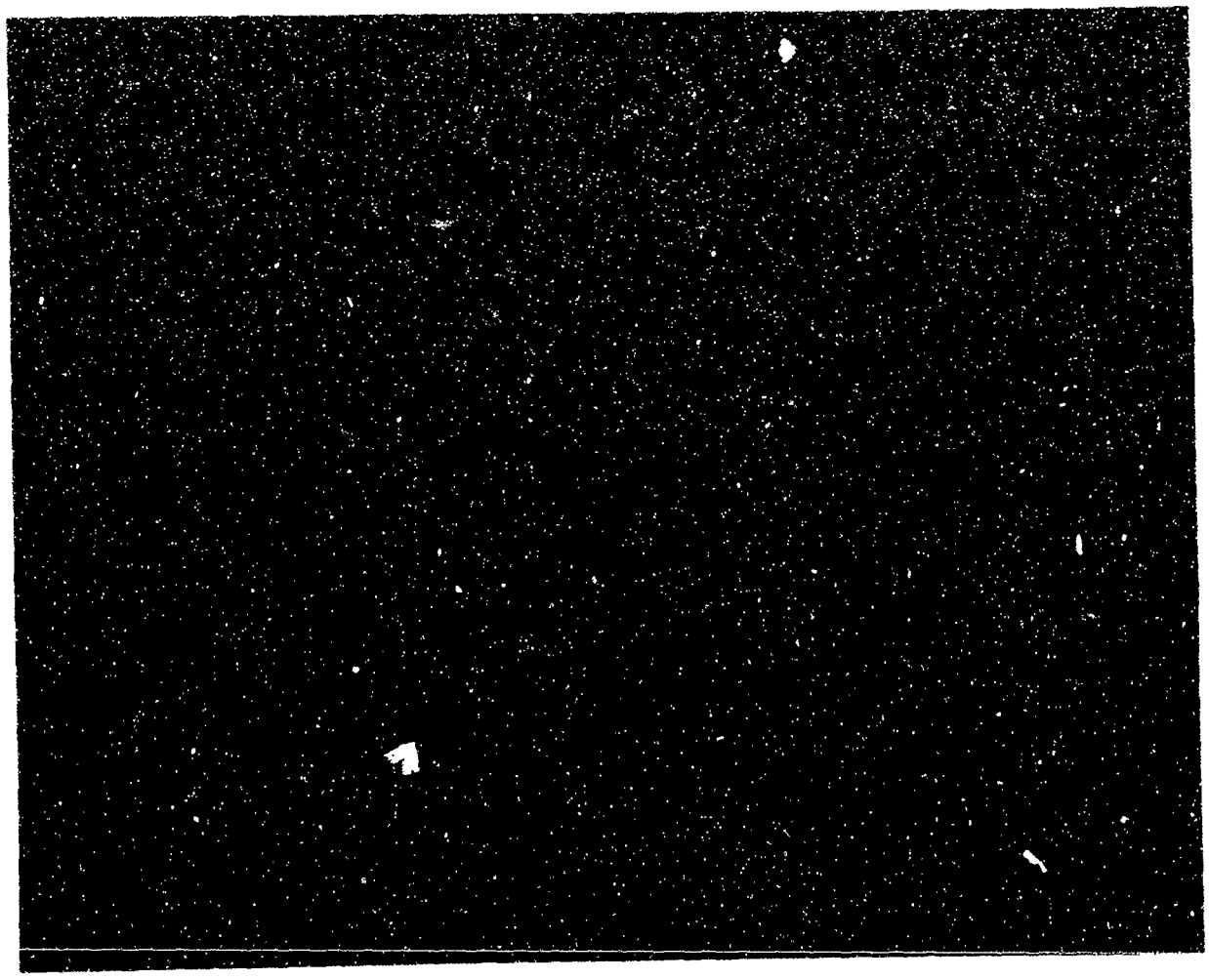

Figure 4.10

Launching Region in Tube II

Tube II differs from Tube I in several other respects as well. The field terminations are provided not by a set of resistors, but rather by a continuous winding of Nichrome V resistance wire which extends from one plate to the other. The diameter of the wire is 0.001 inch and the resistance is 681.9 ohms per foot. It is wound in 47 turns on ceramic spacers in which grooves have been cut by a lathe. The field distortion is thus confined to within about 0.01 inch from the winding. Figure 4.9 shows that Tube II actually has two end plates on either side of the drift space, one inside the other, and two field terminating windings, one for each set of plates. The two coils divide the aperture into a center section $(1.27 \times 0.318)\,cm^2$, and two outer sections $(1.27 \times 5.26)\,cm^2$. The plates on each side are insulated from one another and can therefore be set to different average potentials. Usually the voltage across each winding is the same, making the transverse electric field throughout the device the same also. The variation of the average voltage, from one coil to the other, provides focusing fields on either side of the central winding without changing the transverse electric field which controls the drift. Ideally the structure would look like the drawing of Figure 4.11 in which the only field distortion is produced by the discreteness of the termination. The actual structure, of course, does produce some additional distortion near the outer end plates.

This tube was designed primarily to test the cross field delay line when the beam is launched by secondary emission. The secondary emitter is a glass rod coated with a tin oxide resistance of 60,000 ohms. It is mounted on external supports visible on the end plate at the left

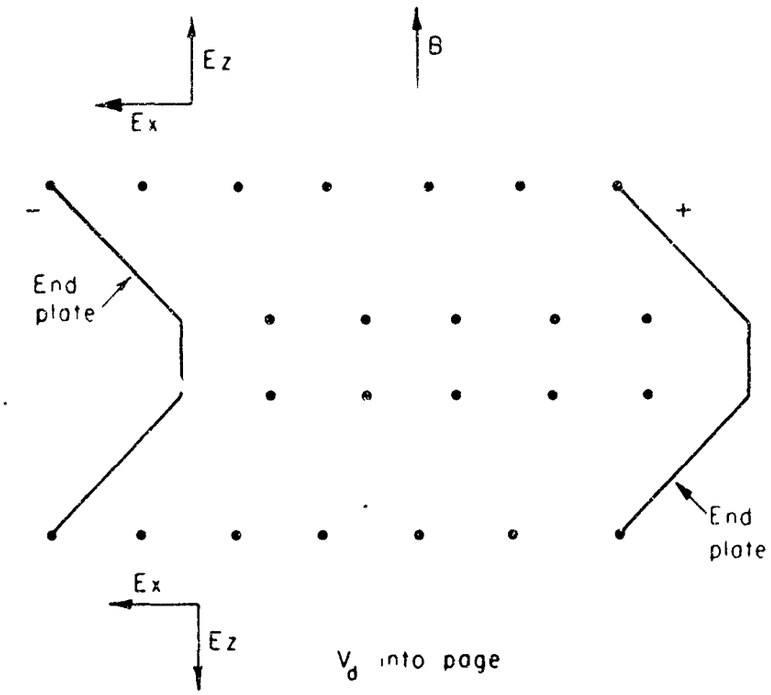

Figure 4.11

Electrode Configuration for Rectangular Delay Line

of Figure 4.9. A similar resistance rod is visible at the right of the figure and it is supported in the same manner. The second resistor is the electron collector and it is connected to leads which conduct the signals through the glass envelope to the external circuits. The voltage drop across each resistance is adjustable, and it is usually set to match the transverse electric field along the resistance to the transverse electric field provided by the external structure. In addition, the resistances are insulated from the main field structures to allow variation in the absolute potential along each resistance. These

resistance rods were replaced in later experiments by titanium oxide resistors that were made by evaporating titanium in vacuum on to thin strips of glass cut from microscope slide covers. Although these resistors oxidized to some extent as soon as they were exposed to air, the oxidation was enchanced by heating these resistors in a small furnace. The resistance was monitored until it rose to the required value.

The nichrome windings in Tube II expand slightly when they are hot. To avoid slackening of the wire the ceramic supports are spring-loaded. One set of springs for the outer winding is visible at the right of Figure 4.9. The spring for the inner winding is shown in Figure 4.12, which also shows the inner coil wound on the inner plates. The two copper rods protruding through the inner plates supported the structure during the winding process and they were removed after the outer plates were assembled.

The completed tube is shown in the photograph of Figure 4.13, which also shows the Bayard-Alpert ionization gauge that was used to monitor the pressure during the experiments.

Tube III, shown in schematic form in Figure 4.14, is built upon the same structural principles as Tube II, and uses the identical electron gun. Like Tube I, however, it is designed to operate in the plasma mode. It therefore has only two end plates and one nichrome winding connecting them, and it has no resistive secondary emitter in the launching region. Also, as in Tube I, the collector is outside the cage which encloses the drift region. The collectors are either metal strips (stainless steel) or thin titanium oxide resistors of the type used in Tube II. These strips are supported by two sets of shelves

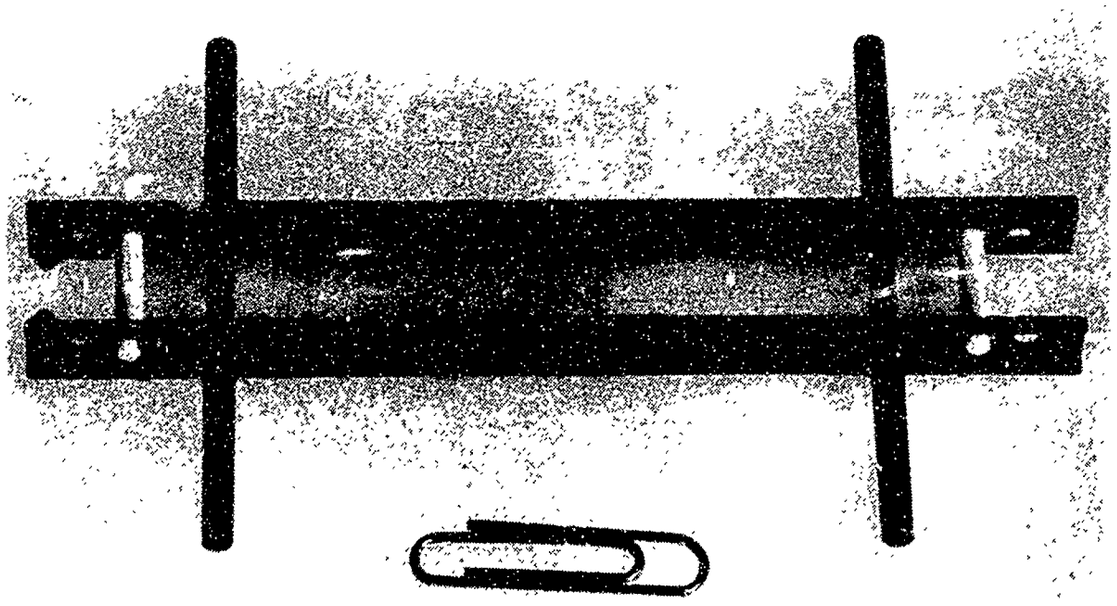

Figure 4.12

Tube II Inner Winding on Subassembly

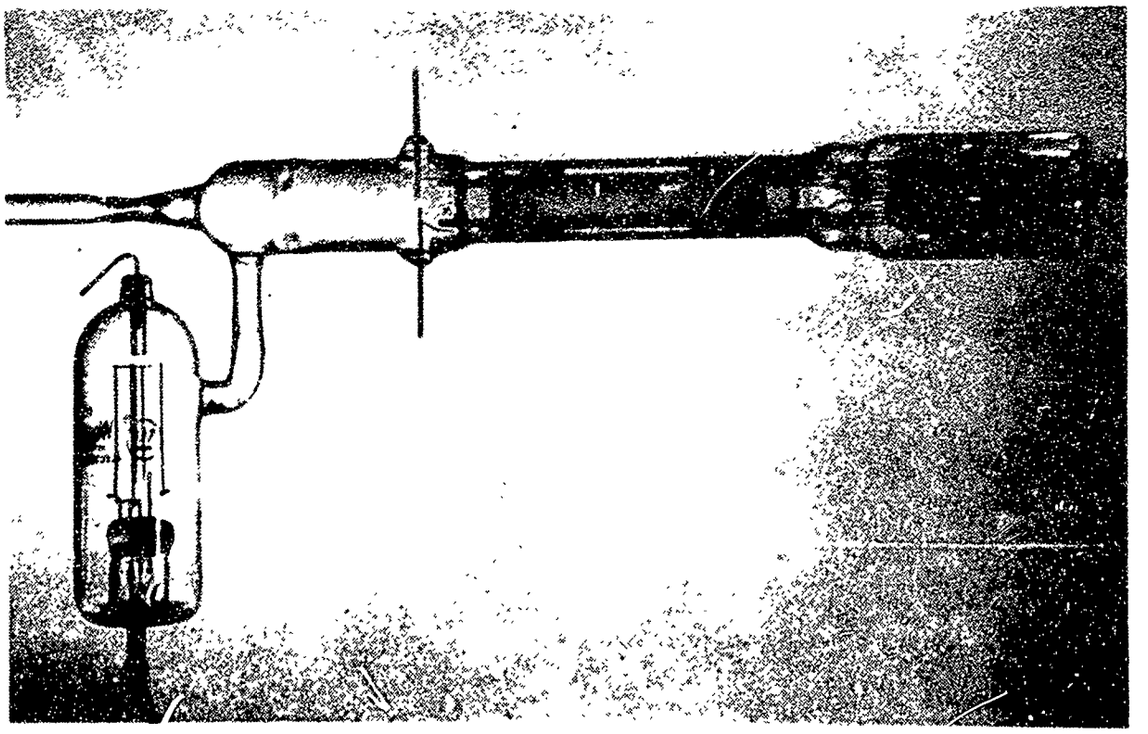

Figure 4.13

Tube II with Bayard-Alpert Pressure Gauge

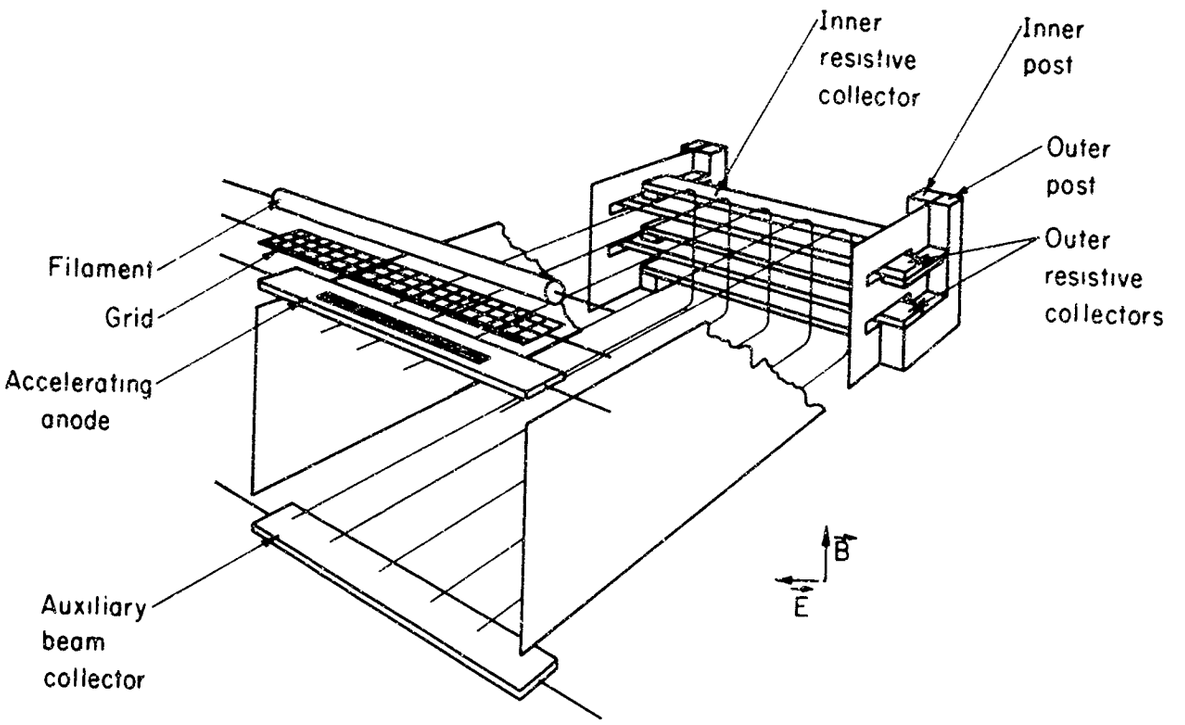

Figure 4.14

Schematic Drawing of Tube III

insulated from the end plates and from each other, as shown in Figure 4.14. The collector strip edges are fixed in place to within 0.02 inch of the cage end. When the resistance collectors are used the signals are conducted through four separate leads to the external circuits.

4.2 The Vacuum System

The vacuum system used in the experiments is shown schematically in Figure 4.15, and part of it is shown in the photograph of Figure 4.16. It had been constructed earlier to test metal vacuum components, and it is more complicated than necessary for the delay line experiments. The metal pipes could just as well be glass, and the second getter-ion pump together with valve no. 2 are superfluous. On the other hand, these parts do not give rise to any problems, and the system, usually operated with valve no. 1 open, and the ion pump no. 1 inactive, provides the necessary vacuum for the experiments.

The first measurements were made on Tube I after it had been filled with helium and sealed off at a pressure of about 0.1 Torr. It soon became apparent, however, that the observed effects were sensitive to pressure, and that the pressure should be a controllable parameter. The following procedure soon became standard.

With the tube connected to the vacuum system, the system was pumped through the cold trap by the fore pump to a pressure of about 10^{-3} Torr. The getter-ion pump was then turned on and after an outgassing period that was sometimes as long as fifteen minutes it suddenly took control of the evacuation process and the pressure dropped rapidly. When the pressure reached 10^{-5} Torr, valve no. 3 was

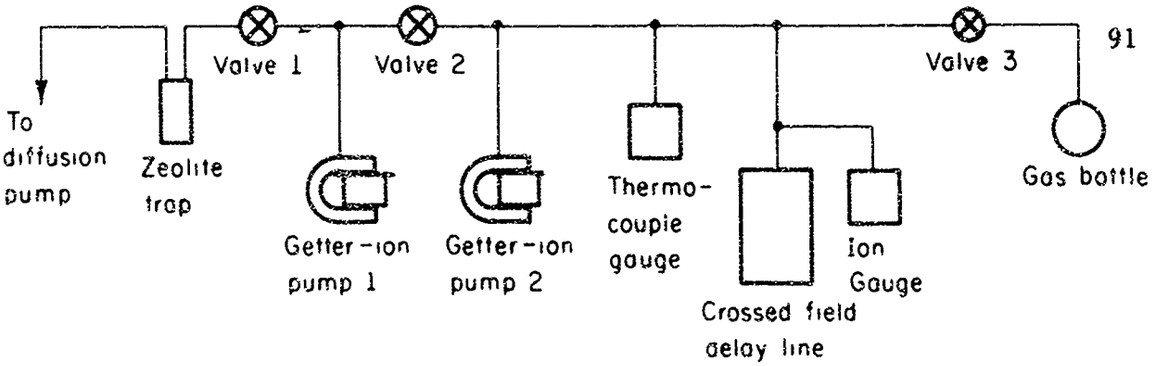

Figure 4.15

Schematic Drawing of Vacuum System

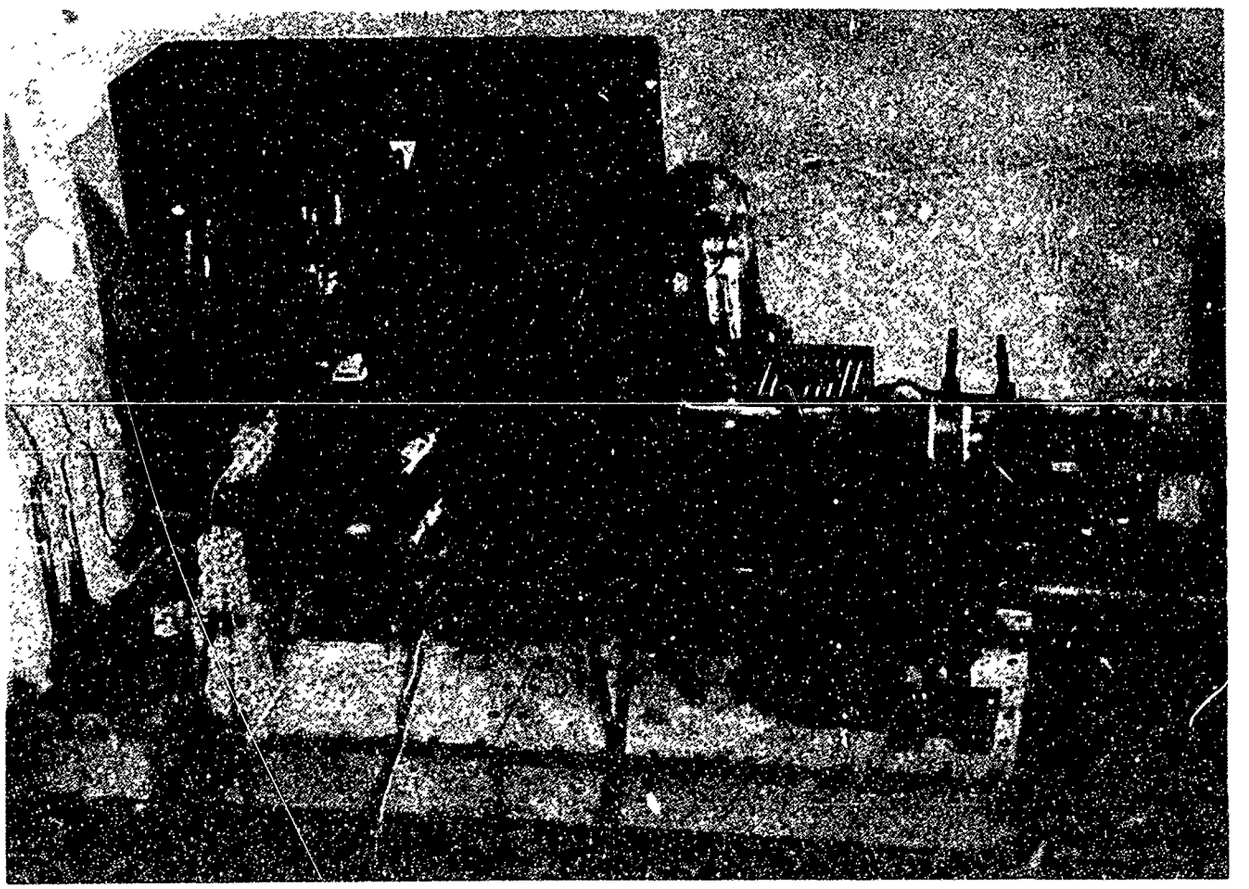

Figure 4.16

Tube III Mounted in Magnet and Connected to Vacuum System. Tube II on Support at Right.

closed, an ordinary heat lamp was used to heat the tube, and in this partially baked condition the system was allowed to pump about eight hours.

Next the filament was brought up to temperature and the ion gauge was outgassed by electron bombardment of the grids. After several hours a pressure in the middle to high 10^{-8} Torr region was usually obtained. The tube was then placed in position in the magnet and connected to the external circuits. The tube was aligned to allow the maximum current to flow through the slit anode to the auxiliary collector, and at the same time the tube was leveled in the magnet so that the magnetic field and the electric field were perpendicular. In the electron delay line mode the tube was then ready for measurement.

In the plasma mode, of course, it was necessary to reconnect the tube to the vacuum system. The above procedure was again followed until a low pressure was obtained. Valve no. 3 was then opened, allowing helium to flood the system and to raise the pressure to about one Torr. The helium was them pumped out by the fore pump and refilled with helium to the desired pressure. High pressures in the neighborhood of 10^{-2} Torr could be maintained simply by closing the valve on either side of the vacuum system containing the tube itself. Low pressures in the neighborhood of 10^{-4} to 10^{-3} Torr were maintained by allowing helium to leak slowly from the gas bottle through valve no. 3 into the system where it was removed by the ion-getter pump.

4.3 The Magnet

In operation the tube is suspended between the poles of an

electro-magnet. The diameter of each pole piece is five inches and the gap between the poles is 1 1/2 inches. This magnet was constructed a number of years ago for physics experiments and the gap was originally one inch. To provide more room for the tube new pole pieces of soft iron were machined to replace the original pole pieces. The two coils in the H frame were wound separately, and in the original application these coils, connected in series, were powered from a specially constructed power supply. This power supply was not available, and a commercial supply was used instead. To provide sufficiently high magnetic fields it was necessary to connect the two coils in parallel. Figure 4.17 shows the relation between the magnetic field at the center of the gap and the current through the coils. Figure 4.18 shows for two coil currents the variation of magnetic field strength as a function of the distance from the center of the gap. These measurements were made with a commercial moving coil Gauss meter (Type 720 R.C. Gaussmeter Probe).

4.4 Circuits and Procedures

Figure 4.19 shows in schematic form the connections from Tube I to the external equipment. For clarity the field terminations have been omitted from the drawing, and the space between the collectors and the cage has been increased. The arrangement for Tube II is similar except that the dual electric field structure and the resistive emitter each require an additional balanced voltage source, and the resistive collector requires a balanced output circuit. Figure 4.20 shows these features. Tube III, when fitted with stainless steel collector strips, is a variant of Tube I and it operates in the circuit shown in Figure 4.19.

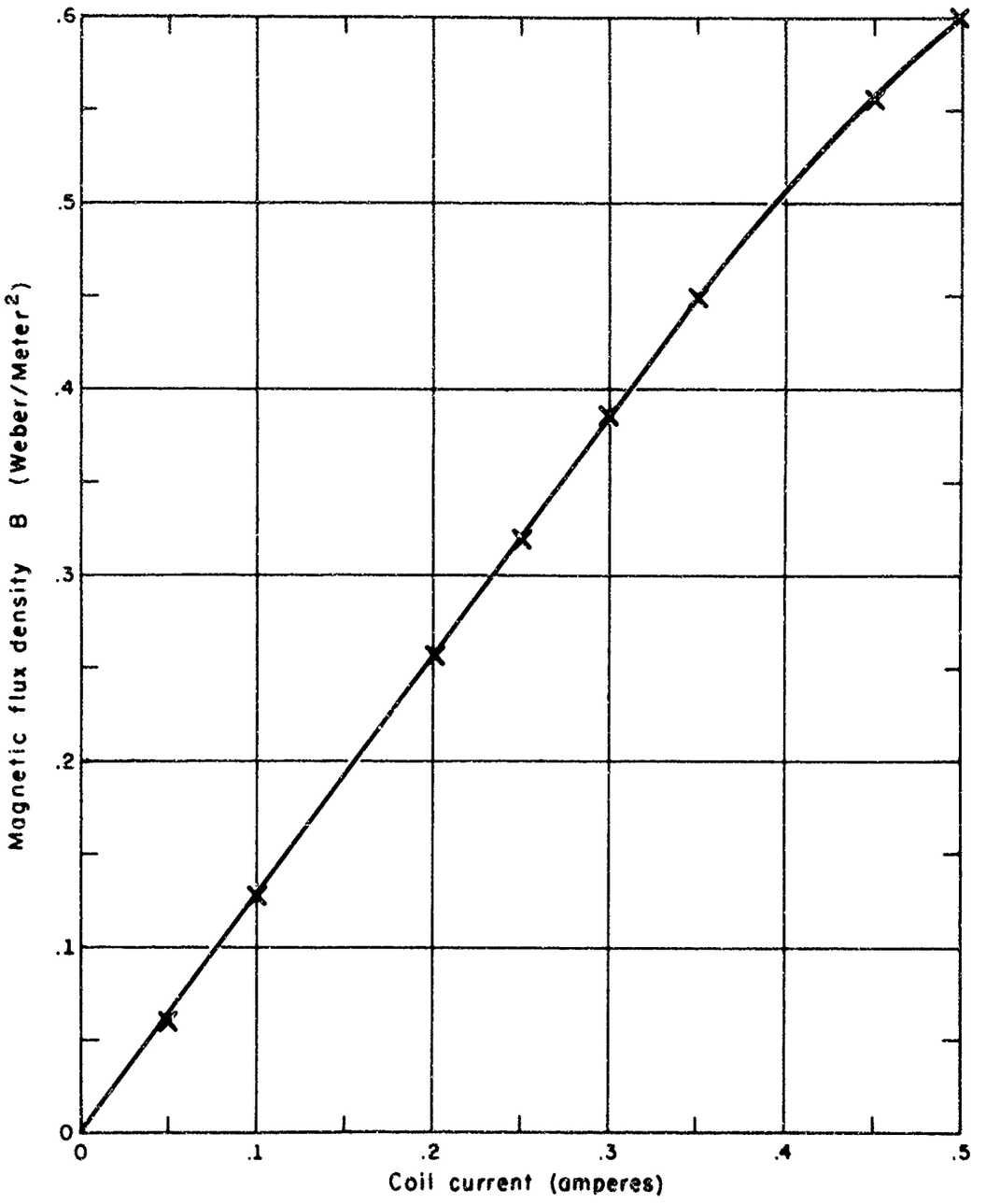

Figure 4.17

Dependence of Magnetic Field Strength on Coil Current

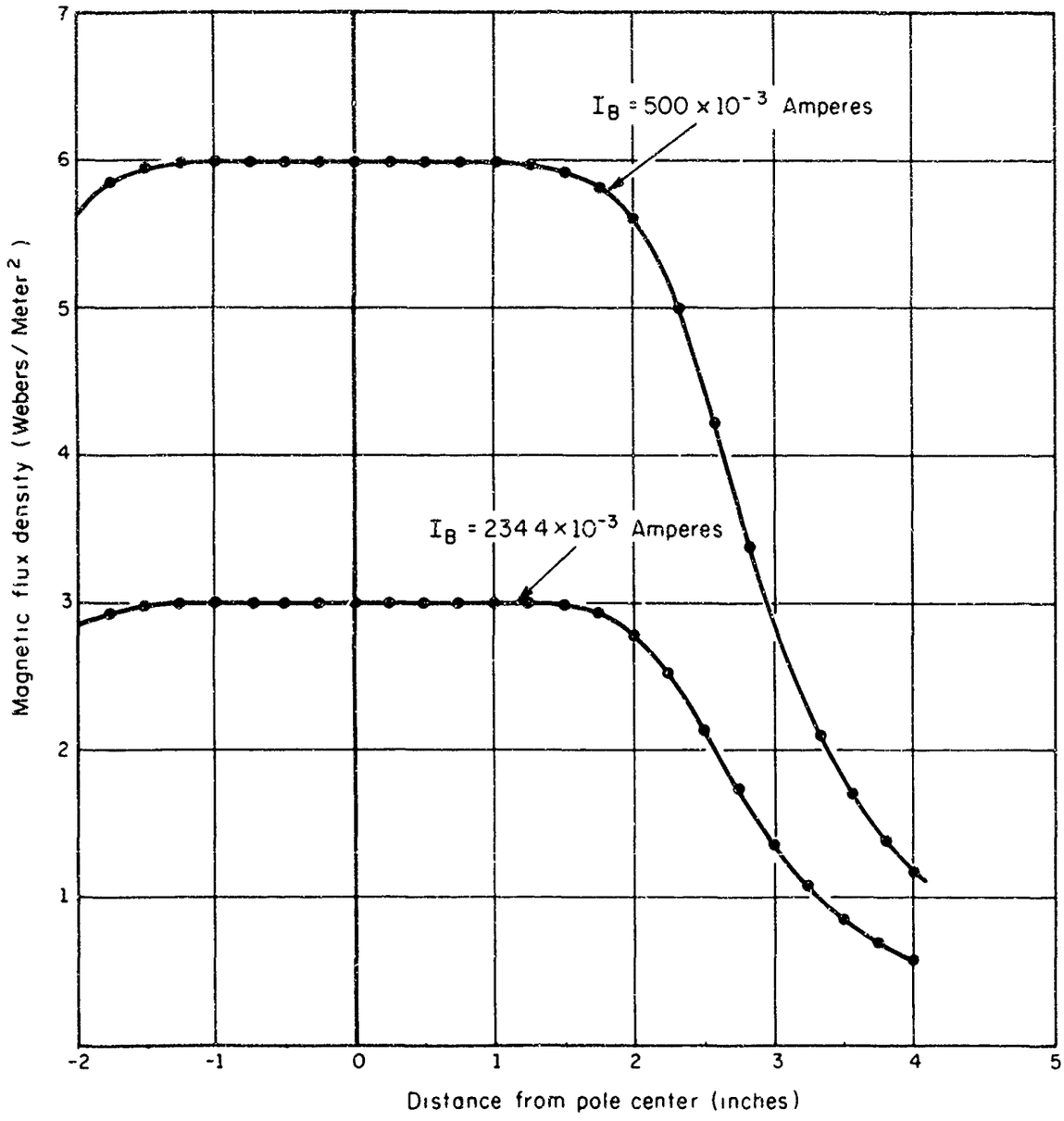

Figure 4.18

Magnetic Field Strength in the Air Gap

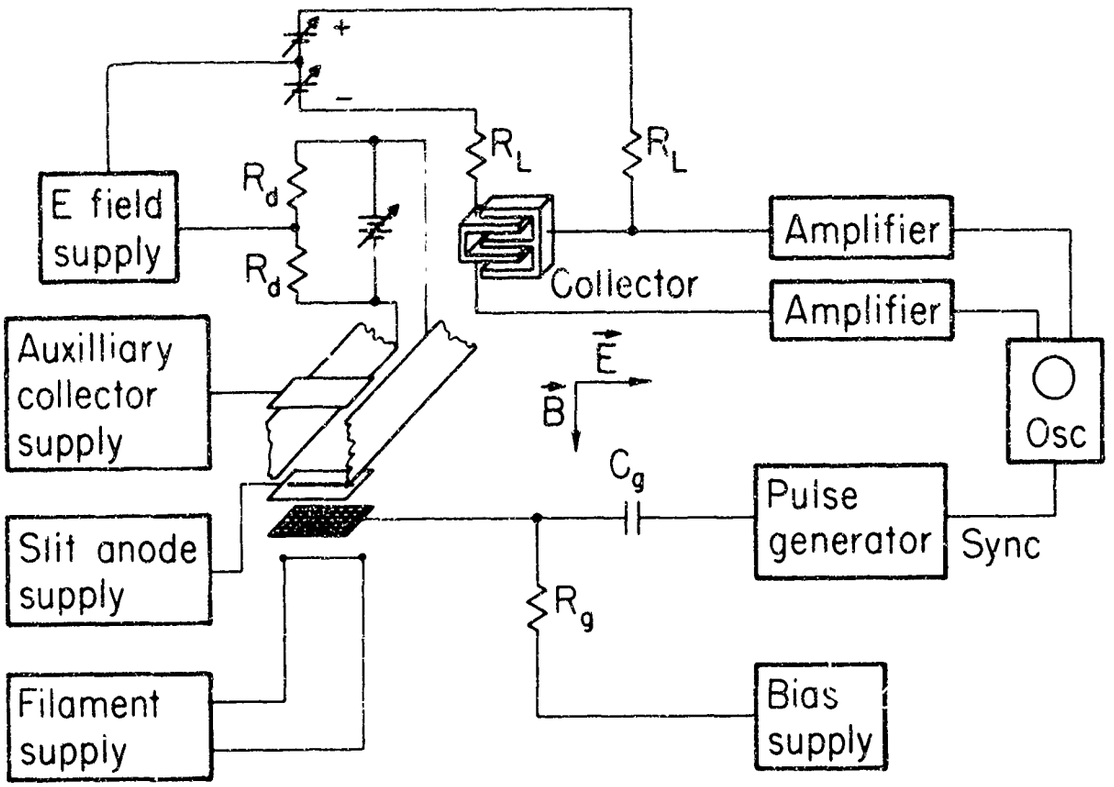

Figure 4.19

Schematic Drawing of Circuit for Tube I

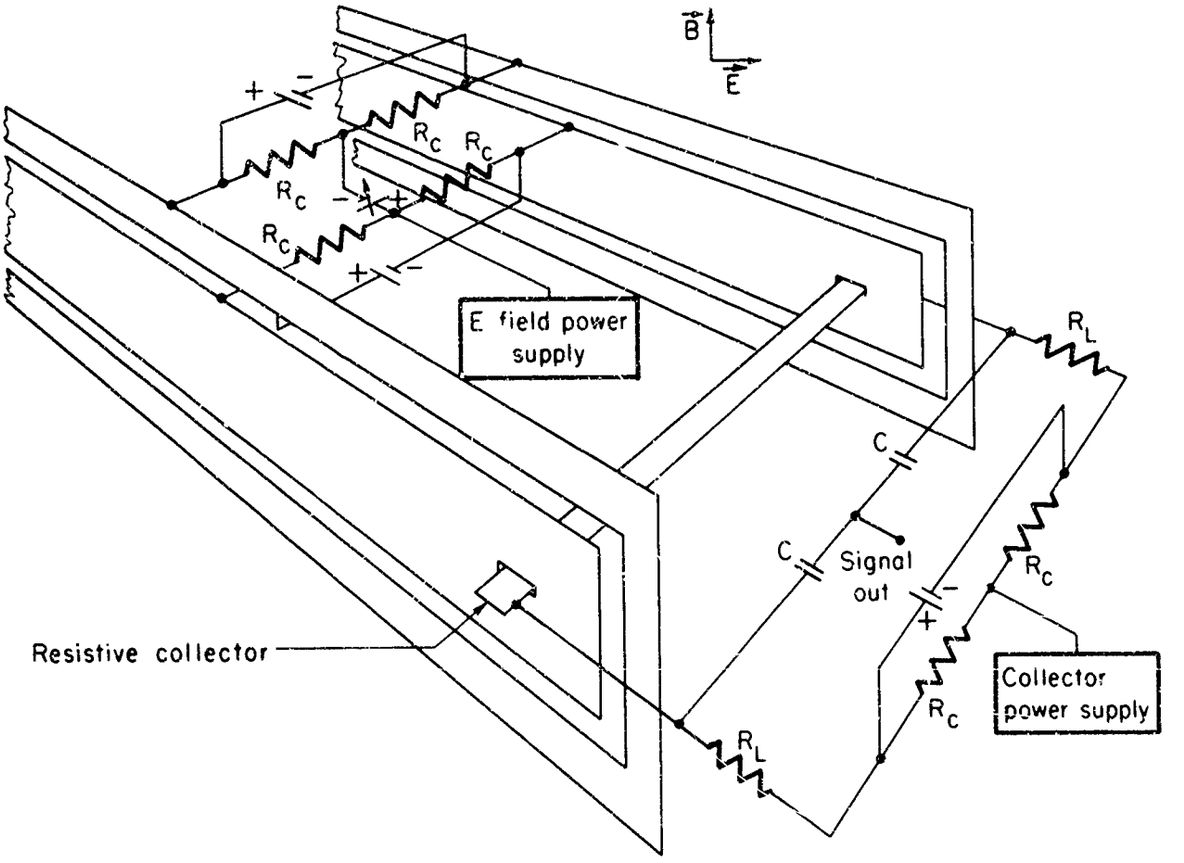

Figure 4.20

Output Circuit for Tube II

When fitted with resistive collectors, however, it requires two sets of balanced output circuits of the kind used in Tube II. These are shown schematically in Figure 4.21.

This output circuit, although simple, is unconventional. It must approximately match the transverse electric field in the output region, and must be capable of coupling signals to the detection apparatus. If the distribution of collection current is symmetrical in the aperture, the signal appears, with the same amplitude and polarity, at each end of the collection resistor. Although the center voltage is depressed slightly with respect to the voltage at the ends, the total voltage drop across the resistor remains unchanged. Since the bridging capacitors neither charge nor discharge, they do not influence the output time constant. Any shunt capacity from these elements to the surrounding structures of course load the circuit in the usual way. The output resistance in Figure 4.20 is $R_L/2$.

As a circuit element, each tube, looking back into the collector, is a current generator feeding the capacitance between the collectors and the end plate structure (which is at A.C. ground). The output impedance seen by the amplifier is this capacitance in parallel with the load resistance. We have measured these capacitances with an LC meter (Tektronix 130) and they are for Tube I, III, and III respectively, 5.8 $\mu\mu$F, 20 $\mu\mu$F, and 20 $\mu\mu$F. In addition we have confirmed these values by driving the impedance with an external current pulse and comparing the current and voltage wave forms.

For very high frequency response the time constant should be small. The shunt capacitance for each tube is of course fixed by the

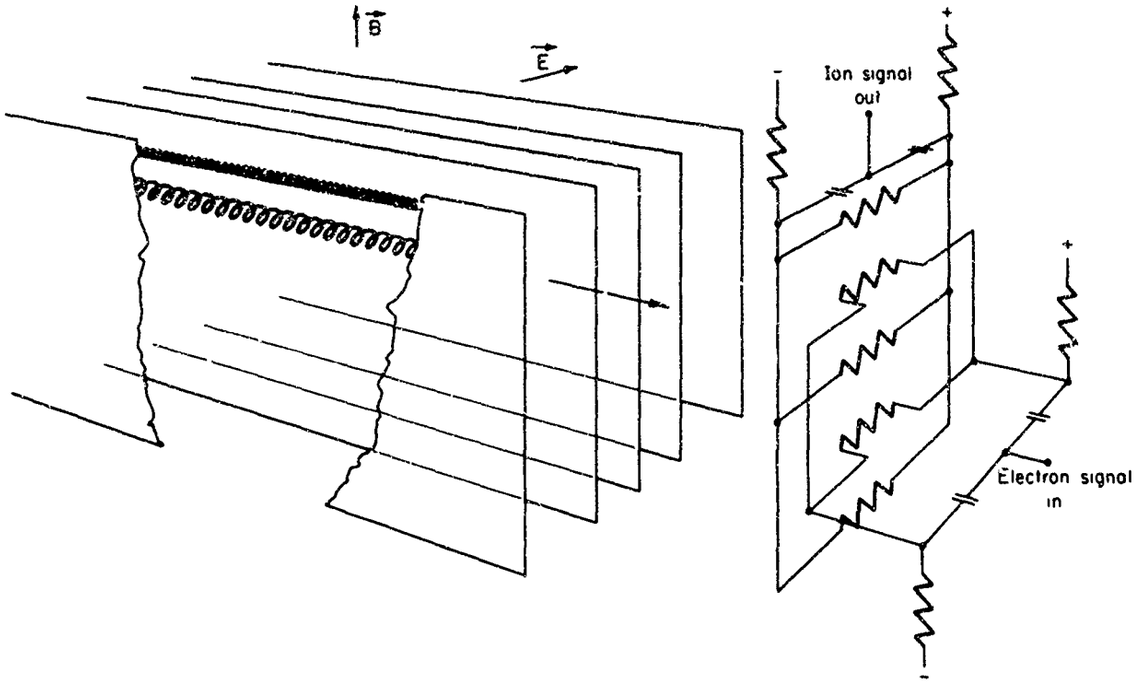

Figure 4.21

Schematic Drawing of Field Matching
Output Circuit for Tube III

structures. To obtain easily interpretable signals we have chosen load resistances in the range of 1,000 ohms to 12,000 ohms.

All three tubes have one feature in common which for a practical delay line would be a serious disadvantage. The field terminating structures intercept the auxiliary beam, and through it capacitance to the collector it transmits signals without any delay. This is not, however, a disadvantage in the experiments on pulse signals because the initial response decays before the delayed signals reaches the collector.

The general procedure for all three tubes and for both modes of operation was essentially the same. The control grid was normally biased beyond cut-off and the auxiliary beam was pulsed on and off by a signal from the pulse generator. As a variant the grid was occasionally set to a voltage such that a current flowed steadily to the output collector. The auxiliary beam was in this case pulsed off and then on. In addition some measurements were made on continuous beams.

In the following chapter we discuss the results of these experiments, and where appropriate we describe the procedures in greater detail.

CHAPTER V

EXPERIMENTAL RESULTS

That the idea of a plasma delay line was the chief influence in the original design of the experiments is shown in all three tubes. None is ideal for an electron delay line. Nevertheless, the observations of electron pulses at high vacuum have proved to be easier to interpret than the plasma results, and we begin this chapter with a discussions of experiments in this mode. The second part of the chapter is a comparable discussion of the plasma mode. In both modes we are interested principally in the time delay, current, and wave form in the output signals.

5.1 Measurements in the Electron Mode

Since the primary electrons in the experimental tubes bombard surfaces on the field terminations and on the auxiliary collectors, they must surely produce secondary electrons. It is not as sure, however, that these secondaries should also escape from the emitting surfaces. To determine whether or not they are actually launched we operated Tube I at pressures less than 10^{-6} Torr and searched for delayed signals.

We discovered that electrons can escape through either of two different processes. One, which we believe is essentially the mechanism that we discussed in Chapter II, apparently launches electrons during the entire time the primary beam is on. The drift pulse distorts, however, under the action of its own space charge, and it is foreshortened when it reaches the collector. The second mechanism is associated with

transient voltages on the emitter, and it launches sharp bursts of electrons when the primary beam is turned off.

In the following sections we discuss, in turn, the measurements on the sharp pulses and the measurements on the foreshortened pulses. We also discuss the conditions under which the drift pulses are formed, and the mechanisms by which we believe the electrons are launched and focused.

5.1.1 Sharp Pulses

Figure 5.1(a), one of the earliest photographs of this effect in Tube I, shows several of its distinctive features. We note first that each rectangular input pulse (upper trace) is followed after 5.8×10^{-6} seconds by a current spike at the collector and that furtherfore the time delay measured from the trailing edge of the pulse is independent of the pulse width. This indicates that the launching process is probably associated with the trailing edge.

We have, in fact, observed sharp spikes, about 2 volts amplitude, at the auxiliary collector at both the beginning and the end of the input pulse. Furthermore, the appearance of the delayed signal depends critically on the potential of the auxiliary collector with respect to the average potential V_i in the drift space. If this voltage is more than about $\pm$ 6 volts, the effect does not appear at all. In addition the potential of the slit anode must be equal to or less than V_i.

From these observations we suggest that electrons in this mode are launched by the following proceso. Electrons that leave the

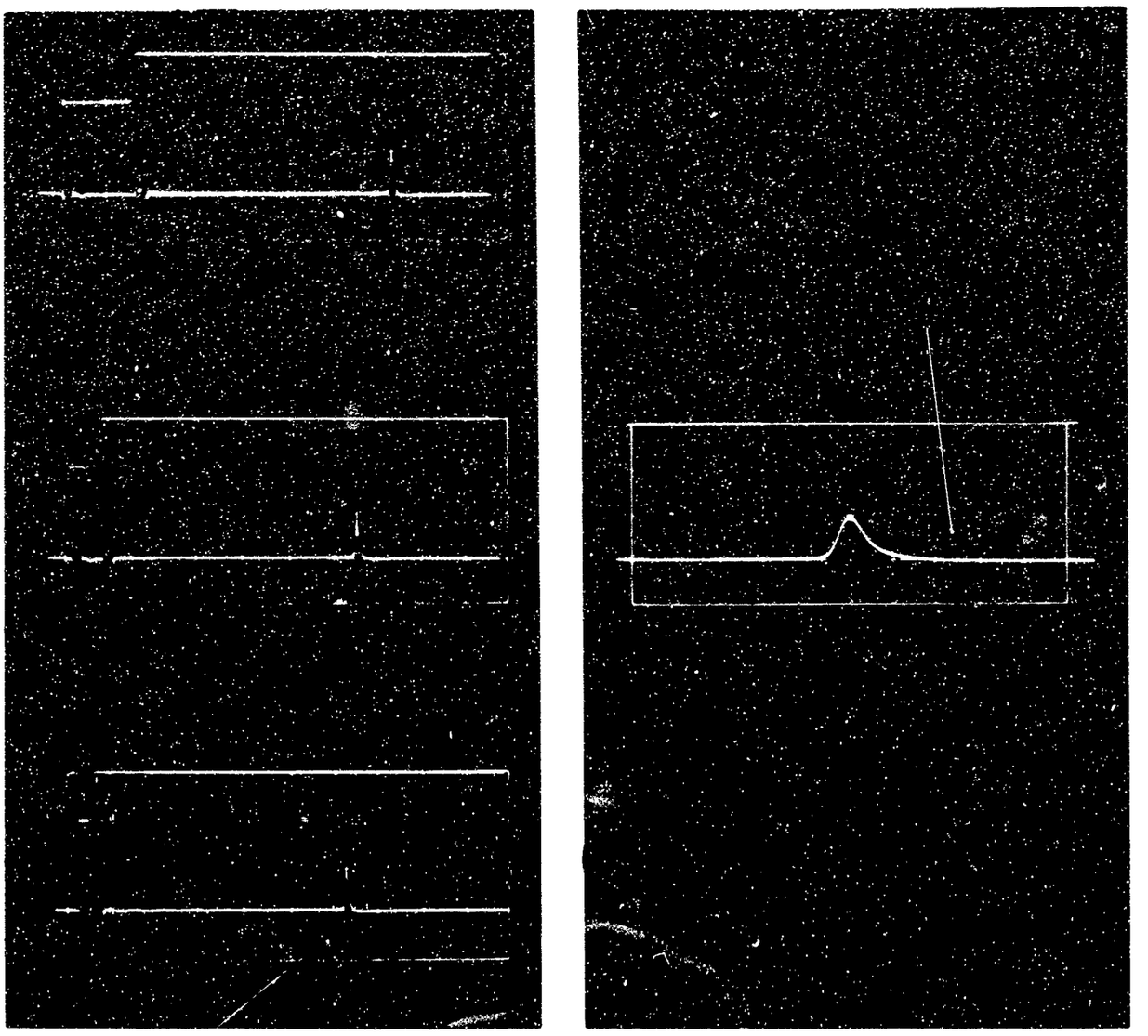

(a) (b)

Amplitude Scales

Upper Traces	50 V/div	1 μa/div
Lower Traces	1 μa/div	

Time Scales

1 μsec/div	0.1 μsec/div

Figure 5.1

Sharp Electron Pulses in Tube I

auxiliary collector with velocity components in the -z direction will be reflected either by the fringing field of the terminating electrodes, or if they penetrate these electrodes, by the stronger field at the slit anode. When they return to the auxiliary collector they are normally collected. Some of the electrons emitted just before the trailing edge of the input pulse lack the energy to return to the auxiliary collector which, because of the voltage spike, is at a lower than normal potential. The electrons are therefore re-reflected in the -z direction. At the same time they are drifting toward the output terminals with a velocity $v_d = E/B$, and we assume that when the auxiliary collector regains its normal potential they will have escaped and will respond then only to the crossed electric and magnetic fields, and as we shall see later, to their own space charge.

One launched, of course, the electrons must be kept from the walls if they are to reach the output collectors, and we attribute the required forces to the fringing fields of the terminating electrodes. Since the electrons are already constrained by the magnetic field, these focusing forces are unusual in that they reflect back into the drift space only those electrons in the positive part of each section (Figure 5.2), allowing the others to escape. Furthermore, we see in Figure 5.2 that if the tube is rotated, these sieves match only at discrete angles, and that at intermediate angles electrons constrained at one side of the drift space escape through the sieve at the other. Our conviction that this is indeed the correct mechanism is strengthened by later observations on Tube II. When this tube was evacuated and sealed we found that the appearance of electrons at the collectors

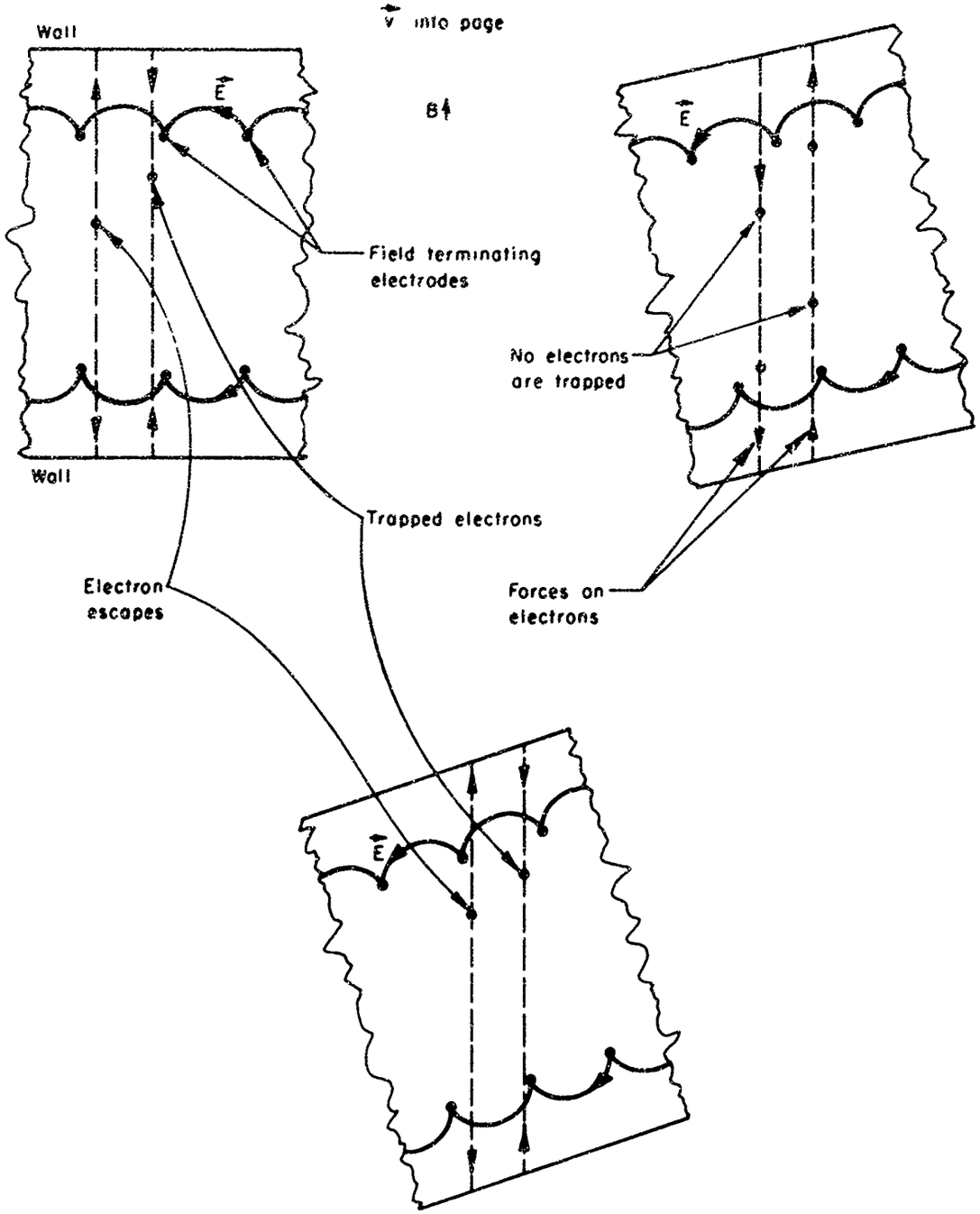

Figure 5.2

Trapping of Electrons by Field Terminating Electrodes

always depended on angle in precisely this way.

When the photograph of Figure 5.1 was taken, the voltage across the one-half inch aperture was 90 volts, and the corresponding electric field was therefore $E = 7.1 \times 10^3$ volts/m. With the magnetic field strength $B = 0.55$ weber/m^2, the drift velocity should be $v_d = 1.29 \times 10^4$ m/sec, and the calculated time delay is 5.83×10^{-6} sec. This agrees with the measured delay, at least to one percent.

Figure 5.1(b) shows the delay pulse of the third trace of Figure 5.1 on an expanded time scale. We see that the total pulse duration is about 0.1×10^{-6} secs. Since the time constant of the output network is only 6×10^{-9} sec, this picture probably provides a reasonably good description of the charge distribution through the delay pulse.

The restrictions on the voltage difference between V_i and the voltage on the auxiliary collector suggested that the launching of electrons might actually be confined to the center of the aperture. This suggestion seems to be confirmed by the following observations.

Figure 5.3 shows a series of photographs in which one output collector was held at -22.5 volts with the respect to the voltage V_i at the center of the drift space, and the other collector was varied from +22.5 volts to -6 volts with respect to V_i. We see that although at 1.5 volts electrons are still collected, at -1.5 volts, while they come close enough to the collector to induce a measurable charge, they are evidently repelled. This result indicates that the electrons are not in the negative half of the drift space and that since there is no reason for them to prefer one half to the other, that they are probably

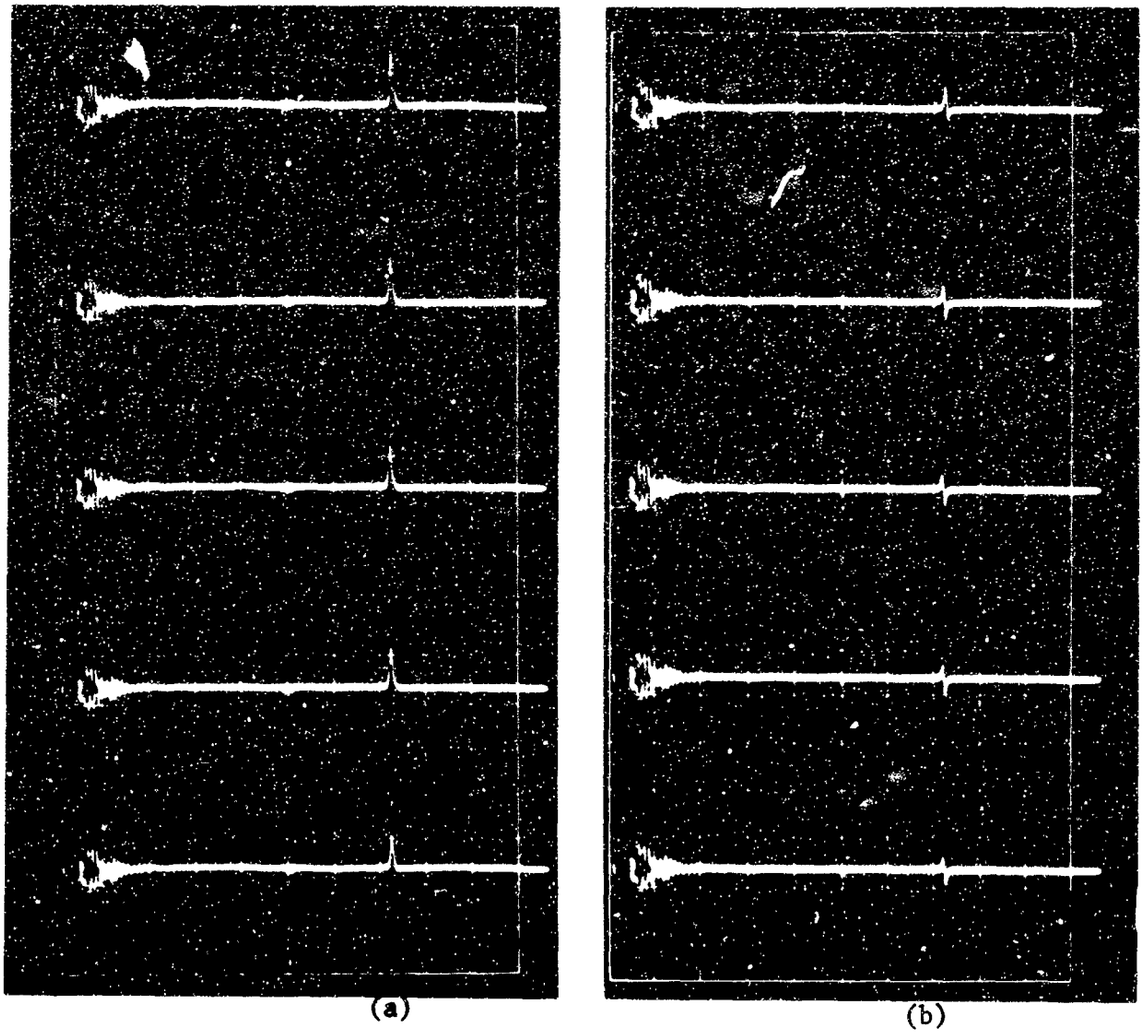

(a) (b)

Amplitude Scales

(a)	(b)
1 μa/div	1 μa/div

Time Scales

(a)	(b)
1 μsec/div	1 μsec/div

Collector Voltage (beginning with Upper Trace)

(a)	(b)
22.5, 6.0, 4.5, 3.0, 1.5	0, -1.5, -3.0, -4.5, -6.0

Figure 5.3

Influence of Collector Voltage on Pulse Shape

in the center.

Later we filled the tube with helium to a pressure of 0.1 Torr, and by simply looking at the ionization trace we discovered that the electron gun was producing not a sheet beam, but a pencil beam in the center of the aperture.

Even at somewhat longer time delays these pulses have reasonably good wave forms. Figure 5.4 shows an input pulse together with a pulse delayed by 13 microseconds, and the third trace shows the delayed pulse on an expanded time scale. From these observations we estimated that it should be possible to pack pulses in the delay line with a separation of about 100 nanoseconds between pulses. This would allow us to pack 130 pulses in the 7.5 centimeter delay line when the time delay is 13 microseconds.

To test the validity of this assumption we introduced two pulses from separate generators into the delay line. We found, however, that as these pulses were brought close together their interaction reduced still further the time separation, and therefore the physical spacing between them. Figure 5.5(b) shows a series of photographs of the two input pulses. These input photographs, taken on a Tektronix 512 oscilloscope, do not adequately show the pulse rise time, which was actually about 40 nanoseconds. Figure 5.5(a), on an expanded scale, shows the delayed pulses displayed as usual on a Tektronix 585 oscilloscope. As the time interval between the two pulses decreases, the interaction increases and the first delay pulse is actually retarded. This effect is clearly evident in the photograph. Finally, when the input pulses are still about 0.7×10^{-6} seconds

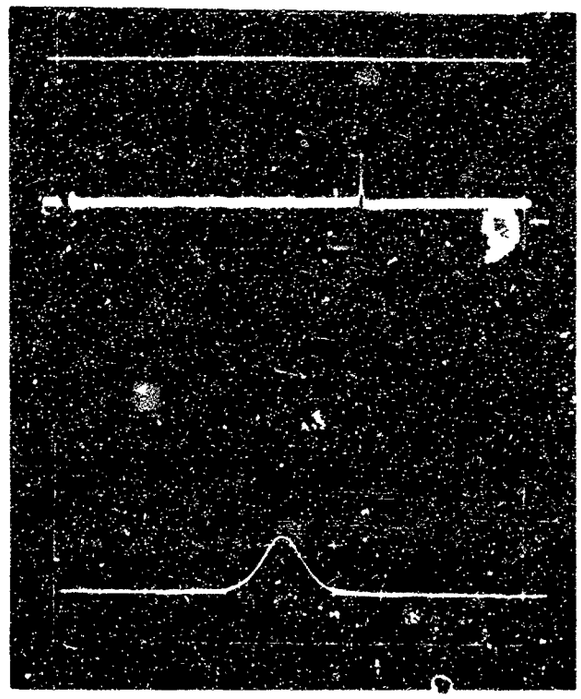

Amplitude Scales

First Trace 100 V/div
Second and
Third Traces 0.4 μ /div

Time Scales

First and
Second Traces 2 μsec/div
Third Trace 0.1 μsec/div

Figure 5.4

Sharp Pulses in Tube I

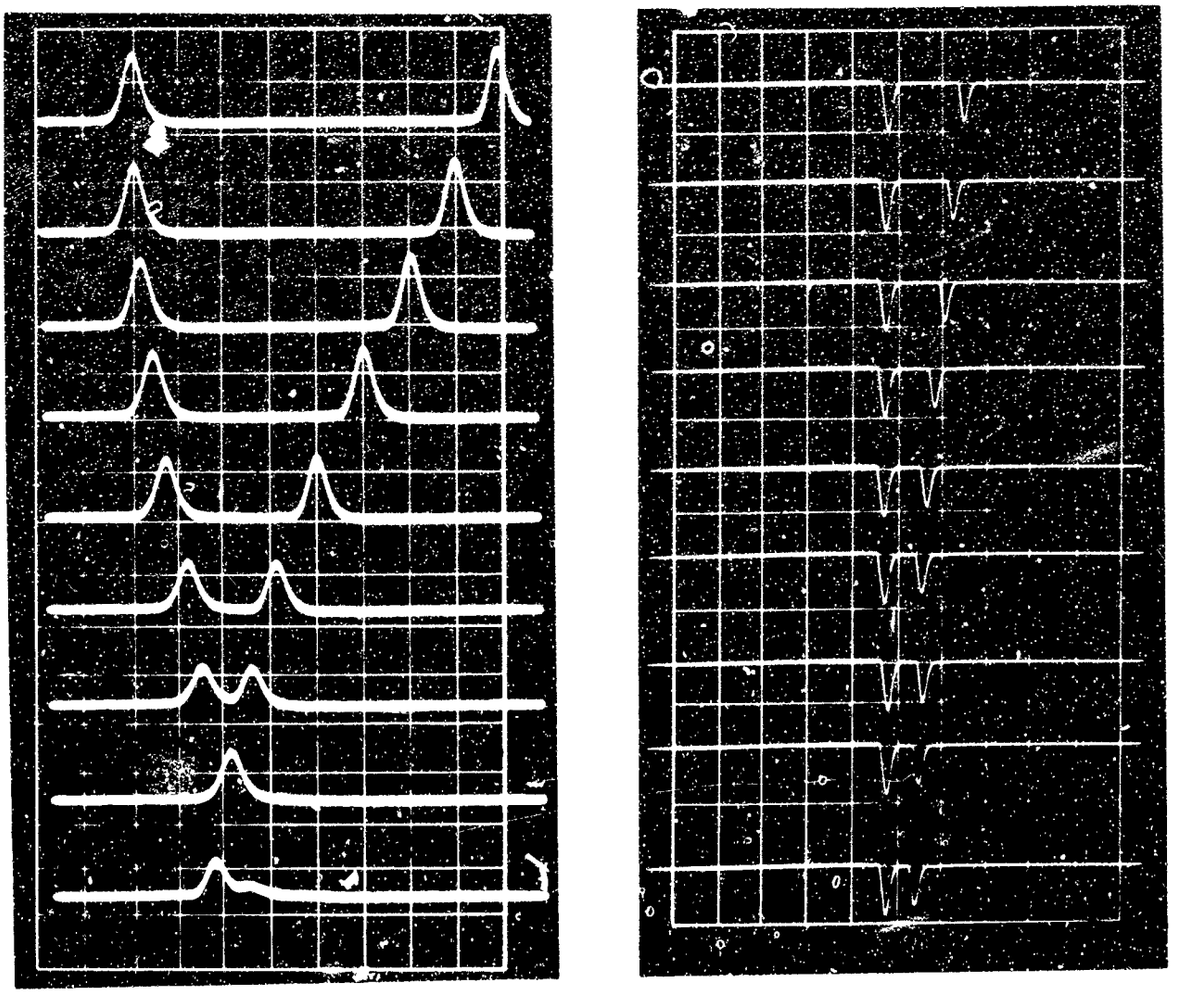

(a) (b)

Time Delay 13 μ sec

Amplitude Scales

0.4 μa/div 50 V/div

Time Scales

0.2 μsec/div 1 μsec/div

Figure 5.5

Space Charge Interaction of Two Electron Pulses

apart, the delay pulses appear to merge.

The explanation for this effect lies in the same crossed field phenomenon that is the basis of the delay line. The mechanism is most easily visualized if the observer is in a frame of reference that moves at the drift velocity of the electrons. In this coordinate system the external electric field disappears, and the electron trajectories are dictated by the magnetic field and the electric field of the space charge. The coulomb forces between the charge clumps give rise to a crossed field drift which in the laboratory coordinate system is superimposed on the main drift. If these charge clumps were actually confined to two points we would then expect to see a rotation of the points around a center that is midway between them. We have made this calculation for the seventh trace in Figure 5.5(b), and we find that the required charge for each clump is 0.35×10^{-12} coulomb.

We next assume that the charge is in fact spread over a time interval of 0.1 microsecond as indicated in the figure, that the wave form is approximately triangular, and that the small spreading of charge does not seriously alter the behavior of the two charge clumps with respect to one another. Under these circumstances the required current at the collector is 3.5 microamperes. The actual measured current is closer to 0.5 microampere.

The charge, of course, is not confined to discrete points, and in fact we have assumed that the electrons oscillate from one side of the drift space to the other. It might appear that a 1/R type force field would be more appropriate. Nevertheless, for the distances involved the actual forces for the two force laws are not very different.

Although the difference between the calculated and observed currents is not completely understood, it may be that as these charges rotate some of them escape through the sievelike focusing mechanism and that the rotation is actually more rapid during the early part of the trajectory.

Figure 5.6 shows the effect of a particular three pulse interaction. As we see from the top trace in Figure 5.7(a), the first two input pulses are initially set to provide a strong interaction. The influence of the third pulse on the first two is negligible. The succeeding photographs show the effect of moving the third pulse closer to the second. As the interaction between these two pulses increases the interaction between pulses 1 and 2 decreases.

Figure 5.7 records a series of observations similar to those in Figure 5.5 except that the drift velocity has been doubled. The physical spacing between these pulses for the same time intervals is therefore doubled, and furthermore, the time during which the interaction can take place is reduced by a factor of 2. That the interaction between these pulses is less is apparent in the photographs.

Sharp pulses of this kind have also been observed in Tube II. In fact, one of the goals of the design of the second tube was to provide a more appropriate environment for the study of this effect. In particular, as we have discussed in Chapter IV, the gun was designed to provide a more uniform illumination of the aperture and a special secondary emitter was provided which approximately matched the electric field in which it was placed. It was hoped that with this arrangement discrete sheets of charge could be produced, and that since the interaction of charge sheets is a sliding, transverse motion instead of a

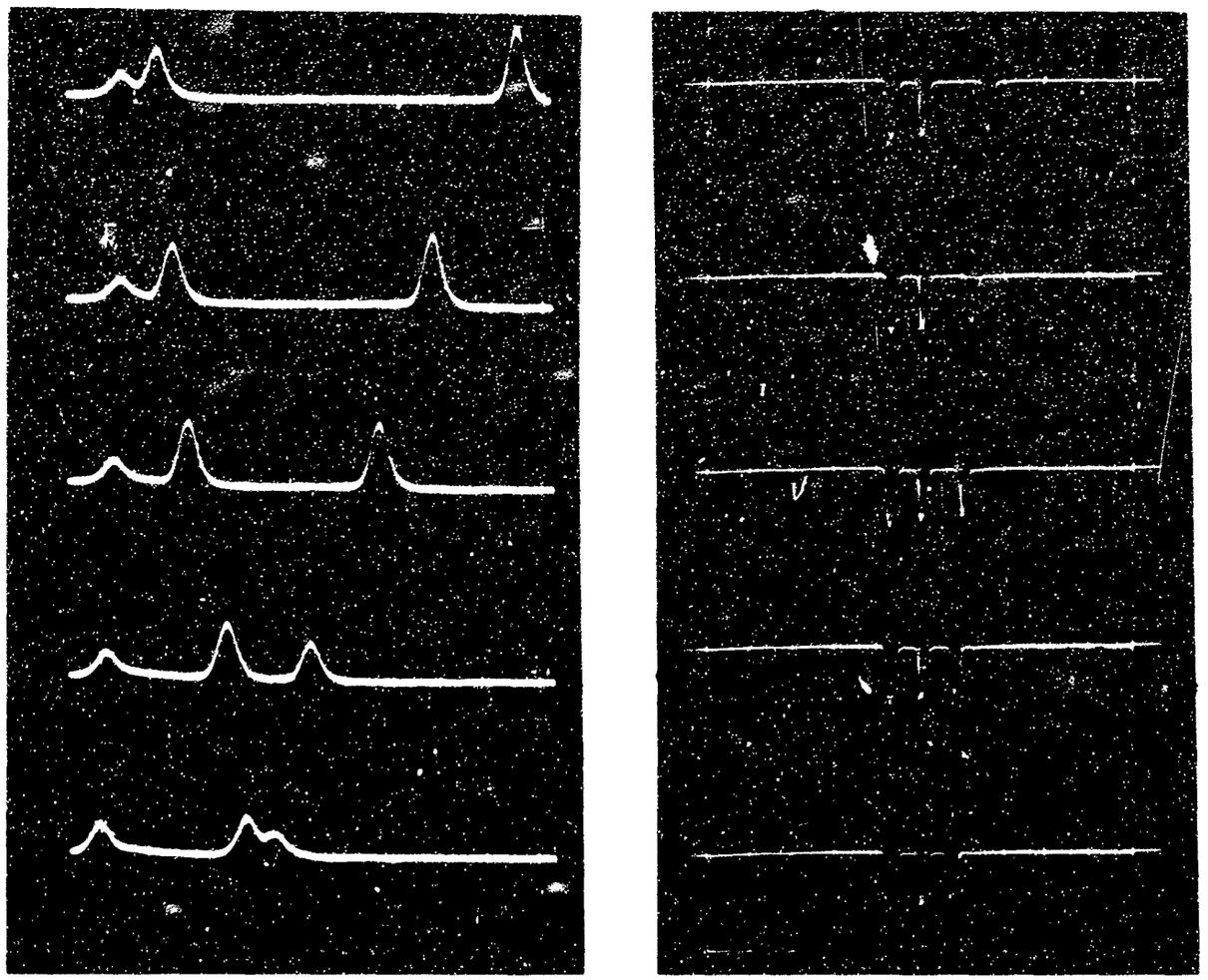

(a) (b)

Time Delay 13 μsecs

Amplitude Scales

0.4 μa/div 50 V/div

Time Scales

0.2 μsec/div 0.5 μsec/div

Figure 5.6

Three Pulse Interaction

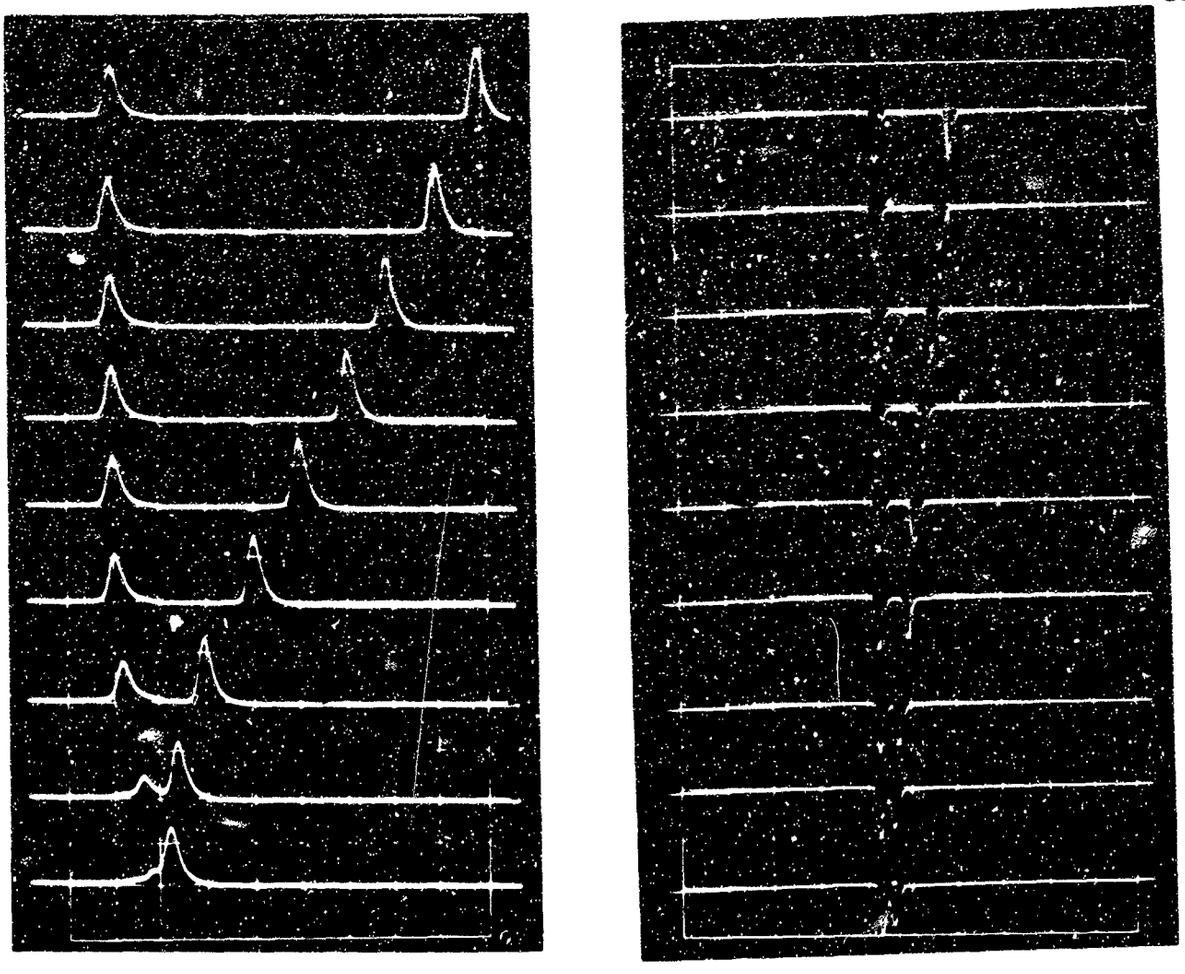

(a) (b)

Time Delay 6.5 μsec

Amplitude Scales

0.4 μa/div 50 V/div

Time Scales

0.2 μsec/div 1 μsec/div

Figure 5.7

Two Pulse Interaction

rotation, the interaction between pulses would in this way be reduced.

These goals have not been achieved entirely. Although results of our observations are similar to those of Tube I, the attained current is actually somewhat less. Nevertheless, there were some new effects as well. We were able to produce pulses which with good wave form remained in the tube for more than 25 microseconds, and we obtained some indication of the result of launching electrons in a region of somewhat higher drift velocity than is found in the main part of the tube. We discuss these results briefly in the following paragraphs.

Figure 5.8(a) shows a sharp pulse delayed by 12.8 microseconds in Tube II and Figure 5.8(b) shows the same pulse on an expanded time scale. Because the output time constant for these observations was 0.24 microsecond the sections between the zero slope points represent the integral of the current pulse. The maximum current is 0.13 microampere. The portion beyond the maximum is just the normal discharge curve of the output circuit. This photograph was taken with an additional capacity of 50 picofarads connected between the control grid and the emitter. We have discovered that this capacity doubled the pulse amplitude. Additional capacity, however, only reduced the amplitude from this maximum and 500 picofarads eliminated the pulse altogether. These observations provide additional evidence for the connection between the launching of these sharp pulses and the transient voltages on the emitter electrode.

Figure 5.9(a) shows the delayed responses to two input pulses separated by 5 microseconds. The signals, although delayed by a little more than 26 microseconds, have clean wave forms. The output time

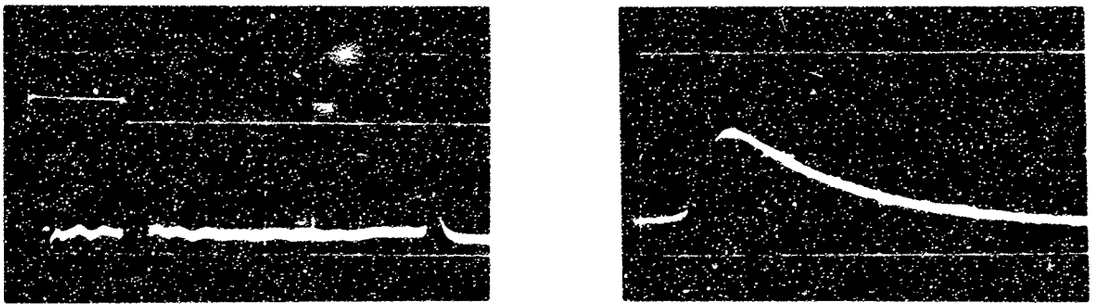

	(a)	(b)
Amplitude Scales		
Upper Trace	50 V/div	50 V/div
Lower Trace	0.2 mV/div	0.2 mV/div
Time Scales		
	5 μsec/div	0.1 μsec/div
Output Circuit		
	$R_L/2 = 12 \times 10^3$ ohms C = 20 μμF	$R_L/2 = 12 \times 10^3$ ohms C = 20 μμF

Figure 5.8

Sharp Electron Pulses in Tube II

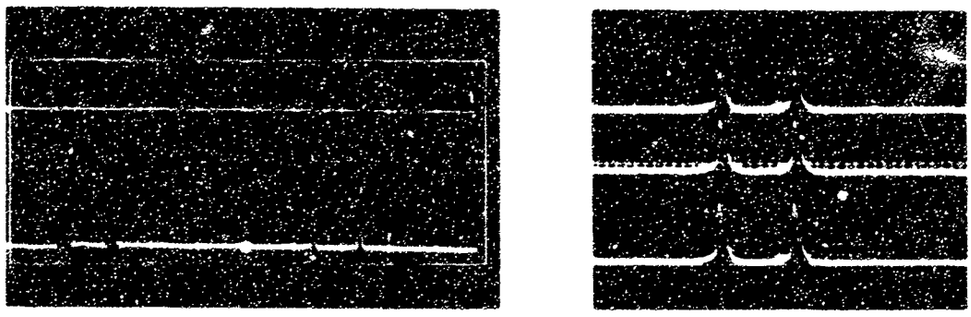

(a) (b)

Amplitude Scales

(a)	(b)
Upper Trace 50 V/div Lower Trace 0.5 mV/div	All Traces 0.5 mV/div

Time Scales

(a)	(b)
5 μsec/div	1 μsec/div

Output Circuits

(a)	(b)
$R_L/2 = 2 \times 10^3$ ohms C = 20 μμF	$R_L/2 = 2 \times 10^3$ ohms C = 20 μμF

Figure 5.9

Sharp Electron Pulses in Tube II

constant for this photograph is 40 nanoseconds, and the current in the pulse is about 0.2 microampere. With 22 volts across the end plates the electric field was 1.72×10^3 volts/m. With B = 0.6 webers/m^2 the calculated drift velocity was 2.89×10^3 m/sec, and the corresponding time delay was 26 microseconds, in good agreement with the measured value. The electric fields, however, at both the emitter and the collector, were raised to 7.08×10^3 volts/m, a little over four times the drift field. We observed that these large fields increased the peak current without appreciably affecting the time delay. Figure 5.9(b) shows this effect more clearly. Each of the three traces shows two pulses delayed by 12 microseconds. For the upper trace the fields were matched, for the second trace the collector field was doubled, and for the third trace both the collector and emitter fields were doubled.

Figure 5.10(a) illustrates the same kind of double pulse interaction that we have discussed in connection with Tube I. The top trace shows on a scale of 5 microseconds/division two input pulses which are about 1.5 microseconds apart. The second and third traces show the delayed signals after 25 microseconds and 12.5 microseconds, respectively. At 12.5 microseconds delay the reduction in the time separation is negligible. At 25 microseconds it has been reduced to about 0.4 microsecond. Figure 5.10(b) illustrates how for a delay of 25 microseconds this interaction is reduced as the current in the drift pulse diminishes.

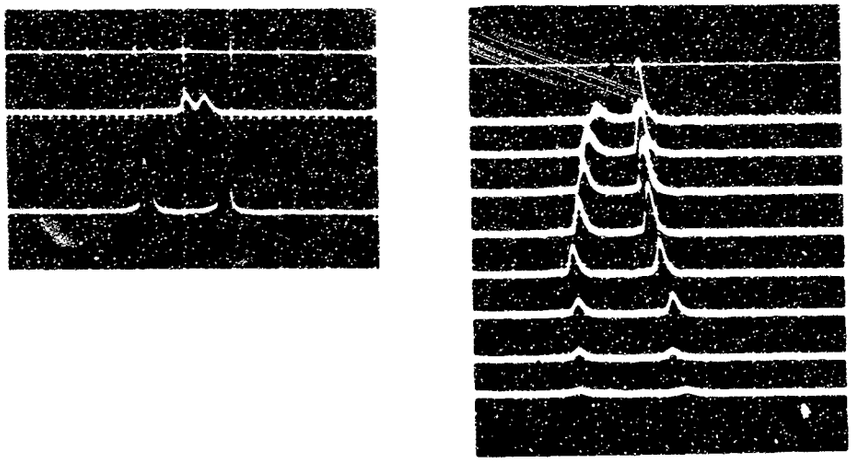

(a) (b)

Amplitude Scales

Upper Trace	50 V/div	50 V/div
Lower Trace	0.5 mV/div	0.5 mV/div

Time Scale

Upper Trace	5 μsec/div	5 μsec/div
Lower Trace	1 μsec/div	1 μsec/div

Figure 5.10

Double Pulse Interaction in Tube II

5.1.2 Broad Electron Pulses

When the input voltage to the grid was less than about 20 volts we did not observe the sharp pulses that we have been discussing. We were able, however, to produce pulses which at very low currents (10^{-8} amperes) resembled the input pulses. When we increased the current in these pulses, generally by raising the emission current, the pulse width diminished as the amplitude grew. These effects are illustrated in Figure 5.11 in which the second trace is actually the super-position of three separate photographs. The explanation again lies in the space charge forces of the electrons, and is closely related to the kind of thin beam instability that we discussed in Chapter II. Here the charge density is not great enough in the center of the pulse to create much distortion. On the edges, however, it can be relatively strong, because the edge electrons respond to the force of their inner neighbors, and these forces are not compensated, as they are in the center of the pulse. As a result the edges curl toward the end plates, and the effect at the collectors is a pulse contraction.

This effect is more difficult to calculate than the case of two isolated charges, and we have made two calculations on the CDC 1604 digital computer to simulate the process in thin electron pulses. Figure 5.12 shows in graphical form some results of one of these calculations. Although the calculations show a definite contraction of the pulse, the results fail to agree with the experimental observations in two respects. First, the curling at the edges in addition to shortening the pulse would also increase the amplitude at the edges with respect to the amplitude in the center of the pulse. Secondly, the calculated

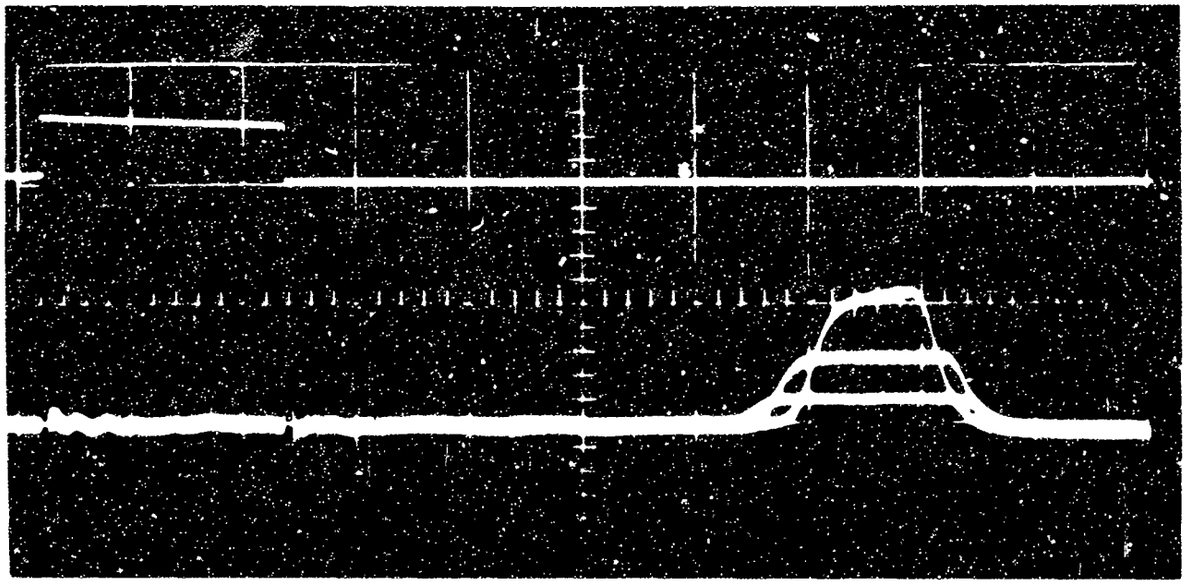

Amplitude Scales

Upper Trace	5	V/div
Lower Trace	1	mV/div (0.83×10^{-7} amp/div)

Time Scale

2 μsec/div

Figure 5.11

Space Charge Effects in Broad Electron Pulses

$t_0 = 1.6\,\mu sec$

$x_0 = y_0 = 0.625 \times 10^{-3} m$

$I = 10^{-7}$ amps

$q = 0.788 \times 10^{-12}$ coul/m

$v_e = 6.25 \times 10^{3}$ m/sec

Pulse duration = 4×10^{-6} sec

Pulse length = 2.5×10^{-2} m

$B = 0.58$ weber/m^2

Line charge approximation

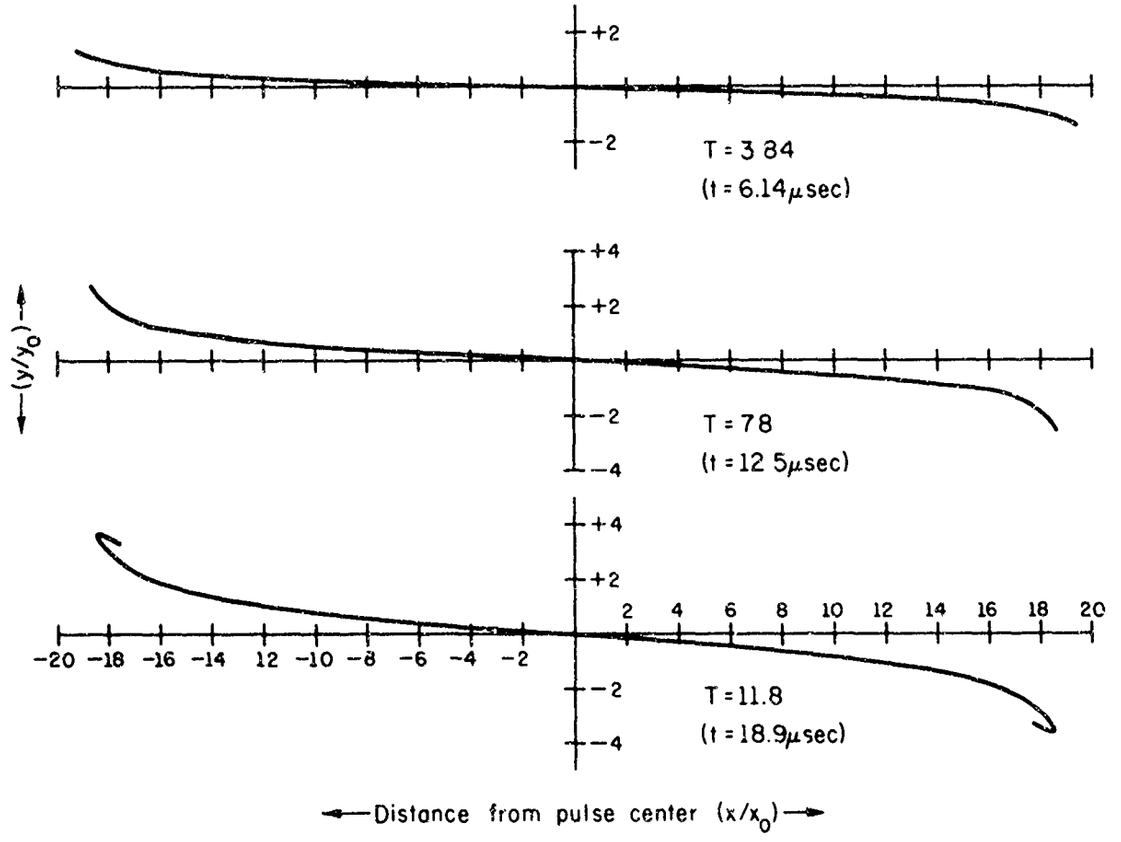

Figure 5.12

Calculated Time Variation of Charge Contour
in Thin Electron Pulse

effect for the same current is less than the experimentally observed effect. We believe here, as in Tube I, that the discrepancies are explained in terms of particle loss. In the experiment we measure only the current at the collector. It seems reasonable to believe that the extra charge on the edge resulting from the curling escapes from the drift space during the transit time and that the charge throughout the pulse during this time interval also suffers attenuation. We discuss this calculation in more detail in Appendix C.

The effect is also shown in the photographs of Figure 5.13, but from a somewhat different point of view. In Figure 5.13(a) the upward going pulse in the upper trace represents the signal which turns the drift beam on. As before the upward going pulse on the lower trace represents the delay signal which clearly has been shortened. The downward going pulses represent the case when the beam is normally on and is turned off by the input pulse. Here the delay pulse is lengthened. In both cases the effect is the same, a curling at the edges of the beam. The actual current in the drift beam is 3.6×10^{-8} ampere and the delay at 5 microseconds/div is 12.5 microseconds. Figure 5.13(b) is a similar composite when the current is reduced to 1.2×10^{-8} amperes. The scale for the lower trace has been magnified by a factor of two from the trace in Figure 5.13(a). For this current we see that the pulse shortening is negligible.

The sequence of photographs in Figure 5.14 shows the effect in still a different way. As before, a pulse on the control grid turns the beam on and off, but in addition a sharp perturbing signal, applied to the ends of the emitter, impairs the electron launching. As the

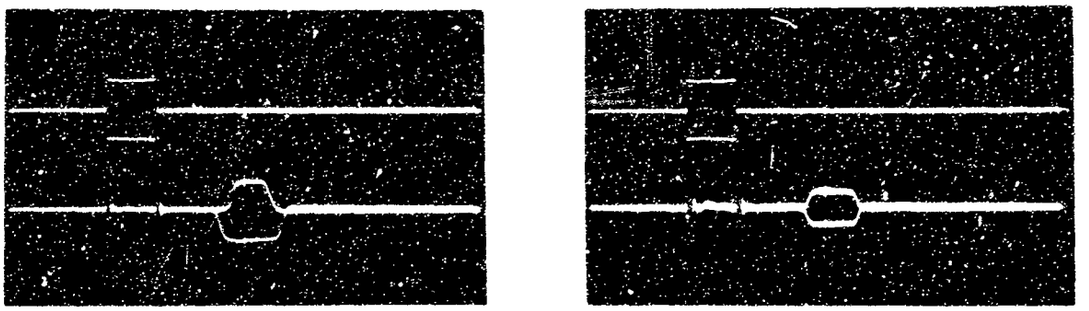

(a) (b)

Amplitude Scales

Upper Trace	20 V/div	20 V/div
Lower Trace	0.83×10^{-7} amp/div	0.415×10^{-7} amp/div

Time Scales

5 μsec/div	5 μsec/div

Figure 5.13

Space Charge Effects in Broad Electron Pulses

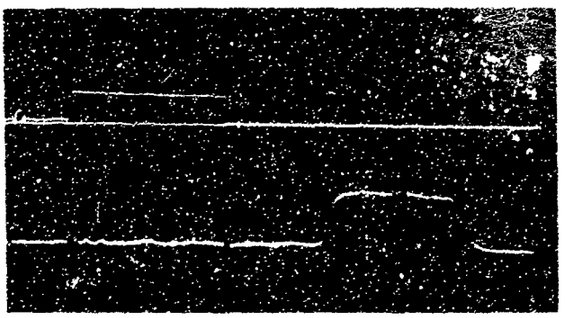

(a)

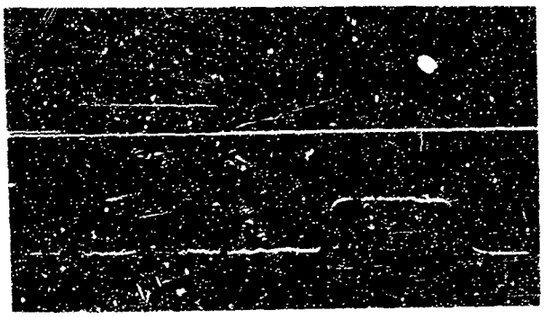

(b)

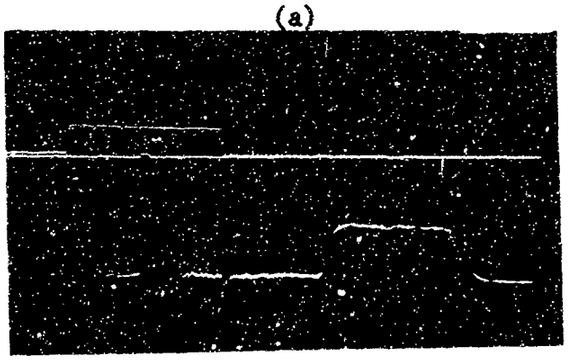

(c)

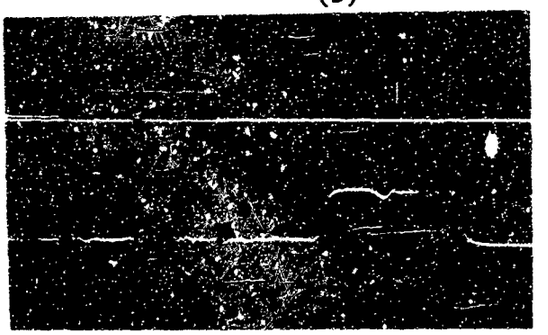

(d)

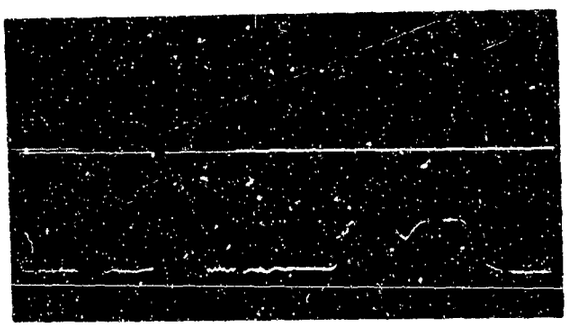

(e)

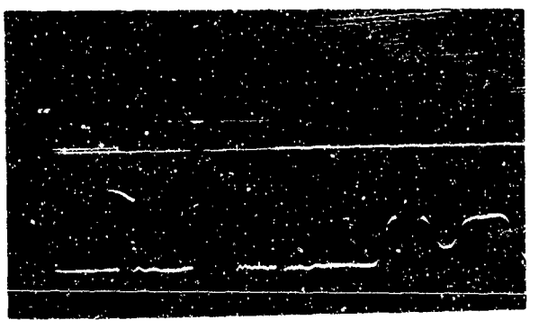

(f)

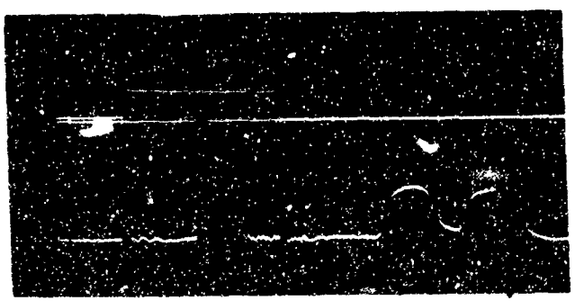

(g)

Amplitude Scale:

Upper Traces 5 V/div
Lower Traces 0.417×10^{-7} amp/div

Time Scale: 2 μsec/div

Figure 5.14

Space Charge Effects in Electron Pulses

magnitude of the disturbance increases, the output signal divides, and curling at the inner edges "amplifies" the separation.

These effects are characteristic of sections of thin beams and we believe that in all cases these observations were made under thin beam conditions. Our procedure was to raise the filament current until the pulses appeared on the oscilliscope and to control the pulse amplitude and width by varying the filament current. Since the temperature was just above threshold for emission, it is reasonable to believe that only the center, where the temperature was highest, actually emitted primary electrons and that only the center of the resistive emitter provided secondary electrons for the drift space. Furthermore, the photographs of Figure 13 were taken when the filament was bowed, and only the center of the aperture could be illuminated.

In a thick beam section we would expect, instead of curling, a migration of particles around the pulse. Although this would produce distortion, it should not shorten the pulse duration appreciably. Figure 15 shows the results of an attempt to produce a thick section by filling the aperture with electrons. As the filament current increased beyond the emission threshold, a pulse appeared which, at first, contracted as its amplitude increased, but at still higher temperatures it regained much of its initial breadth. The pulse shape, however, exhibited characteristics which we do not yet understand. Although the leading edge and the main body of the pulse reflect the shape of the input pulse, the trailing edge invariably developed a step like distortion. In addition, the current was limited by the outbreak of noise.

A more natural mechanism for filling the aperture is the

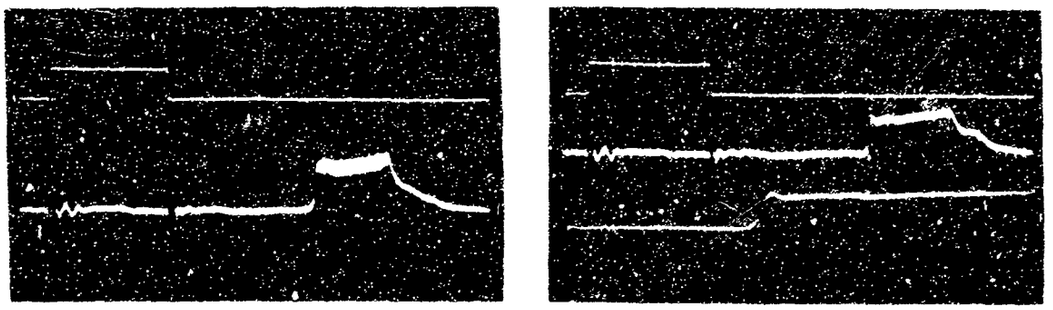

(a) (b)

Amplitude Scales

Upper Trace	10V/div	10V/div
Lower Traces	10^{-7} amp/div	10^{-7} amp/div

Time Scales

2 μsec/div	2 μsec/div
Third Trace	0.5 μsec/div

Figure 5.15

Electron Pulses that Fill Aperture in Tube II

ionizing action of the auxiliary beam in the plasma delay line. In the following section, we discuss our measurements in this mode.

5.2 Results in the Plasma Mode

Our first observations on Tube I were encouraging. Electrons were effectively launched by the ionizing beam, and their transit times depended in the predicted way on electric and magnetic fields. It soon became clear, however, that the tube could not be functioning properly. The electron signals exhibited the same contraction that we observed later at high vacuum, no ions were observed at the collector, and the electric fields in the collector region were distorted by the collectors themselves. When we realized that the ionizing beam did not fill the aperture but was instead confined to a narrow region in the center, we decided to defer the study of the plasma mode until a better tube was available.

Tube III seems to provide an almost ideal environment for the plasma mode. The field is uniform, the ionizing beam fills the aperture, and with appropriate strip resistors the fields in the collector region are matched. We first assembled the tube with resistors that we made by spraying Aquadag on mica strips. The output signals, although delayed by the correct time intervals, were erratic. They appeared and disappeared spontaneously, and they fluctuated almost continuously in amplitude and in wave form. Because the launching region was so similar to that of Tube II we believed that the difficulty was probably due to peculiarities in the behavior of the Aquadag resistor. At this time we had not yet learned how to make satisfactory

titanium oxide resistors; therefore, to test this hypothesis we [illegible] the Aquadag resistors with stainless steel strips. Under these conditions the tube behaved normally, and our observations were both consistent and reproducible. All of the results which we discuss in this section were obtained from measurements on Tube III in this fo[illegible] Although the environment under these conditions is somewhat less than ideal, the actual results were interesting and their contrasts with the broad pulse results in the electron mode are informative.

Eventually we learned to make acceptable titanium oxide resistors. Two of these were installed in Tube II and functioned properly as emitter and collector. Nine of them were eventually installed in the collection region of Tube III. However, we have not yet tested the tube in this form.

Our observations in the plasma mode have in some respects been surprising. We found first of all that we could collect particles only on the set of plates which included the outer pair. This seems to indicate that although the ions and electrons are launched properly by the ionizing beam they do not diffuse in the manner that we discussed in Chapter III, but are probably focused by the field terminating electrodes as are the electrons at high vacuum. We found, furthermore, that although we could collect both electrons and ions, that the ion current was always larger, that its wave form was always better, and that as we lowered the pressure from about 10^{-2} Torr the ion signal increased whereas the electron signal decreased until it disappeared altogether. Unlike the broad electron pulses the ion pulses showed no contraction, and although the rise time suffered at long delays, we

observed pulses with good wave form that were delayed by over 50 microseconds. We also discovered that the rise time associated with the ion pulses decreased as we decreased the pressure. In this section we discuss these results in detail.

Figure 5.16(a) shows an input pulse and an output pulse delayed by about 18 microseconds. It is interesting to compare this photograph with that of Figure 5.13. Although the current is 3×10^{-7} amperes, 9.5 × the current in the thin electron pulse, and although the delay time is longer, there is no evidence of pulse contraction. Figure 5.16(b) shows the same input pulse with a superimposed sine wave at 0.55×10^{6} cycles/sec. The phase of the sine wave with respect to the beginning of the pulse is fixed at the time of launching, and this phase relation is maintained when the time delay is varied. The small sinusoidal signal that is visible when the beam is turned off arises from capacative coupling within the tube. At higher frequencies this coupling increases, and when it is comparable to the signal carried by the pulse, beats can be observed when the time delay is varied. We are able to observe signals carried by the pulse in this way with frequencies up to 2 megacycles/sec.

The photographs of Figure 5.17 were taken to provide a contrast with the results of Figure 5.14, which showed the division of a broad electron pulse into two parts. Here the variation in the number of particles launched was controlled by varying the grid potential at about the mid-point of the input pulse. Here again there is no evidence of contraction. There is, however, some distortion in the signal, provided probably by particle dispersion.

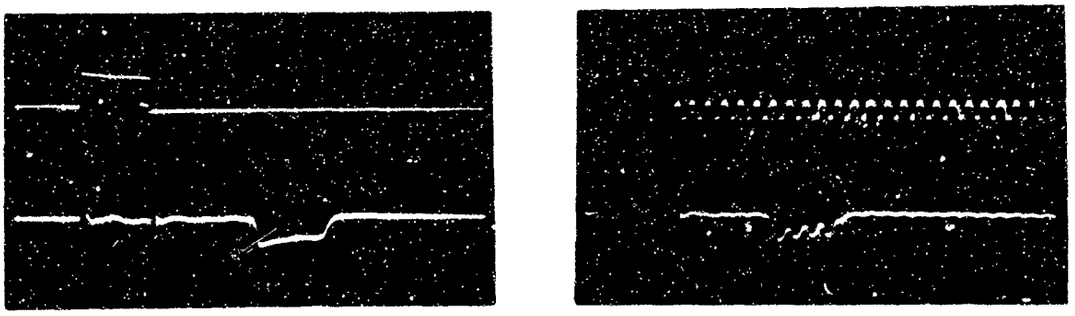

(a) (b)

Amplitude Scales

Upper Trace	10 V/div	10 V/div
Lower Trace	0.5μa/div	0.5 μa/div

Time Scales

5 μsec/div	5 μsec/div

Figure 5.16

Ion Pulses in Plasma Delay Line

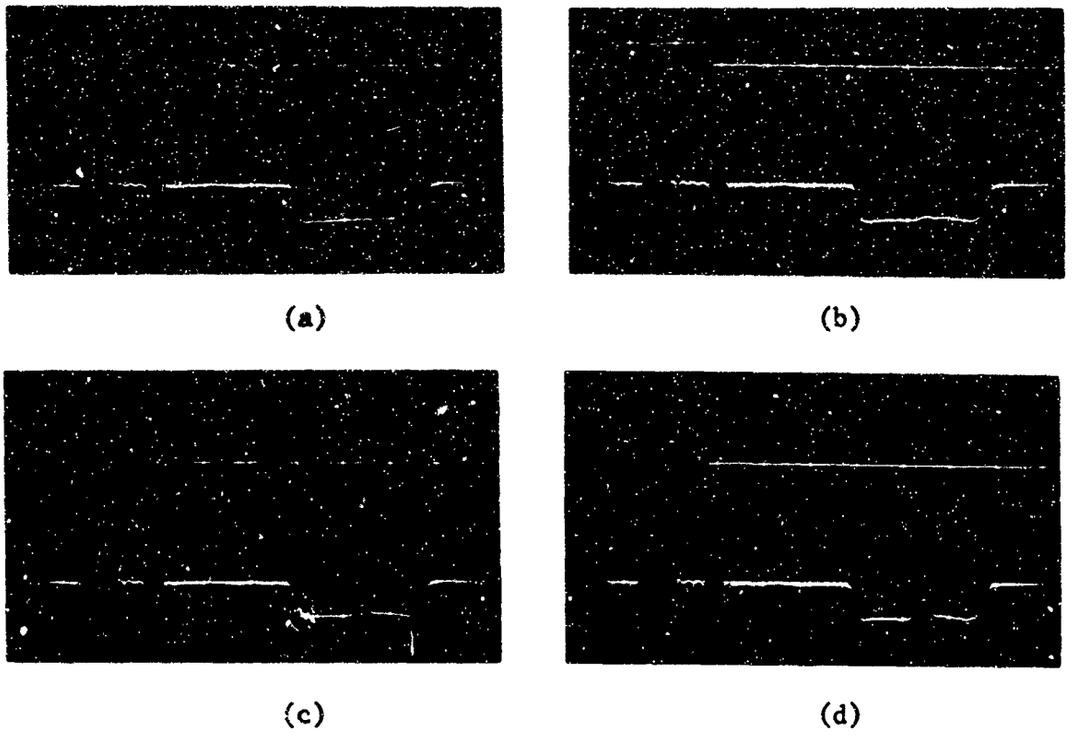

(a) (b)

(c) (d)

(e)

Amplitude Scales

Upper Traces 10 V/div
Lower Traces 0.5 μa/div

Time Scales

5 μsec/div

Figure 5.17

Formation of Two Ion Pulses in Plasma Delay Line

Figure 5.18(a) is a superposition of four photographs, each taken with a successively larger input signal. Unlike the similar records of Figure 5.11 these pulses show no contraction. In addition they give some indication of the linearity of the delay line. The trace for the strongest signal also shows the beginning of an oscillation (about 0.3×10^6 cycles per second). The onset of this type of instability seems to be a characteristic of a device when the space charge approaches 10^{-12} coul/cm^3. We shall discuss this effect later in the chapter.

Figure 5.18(b) is simply an input pulse and a delayed pulse together with an expanded picture of the leading edge of the delay pulse. The pressure for the photograph in Figure 5.18(a) was 1.12×10^{-4} Torr.

From our discussion in Chapter III we expect to see two pressure dependent effects. First, since the ionization efficiency increases linearly with pressure, we expect a similar relation between beam current and pressure. Secondly, we expect the pressure through its control of diffusion effects to influence the rise time of the pulse edges. Figure 5.19, which plots measurements on a continuous beam with $V_d = 0.5 \times 10^4$ m/sec, shows that the collection current actually falls off more rapidly with pressure than we would expect. Although we do not completely understand this effect, we believe it is connected with the fact that the plasma is very tenuous. Even at 10^{-6} coul/m^2, the Debye length for the helium ions is about one-half a millimeter, and for the electrons it is about one-half centimeter. Since the half aperture width is only 0.625 centimeter, we cannot under

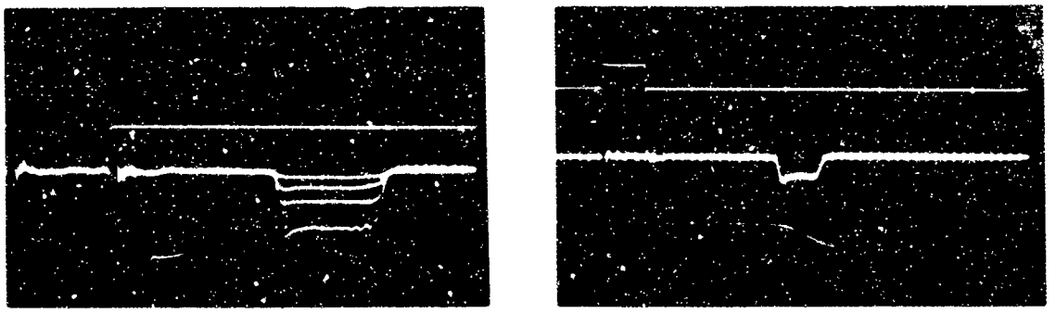

(a) (b)

Amplitude Scales

Upper Trace	5 V/div	10 V/div
Lower Trace	0.5 μa/div	0.5 μa/div

Time Scales

5 μsec/div	Upper Traces 5 μsec/div
	Lowest Trace 0.5 μsec/div

Figure 5.18

Ion Pulses in Plasma Delay Line

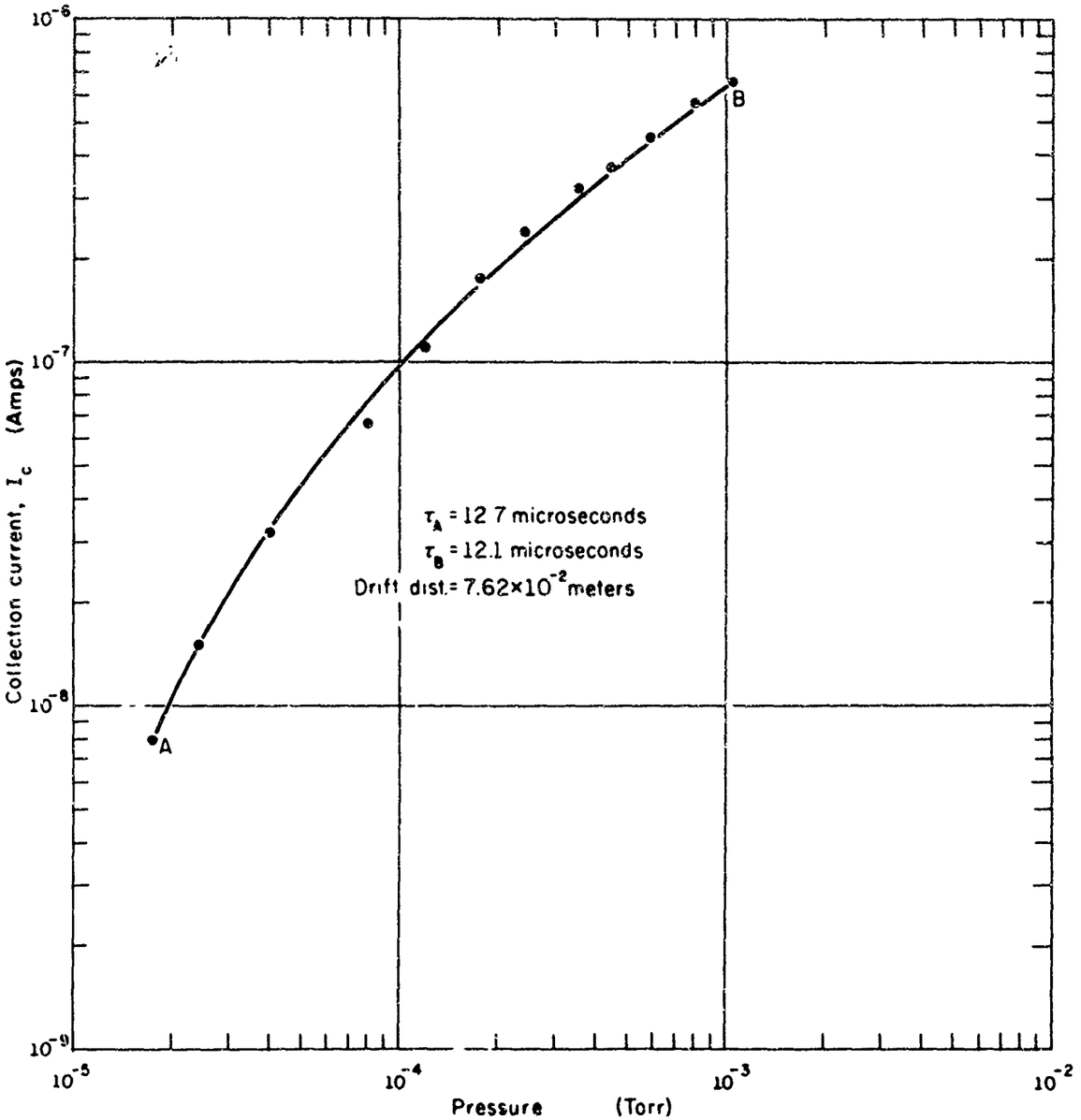

Figure 5.19

Effect of Pressure on Collection Current

these circumstances expect complete neutralization. At much lower charge density the two species of charge particles behave independently of one another. It seems possible that as the particle density in the beam rises with pressure in this region, the increasing charge neutralization partially compensates for space charge repulsion of particles, and to some extent enhances the ability of the fields to contain particles.

The series of photographs in Figure 5.20 shows the effect of pressure on the leading edge of the delayed pulse. As in Figure 5.18(b) the first trace represents the input signal, the second trace represents the delayed signal, and on an expanded scale, the third trace shows the leading edge of the delayed pulse.

In Chapter III we discussed the process by which diffusion can degrade the pulse shape, and in Figure 3.6 we plotted the relation between pressure and rise time for both electron and ion controlled diffusion. In Figure 5.21 we plot these relations for the experimental conditions of Figure 5.20. We see from Figure 5.21 that predictions of the effects of electron control diffusion are too low, by about an order of magnitude. However, the predictions of ion controlled diffusion agree reasonably well with the observed effects, at least at higher pressures. Table 5.1 lists for each of the six traces the pressure, the diffusion coefficient, the calculated rise time, and the observed rise time. Since below $p = 10^{-3}$ Torr the rise time does not decrease, we assume that in this pressure region diffusion can no longer be the dominant influence.

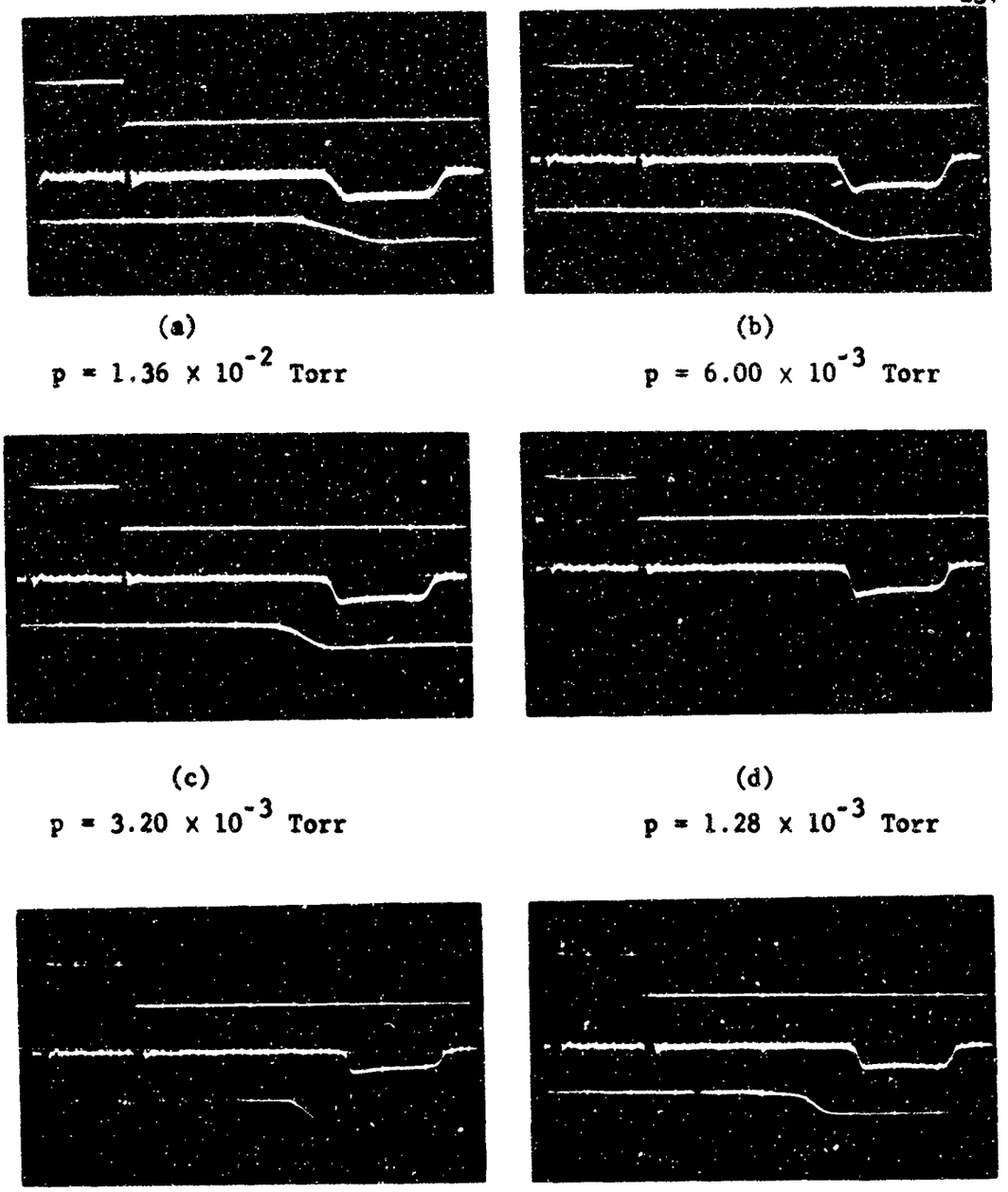

(a)
$p = 1.36 \times 10^{-2}$ Torr

(b)
$p = 6.00 \times 10^{-3}$ Torr

(c)
$p = 3.20 \times 10^{-3}$ Torr

(d)
$p = 1.28 \times 10^{-3}$ Torr

(e)
$p = 1.08 \times 10^{-3}$ Torr

(f)
$p = 6.00 \times 10^{-4}$ Torr

Amplitude Scales		Time Scales	
Upper Traces	5 V/div	Upper Traces	2 μsec/div
Lower Traces	0.5 μa/div	Lower Traces	0.5 μsec/div

Figure 5.20

Influence of Pressure on Rise Time in Plasma Delay Line

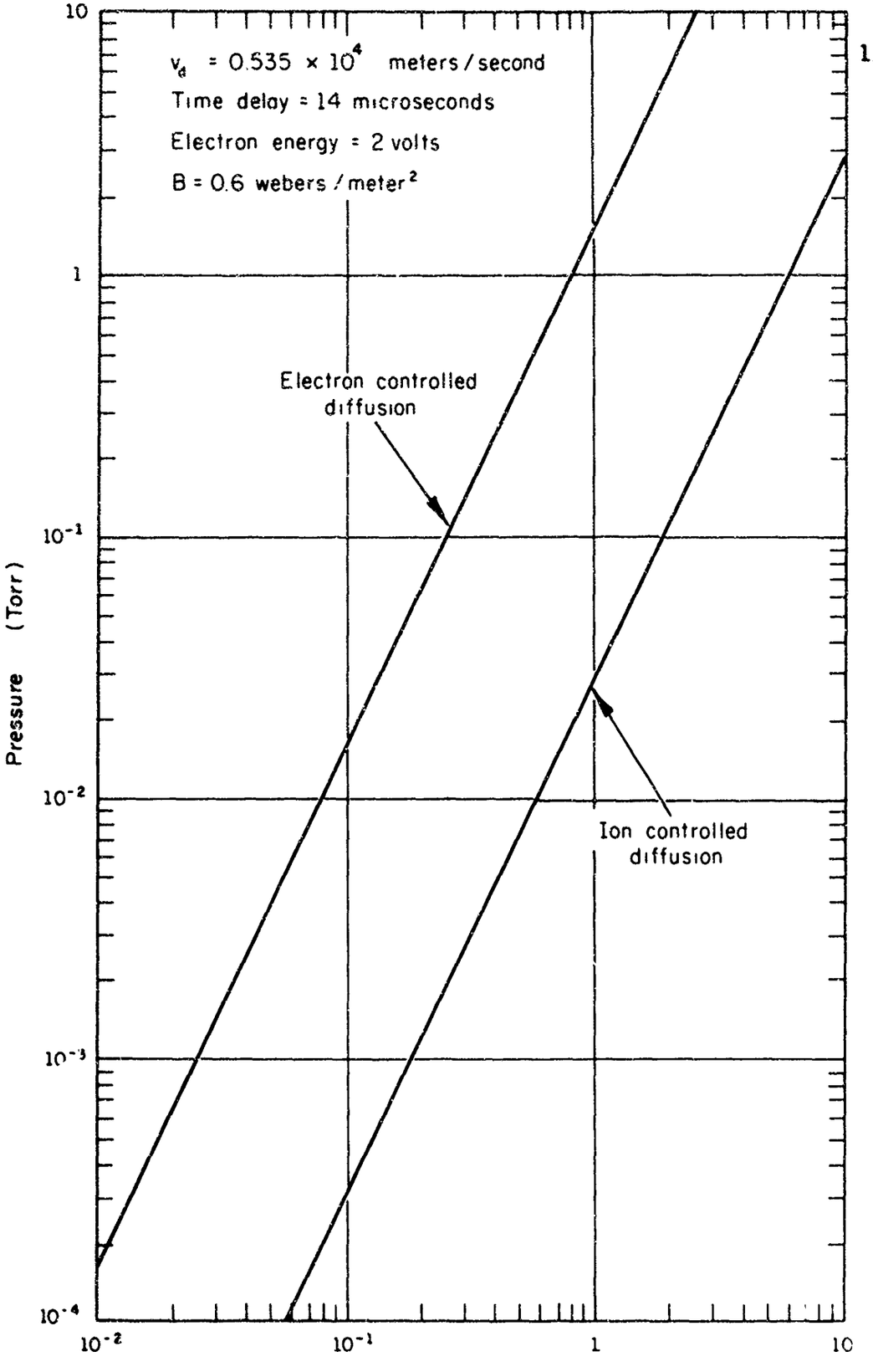

Figure 5.21

Calculated Relation between Pressure and Rise Time for Conditions Illustrated in Figure 5.20

P (Torr)	D(cm^2/sec)	Rise Time (μsec)	
		Calculated	Measured
1.36×10^{-2}	495	0.67	0.80
6.00×10^{-3}	219	0.42	0.65
3.20×10^{-3}	106	0.31	0.40
1.28×10^{-3}	46.6	0.20	0.30
1.08×10^{-3}	39.4	0.18	0.25
6.00×10^{-4}	21.8	0.14	0.25

Table 5.1

In planning these experiments we assumed that the charged particles would drift in the crossed fields with the drift velocity predicted by the classical theory. In this respect our experimental results offered no surprises, and within the accuracy of the measurements, they confirmed the predictions. For completeness we show in Figure 5.22 some data relating the measured time delay of the ion pulses to the measured value of the magnetic field. The solid line is a straight line fit to the data, and the dotted line is calculated from the measured value of the fields. Figure 5.23 is similar except that time delay τ is plotted against the reciprocal electric field.

The data for Figure 5.23 was taken from the oscillograph of Figure 5.24(a), which also shows changes in the pulse shape as the time delay increases.

Figure 5.24(b) shows an ion pulse delayed by 52 microseconds. The current in the pulse was only 3×10^{-8} amperes. Also for this photograph the output resistance was raised to 12×10^{3} ohms.

Earlier in this section we mentioned that although plasma pulses are apparently launched by the ionization processes, ions and electrons are not collected in equal numbers and that at low pressures they are not detected at all. Figure 5.25 shows this effect. The upper delayed signal in Figure 5.25(a) is an electron pulse, and the lower signal is an ion pulse. The pressure was 1.6×10^{-2} Torr. At $p = 8 \times 10^{-3}$ Torr we see from Figure 5.25(b) that the electron pulse has almost vanished, and the ion pulse magnitude has grown.

A possible mechanism for the electron loss is that at the lower pressure the electrons stream to the walls along the magnetic

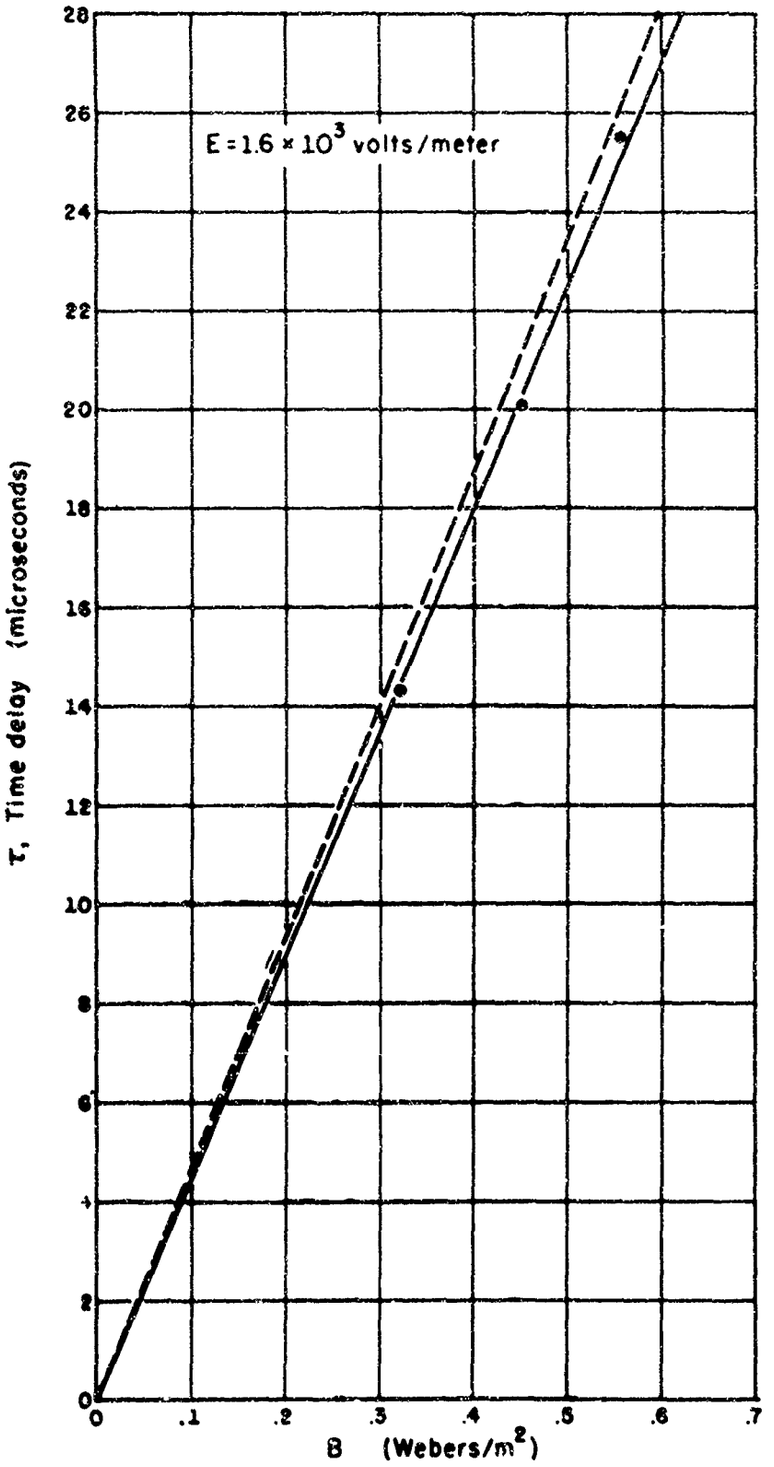

Figure 5.22

Time Delay vs Magnetic Field Strength for Ion Pulses

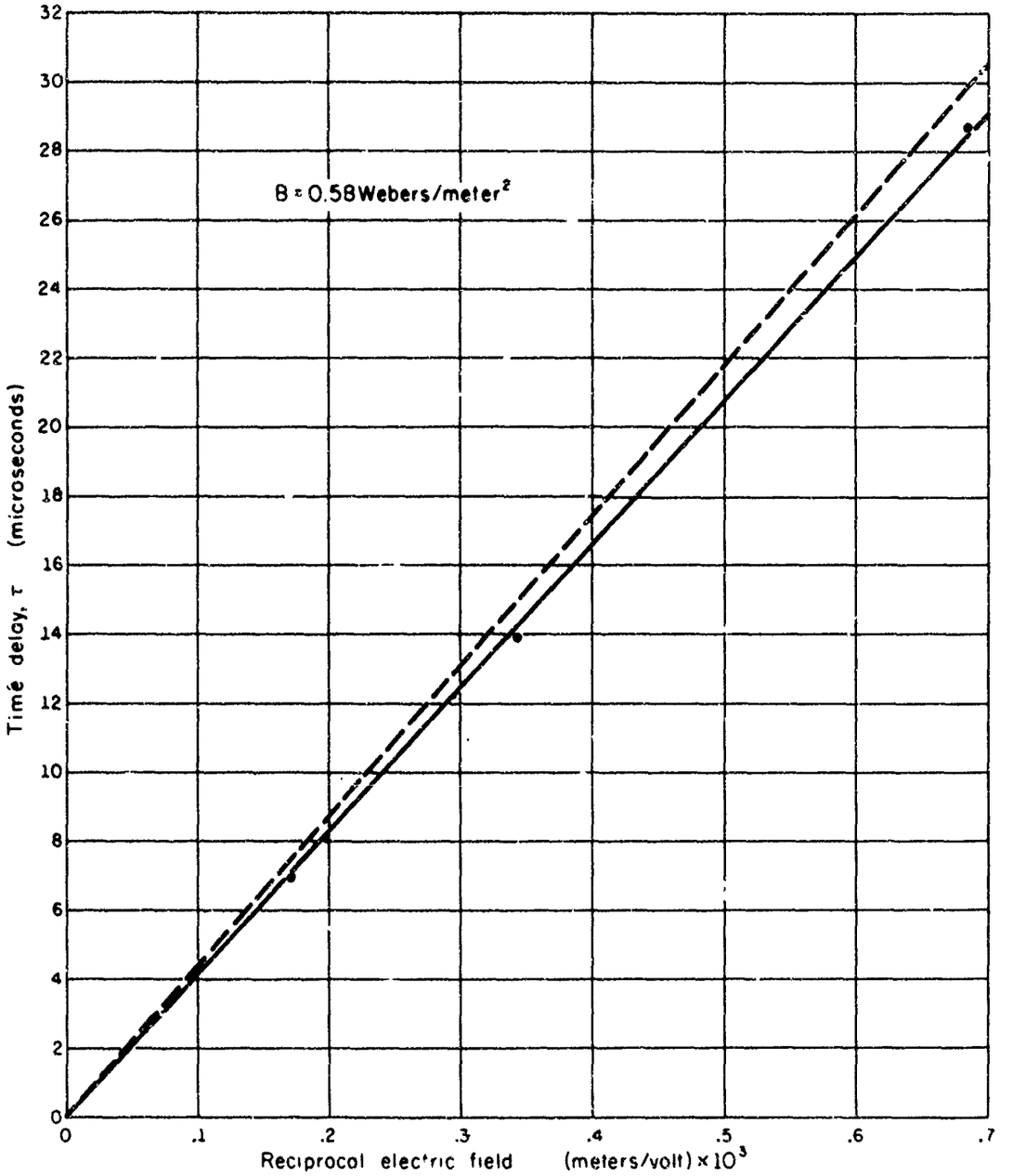

Figure 5.23

Time Delay vs Reciprocal Electric Field Strength for Ion Pulses

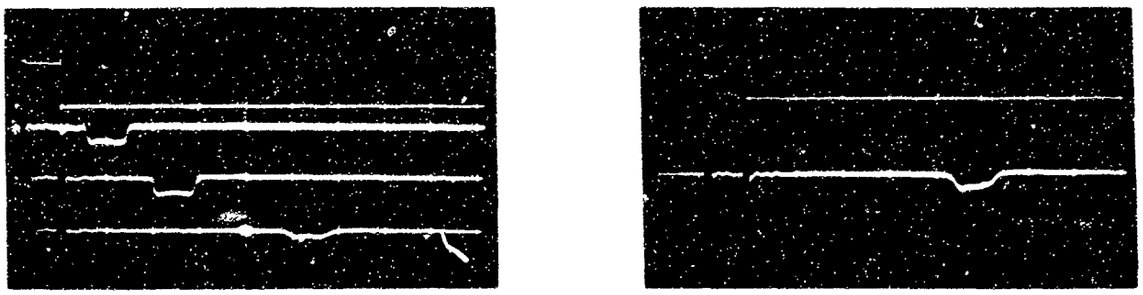

(a) (b)

Amplitude Scales

Upper Trace	5V/div	5V/div
Lower Trace	0.5×10^{-6} amp/div	0.42×10^{-7} amp/div

Time Scale

5 μsec/div	10 μsec/div

Figure 5.24

Low Velocity Ion Pulses

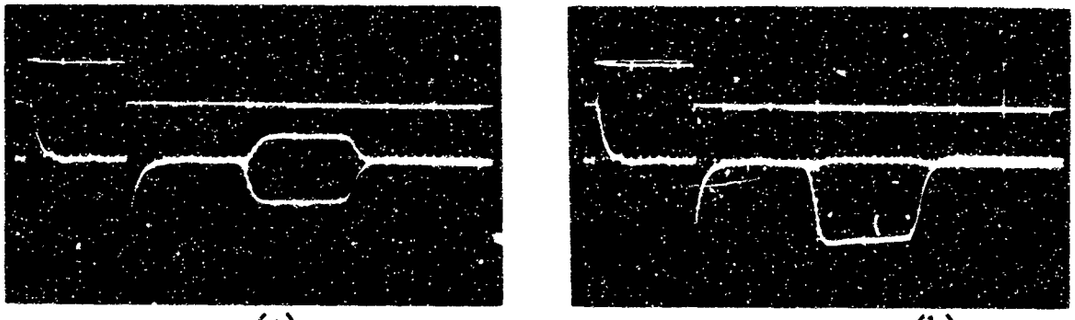

(a) (b)

Amplitude Scales

	(a)	(b)
Upper Trace	5V/div	5V/div
Lower Trace	0.83×10^{-7} amp/div	0.83×10^{-7} amp/div

Time Scale

(a)	(b)
2 μsec/div	2 μsec/div

Figure 5.25

Plasma Pulses Showing Loss of Electrons as Pressure is Lowered

field lines with too much energy to be trapped by the ions or by the fringing fields. At the higher pressures elastic collisions of electrons with neutrals can reflect electrons and can convert some of the longitudinal energy to rotational energy, thus allowing the electrons to be trapped.

The presence of the electrons in the collection region may impede the flow of ions to the collector plates, thereby reducing the ion current.

These explanations are, so far, only speculative. We hope, by varying the drift velocity in different regions of the tube, to learn where the loss takes place and to reach a better understanding of the effects.

The idea of a plasma delay line is based on a neutralized plasma, which in turn requires a small Debye length. Our efforts to produce such a plasma by the means that we have described have always been frustrated by an abrupt increase of noise when the density approached $\rho = 10^{-6}$ coul/m^3. This is just the density at which the Debye length for the electrons is comparable to the aperture. We believe the effect is related to the diocotron instability, or is a plasma oscillation, but more definite statements are unwarranted until further study is made.

CHAPTER VI

CONCLUSIONS

Our research into the properties of crossed field delay lines has been marked by some successes and, if not failures, by some disappointments. In some cases we learned more than we had expected; in others we achieved less than we had hoped. Nevertheless, we believe that on balance our studies have significance in two ways: first, we have demonstrated experimentally that the crossed field mechanism is suitable for the delay of video signals; secondly, we have achieved an understanding of this device that could lead to the development of practical delay lines for a variety of applications. In this chapter we review our results briefly, and we discuss the directions of research that we believe will be fruitful.

6.1 Summary of Results

In our experiments on the delay line we have observed video signals delayed by over 20 microseconds as they traverse the 7.5 centimeters from the launch region to the collectors. Within errors of a few percent the time delays always depended on the electric and magnetic fields as the simple theory predicts. We have shown furthermore that at high vacuum electrons can be launched into the drift space by secondary emission processes, and that at pressures above about 10^{-4} Torr tenuous plasmas can be launched by processes of ionization. We have distinguished between these two modes of operation by the terms "electron mode" and "plasma mode".

In the electron mode we have found that a pulsed signal carried by a section of thin electron beam tends under the action of its space charge to curl at the edges and therefore to present at the collectors a contracted signal. Furthermore, if a single broad pulse is perturbed some time between the leading and trailing edges, the two sections seem to draw away from one another and to appear at the collectors with an increased time separation between them. These phenomena are aspects of the diocotron instability.

Although for small signals on continuous beams the effect actually provides a gain mechanism; because the perturbations become nonlinear this does not seem to be a suitable mode for a practical delay line except for very small currents. Just how small is shown by the curves of Chapter II.

The most surprising result in experiments in the electron mode was that with sharp voltage spikes on an electrode in the launching region it was possible to inject discrete bursts of electrons into the drift space. These electron packets typically had spatial dimensions of about a millimeter, and at time delays of about 12 microseconds exhibited rise times of about 0.1 microsecond. We discovered also that when these electron packets were close together they would interact in such a way as to decrease the normal time interval between them by the time they reached the collectors. We believe this to be simply a coulomb interaction which in the moving coordinate system causes the two discrete pulses to rotate around one another.

Despite the interaction between these discrete pulses we believe that this mode of operation provides a practical means of delaying

information in digital form.

Although in the plasma mode we were successful in producing both electrons and ions in the drift space, we were never able to produce a completely neutralized drifting plasma. Whenever the ion density reached a value of about 10^{-6} coul/m^3, as measured by ion current at the collector, spontaneous oscillation would suddenly break out and would limit the charge density to this figure. The corresponding Debye length for ions is about 0.5 millimeter, but the Debye length for electrons assuming an average energy of about two volts is about a half centimeter. It is clear that the plasma is only partially neutralized. Despite these figures the signals carried by the ions were good replicas of the input signals.

From these experiments and their interpretation the following picture of the crossed field delay line has emerged.

The bandwidth of the crossed field delay line is limited fundamentally only by shot noise, but practically there is a hierarchy of effects which reduce the bandwidth. If particles are collected when their energy is largely rotational, the cyclotron frequency sets an upper limit which is so high (15 kmc for B = 0.5 weber/m^2) that it can hardly be called restrictive. Although for ions the cyclotron frequency is in the low megacycle region, the trajectories are almost simple cycloids, the energy is not principally rotational, and the bandwidth is therefore not limited by the cyclotron frequency.

The spread in rotational energy of the particles or of the positions of the guiding centers are more restrictive. For low energy electrons, however, the corresponding rise times are still in the sub-

microsecond region, and for high energy electrons (10^4 volts) the effect can be essentially eliminated by proper launching. The finite dimensions of coupling regions smear the signals and thereby limit the frequency response. This effect can be reduced either by making these regions very small, or by separating them from the drift region by transition regions.

Most restrictive of all are those influences which cause the charge particles to disperse. These influences can be divided into two classes: those that are caused by characteristics of the external electric field, and those that arise from the space charge forces of the particles themselves. The influence of the first class can be minimized by proper electrode design, and in particular we have shown that for a circular line, properly terminated electrodes that are sections of hyperboloids of revolution provide fields which are precisely correct. In addition we have shown that this kind of electrode is correct even in the presence of space charge, provided that the space charge density is constant and less than a limiting value. The space charge influences can of course be reduced enormously simply by operating at very small currents. The graphs in Chapter II show how small these currents must be to meet various performance specifications in the delay line.

There are actually two ways in which we can think about the compensation both for space charge fields and for dispersive external electric fields. When the Larmor circles are small we imagine that the electrons drift along the equipotential lines. It is therefore necessary to design the electrodes such that the time of flight of

electrons on the different equipotentials are the same. Equal flight times can also be maintained if the electrons follow essentially the same trajectories even though the electric field varies from one part of the Larmor circle to another. In this way electrons with large Larmor circles average out the variations in the electric field throughout the trajectory, and the same flight time for all electrons is maintained. Electrons with these characteristics can also negotiate transition regions with little dispersion, and their use is therefore indicated in lines of this type. All of the ideas for minimizing the influences that degrade bandwidth can, in fact, be combined. Thus, we can visualize a delay line in which high energy electrons are launched in a rectilinear beam, are guided through a region of increasing electric and magnetic fields from which they emerge into a low velocity drift region. Again, at the output the electrons are guided from the low velocity region into a high velocity region where the signals are detected. In addition, the drift region can be circular and can be so arranged that the electrons actually traverse essentially the same circle several times, thus realizing the advantages of the longer drift distance for the same time delay.

6.2 Suggestions for Further Research

Further work on the crossed field delay line divides into several classes. First, there are those measurements that relate directly to the work we have described, and whose objectives are to understand the functioning, as delay lines, of the devices we have already constructed. Secondly, there are those measurements that should lead to an understanding of particular effects that we have

observed in these tubes, but which have general interest apart from their connection with delay lines. Thirdly, there are those lines of development whose objectives are the ultimate production of variable delay lines.

As we discussed in Chapter V, Tube III, the plasma tube, was finally assembled with the resistive collectors that could match the electric field in the collection region. Measurements should be made on the tube in this form to compare with those made on the tube with the metallic collectors. It would also be desirable to perform these same experiments with different gases. Finally, to separate the effects of launching from the interaction effects in the drift region it would be desirable to control the drift velocities in the different regions of the tube by appropriately modulating the transverse electric field.

The abrupt appearance of noise in these tubes is probably related to the unusual noise properties of the much higher velocity crossed field beams used in M type travelling wave tubes. These beams have been the subject of considerable study in recent years, and a detailed investigation of the noise structure in our tubes would complement this work.

Another effect that might be worth studying in more detail is the relation between the shape of pulses and the diffusion of charged particles in crossed fields. It is possible that the effect could, under some circumstances, be used to measure the diffusion.

The original motivation for this research was the belief that the crossed field drift mechanism could provide the basis for

a wide band variable delay line. We now believe that the crossed field line can be realized in a number of ways. For the widest bands, however, and the longest delays, we believe that the most promising approach is to take advantage of the field averaging properties of high energy electrons, to inject and extract signals in regions of high velocity, and to use a curved drift space. We also suggest that serious consideration be given to the use of secondary electron multiplication in the output region. In particular, the coupling of a crossed field delay line to the kind of crossed field secondary multiplier described by Gaddy and Holshouser [23] could produce a versatile component for modern communications systems.

BIBLIOGRAPHY

1. Cumming, R.C., "The Serrodyne Frequency Translator," Proc. IRE, 45, 175-186 (February, 1957).

2. Wong, E.K., "Transit Time Modulation of Variable Artificial Delay Lines," TR No. 1601-1, Stanford University, Stanford, California (May, 1962).

3. Cooper, D.H., "Unified Analysis of Tracing and Tracking Error," IEEE Trans. on Audio, AU-11, No. 4, 141-148 (July-August, 1963).

4. Lavatelli, L., "A New Type of Electric Delay Line," Control Systems Laboratory, University of Illinois, Urbana, Illinois, Report R-80 (March, 1956).

5. Klüver, J.W., "An Electronically Variable Delay Line," Proc. IRE (Correspondence), 50, 2487 (December, 1962).

6. Alfven, H., Cosmical Electrodynamics, Clarendon Press, Oxford (1950).

7. Spitzer, L., Physics of Fully Ionized Gases, Interscience, New York (1956).

8. Klüver, J.W., "Elimination of Slip and Instability Effects in Certain M-type Electron Beams," Proc. IEEE (Correspondence), 51, 868 (May, 1963).

9. Hutter, R.G.E., Beam and Wave Electronics in Microwave Tubes, D. Van Nostrand, Princeton (1960).

10. Buneman, O., "Ribbon Beams," Journal of Electronics and Control," 3, 5, 507-509 (November, 1957).

11. Gould, R.W., "Space Charge Effects in Beam Type Magnetrons," Journal Appl. Phys., 28, 5, 599-605 (May, 1957).

12. Kyl, R.L. and H.F. Webster, "Breakup of Hollow Cylindrical Electron Beams," IRE Transactions on Electron Devices, ED3, 4, 172-183, (October, 1956).

13. Hoch, O.L. and D.A. Watkins, "A Gun and Focussing System for Crossed Field Traveling Wave Tubes," IRE Transactions Electron Devices, ED-6, 18, (1959).

14. Bruining, H., Physics and Applications of Secondary Electron Emission, Pergamon Press, New York (1954).

15. Gaddy, O., private communication.

16. Field, L.M., K.Spangenberg, and R. Helm, "Control of Electron Beam Dispersion at High Vacuum by Ions," Elec. Comm. 24, 1, 108-121 (March, 1947).

17. Atkinson, H.H., "Limiting Currents and Neutralization in Cylindrical Electron Beams," 4th Int. Congress of Microwave Tubes, Schevingen, Holland, (3-7 September, 1962).

18. Harman, W.W., Fundamentals of Electronic Motion, McGraw Hill, New York (1953).

19. Allis, W.P., "Motions of Ions and Electrons," Handbuch der Physik, Springer, Berlin (1956).

20. Cramer, W.H. and J.H. Simons, "Elastic and Inelastic Scattering of Low-Velocity He^+ Ions in Helium," Journal Chem. Physics, 26, 1272-1275 (May, 1957).

21. Glasstone, S. and R.H. Lovberg, Controlled Thermonuclear Reactions, D. Van Nostrand, Princeton (1960)

22. Brown, S.C., Basic Data of Plasma Physics, Tech. Press of M.I.T. and John Wiley, New York (1959).

23. Gaddy, O. and D. Holshouser, "A Microwave Frequency Dynamic Crossed-Field Photomultiplier," Proc. IEEE, 51, 1, 153-162 (January, 1963).

APPENDIX A

MOTION OF ELECTRONS IN UNIFORM MAGNETIC FIELD AND NONUNIFORM ELECTRIC FIELD

The equation of motion for an electron in electric and magnetic fields is

$$\ddot{\vec{r}}' = \eta[\vec{E} + \dot{\vec{r}}' \times \vec{B}], \tag{A.1}$$

where the prime incidates the laboratory coordinate system. In a frame of reference moving with uniform velocity $\vec{v}$ the equation is

$$\ddot{\vec{r}} = \eta[\vec{E} + \vec{v} \times \vec{B}] + \eta\dot{\vec{r}} \times \vec{B}, \tag{A.2}$$

where

$$\dot{\vec{r}}' = \dot{\vec{r}} + \vec{v} \tag{A.3}$$

and the particle "sees" the additional electric field $\vec{v} \times \vec{B}$.

If $\vec{B}$ and $\vec{E}_1$ are uniform fields, and if we let

$$\vec{v} = (\vec{E}_1 \times \vec{B})/B^2, \tag{A.4}$$

then Eq. (A.2) becomes

$$\ddot{\vec{r}} = \eta[\vec{E}-\vec{E}_1] + \eta\dot{\vec{r}} \times \vec{B}\ , \tag{A.5}$$

and we see that by suitably choosing $\vec{v}$, we can transform out of the equation any constant part of $\vec{E}$ that we wish. In particular, if $\vec{E}$ is uniform, and if we choose $\vec{v} = (\vec{E} \times \vec{B})/B^2$, then the electric field in the moving system vanishes, the electron motion is purely circular, and $\vec{v}$ is the drift velocity of the electron in the laboratory system.

We now turn our attention to the motion in the x-y plane when $\vec{B} = \vec{k}B$, and $E_x = 0$. We assume that E_y has the form

$$E_y = E_0 + f(y) \tag{A.6}$$

where E_{yo} is the field magnitude at $y = 0$. Then in a reference frame moving with the velocity $\vec{v} = (\vec{E}_0 \times \vec{B})/B^2$, Eq. (A.2) gives

$$\ddot{x} = \omega_c y \tag{A.7}$$

$$\ddot{y} = \eta f(y) - \omega_c \dot{x} \tag{A.8}$$

where $\omega_c = \eta B$.

From Eq. (A.7)

$$\dot{x} = \omega_c y + K \tag{A.9}$$

and substitution in Eq. (A.8) gives

$$\ddot{y} + \omega_c^2 y - \eta f(y) = -\omega_c K \ . \tag{A.10}$$

If f(y) is nonlinear, but continuous, we know from the mean value theorem that f(y) can be expressed exactly in the form

$$f(y) = (\partial E/\partial y')y \tag{A.11}$$

where $\partial E/\partial y'$ is just $\partial E/\partial y$ evaluated at an appropriate point y' between 0 and y. Eq. (A.10) becomes

$$\ddot{y} + (\omega_c^2 - \eta(\partial E/\partial y'))y = -\omega_c K \tag{A.12}$$

and we note that $\partial E/\partial y'$ is a function of y.

With K = 0 the solution to Eq. (A.12) represents an oscillation about y = 0, and in the method of variation of parameters it is expressed as

$$y = A \cos(\omega_c t + \theta) \tag{A.13}$$

where A and θ are slowly varying functions of time. With $\phi = \cos(\omega_c t + \theta)$ the derivatives are

$$dA/dt = (-\eta/\omega_c) f(A \cos \phi) \sin \phi \tag{A.14}$$

$$d\theta/dt = (-\eta/\omega_c A) f(A \cos \phi) \cos \phi. \tag{A.15}$$

In this method dA/dt and $d\theta/dt$ are replaced by their averages over a cycle

$$\left.\frac{dA}{dt}\right|_{Av} = (-\eta/2\pi\omega_c) \int_{-\pi}^{\pi} f(A \cos \phi) \sin \phi d\phi \tag{A.16}$$

$$\left.\frac{d\theta}{dt}\right|_{av} = (-\eta/2\pi\omega_c A) \int_{-\pi}^{\pi} f(A\cos\phi)\cos\phi d\phi \,. \qquad (A.17)$$

Since $f(A\cos\phi)$ is an even function of ϕ, $f(A\cos\phi)\sin\phi$ is an odd function of ϕ, and

$$\left.\frac{dA}{dt}\right|_{av} = 0. \qquad (A.18)$$

Substitution of Eq. (A.11) into Eq. (A.17) gives

$$\left.\frac{d\theta}{dt}\right|_{av} = (-\eta/2\pi\omega_c) \int_{-\pi}^{\pi} (\partial E/\partial y')\cos^2\phi d\phi \qquad (A.19)$$

or

$$\left.\frac{d\theta}{dt}\right|_{av} = (-\eta/2\omega_c)(\overline{\partial E/\partial y'}), \qquad (A.20)$$

where $\overline{\partial E/\partial y'}$ is just a weighted average of $\partial E/\partial y'$. We note that the weighting factor, $\cos^2\theta$, gives the greatest weight to values of $\partial E/\partial y$ that correspond to ϕ near $\phi = 0$, or y near y = A.

Eq. (A.13) thus gives

$$y = A\cos[\omega_c - (\eta/2\omega_c)(\overline{\partial E/\partial y'})]t \qquad (A.21)$$

or with

$$\gamma = \omega_c - (\eta/2\omega_c)(\overline{\partial E/\partial y'}) \qquad (A.22)$$

$$y = A\cos\gamma t \qquad (A.23)$$

where A is now a constant.

From Eq. (A.9)

$$\dot{x} = \omega_c A\cos\gamma t \qquad (A.24)$$

and

$$x = (\omega_c/\gamma)\, A\sin\gamma t. \qquad (A.25)$$

We see that an electron which, on the average, is at rest in the moving

system, oscillates with constant amplitude about y = 0. The complete orbit is elliptical, and when $\gamma \approx \omega_c$ it is almost circular.

The validity of this analysis rests on the assumption that the relative changes in both A and θ during a cyclotron period are small,

$$(2\pi/A\omega_c)(dA/dt) \ll 1 \tag{A.26}$$

$$(1/\omega_c)(d\theta/dt) \ll 1 \ . \tag{A.27}$$

Eq. (A.11) and Eq. (A.14) show that

$$(2\pi/A\omega_c)(dA/dt) = -(\eta/\omega_c^2)(\partial E/\partial y')(2\pi \cos \phi \sin \phi). \tag{A.28}$$

Similarly Eq. (A.11) and Eq. (A.15) show that

$$(1/\omega_c)(d\theta/dt) = -(\eta/\omega_c^2)(\partial E/\partial y'). \tag{A.29}$$

The restrictions of Eq. (A.26) and Eq. (A.27) are thus essentially the same, namely that

$$\left|(\eta/\omega_c^2)\overline{(\partial E/\partial y')}\right| \ll 1 \tag{A.30}$$

where we have ignored the factor $2\pi \cos \phi \sin \phi$, whose average is π, and we have substituted $\overline{\partial E/\partial y'}$ for $\partial E/\partial y'$.

We can interpret this restriction in several ways. First, since $\omega_c = \eta B$, and $v_r = R\omega_c$, we can express Eq. (A.30) in the form

$$\left|(R/B)\ \overline{\partial E/\partial y'}\ \right| \ll v_r \tag{A.31}$$

which states that in a beam with a spread of guiding centers, the <u>change</u> in the drift velocity in a distance of one radius is much less than the rotational velocity. Second, if the perturbing electric field arises from space charge, then

$$\frac{\partial E}{\partial y'} = \frac{\rho'}{\epsilon},$$

where ρ' is the space charge density at $y = y'$.

Since the plasma frequency is

$$\omega_p^2 = \eta \rho/\epsilon \tag{A.33}$$

Eq. (A.30) can be expressed as

$$\omega_p^2 \ll \omega_c^2 , \tag{A.34}$$

and the corrected frequency is

$$\gamma = \omega_c(1 - 1/2\ \omega_p^2/\omega_c^2) . \tag{A.35}$$

We have shown that, with this restriction, an electron in a uniform magnetic field and a nonuniform electric field will describe an almost circular trajectory superimposed on a drift velocity $\vec{v} = (\vec{E}_0 \times \vec{B})/B^2$ where $\vec{E}_0$ is the electric field at the guiding center. The frequency is slightly greater or slightly less than the cyclotron frequency, and when the perturbing field arises from space charge it is always less.

It is interesting to note that when E_y varies linearly with y, $\partial E_y/\partial y$ is constant, and the differential equations, now linear in x and y, can be solved exactly without any restrictions. With space charge induced perturbations the exact expression for the corrected frequency is then

$$\gamma = \sqrt{\omega_c^2 - \omega_p^2} , \tag{A.36}$$

and we note that when $\omega_p = \omega_c$, $\gamma = 0$, and there is no circular motion. This is just the condition for Brillouin flow.

APPENDIX B

PROPERTIES OF HIGH ENERGY ELECTRONS IN CROSSED ELECTRIC AND MAGNETIC FIELDS

We consider in this section some properties of electrons, first when the Larmor diameters are equal to the beam width, and secondly, when they are less than but still comparable to the beam width. We assume that the electron beam is infinite in the drift direction x, and in the magnetic field direction z, and that there are n circular orbits per meter. Furthermore, we assume that the distance in x between neighboring guiding centers is small compared to the Larmor radius. This last assumption is valid when the drift velocity v_d is small compared to the rotational velocity v_r of the electrons.

If a charge q is uniformly distributed on a ring illustrated in Figure B.1, the charge in an element $rd\theta$ is just

$$\lambda = (q/2\pi)d\theta \quad . \tag{B.1}$$

Above the plane $y = s + R \sin\theta$ the charge on the ring is

$$\begin{aligned} q_a &= (q/2\pi)\int_{\theta}^{\pi/2} d\theta \\ &= q(1/2 - \theta/\pi), \end{aligned} \tag{B.2}$$

and the charge below $y = s + R \sin\theta$ is

$$q_b = q(1/2 + \theta/\pi). \tag{B.3}$$

The difference is

$$q_b - q_a = 2q\theta/\pi$$

or in terms of y

$$q_b - q_a = (2q/\pi)\sin^{-1}((y-s)/R). \tag{B.5}$$

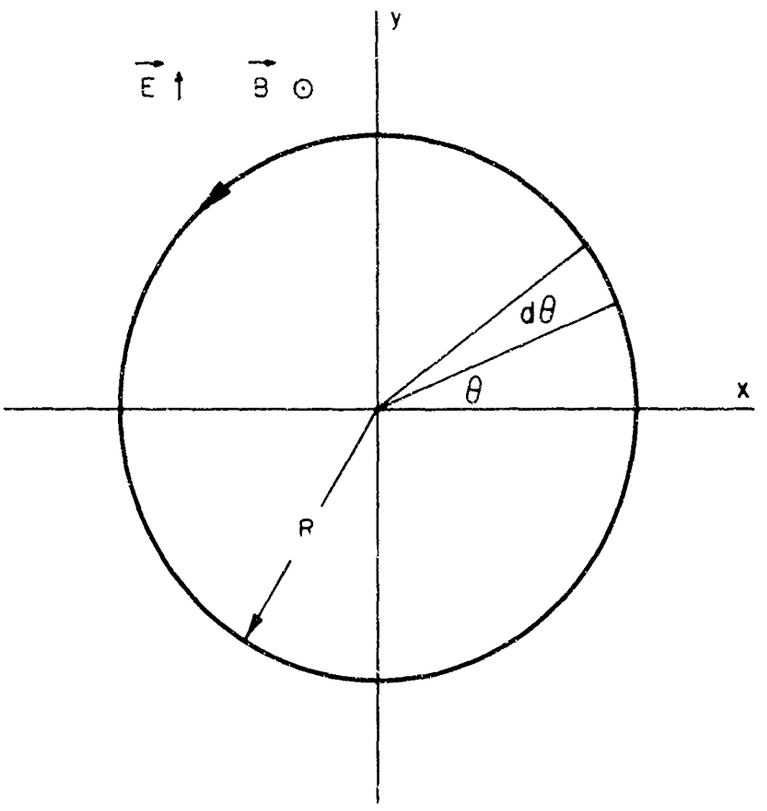

Figure B.1

Uniformly Charged Ring

If we interpret the ring as a cross section of an infinite cylinder, q_a and q_b represent linear charge densities on the cylinder.

Since there are n orbits per unit length in x the difference in charge density above and below $y = s + R \sin\theta$ is

$$n(q_b - q_a) = (2nq/\pi) \sin((y-s)/R). \qquad (B.6)$$

From Gauss's law the electric field at y is

$$E_y = (\lambda/\pi\epsilon) \sin((y-s)/R) \qquad (B.7)$$

where $\lambda = nq$. When $y - s > R$, E_y is constant, and equal to the value at $y = R + s$

$$E_y\Big|_{y - s \geq R} = \lambda/2\epsilon. \qquad (B.8)$$

We have assumed a particular form for the electron trajectories, and have derived the space charge field that this assumption implies. In general we should show that this field, together with the external field, will actually produce the assumed trajectory. We have already shown, however, in Appendix A that with $\omega_p^2 \ll \omega_c^2$, the orbital motion is essentially independent of the space charge field, and that the drift velocity depends only on the electric field at the guiding center. The assumed trajectories and the derived fields in Eq. (B.7) are therefore self consistent.

To the extent that the guiding centers are confined to a plane, $y = s$, in which the electric field magnitude is constant, the electrons drift with the same velocity, and there is no particle dispersion. When the guiding centers, however, are distributed through an interval in y there will be, across the beam, a velocity slip that is proportional to the variation in electric field across the interval.

In calculating this effect we again adopt the viewpoint of an observer who in the moving frame of reference sees only the space charge field.

For simplicity we assume that the guiding centers are distributed uniformly between $y = A - R$ and $y = -A + R$ in a beam whose thickness is 2A, as in Figure B.2. The number of electron orbits in the interval ds is $\rho' ds$, and the contribution of these electrons to the electric field at y is

$$dE_y = (\rho' ds/\pi\epsilon) \sin^{-1}((y-s)/R). \tag{B.9}$$

If $(y-s) \geq R$, then

$$dE_y = (\rho' ds)/2\epsilon, \tag{B.10}$$

and if $(s-y) \geq R$, then

$$dE_y = -(\rho' ds)/2\epsilon . \tag{B.11}$$

The integral of Eq. (B.9) is

$$I = (\rho'/\pi\epsilon)\left[\frac{y-s}{R} \sin^{-1}\frac{y-s}{R} + \sqrt{1 - \frac{(y-s)^2}{R^2}}\right]_{s=a}^{s=b} \tag{B.12}$$

where

$$a = \begin{cases} y - R & \text{if } y - R > -A + R \\ -A + R & \text{if } y - R \leq -A + R \end{cases}$$

$$b = \begin{cases} y + R & \text{if } y + R < A - R \\ A - R & \text{if } y + R \geq A - R. \end{cases}$$

The integral of Eq. (B.10) is

$$II = (\rho'/\pi\epsilon)(y+A-2R) \tag{B.13}$$

and it is defined only when $y \geq -A + 2R$.

Similarly the integral of Eq. (B.11) is

$$III = (\rho'/\pi\epsilon)(y-A+2R) \tag{B.14}$$

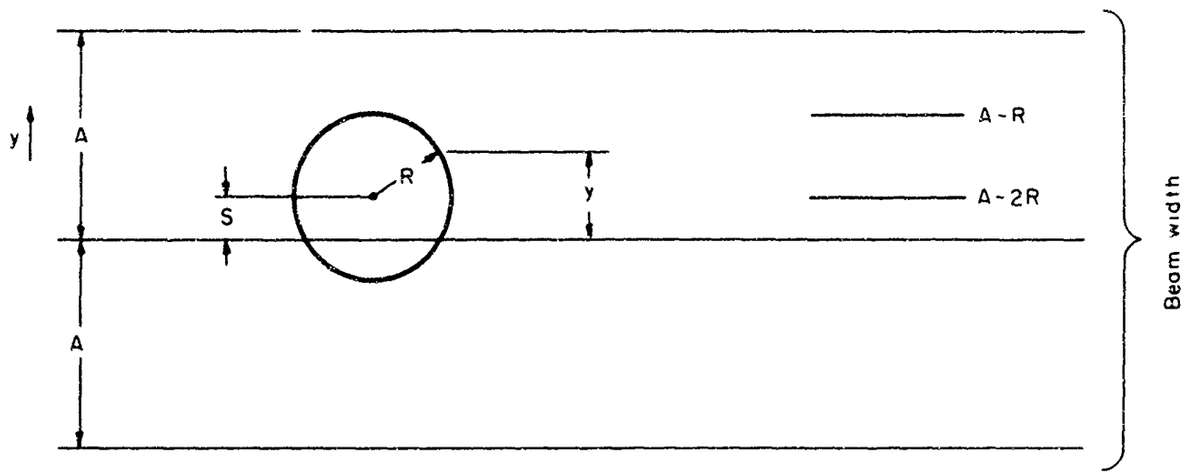

Figure B.2

Electron Orbit in Thick Beam

and it is defined only when $y \leq A - 2R$.

These integrals add to give E_y, but for any y at least one integral is zero or is not defined. For example, when $R < 0.5A$, E_y is given by I and II if $y > A - 2R$, but if $-A + 2R < y < A - 2R$, I vanishes and II and III combine to give E_y. Similarly when $R > 0.5A$ and $y > -A + 2R$, I and II again give E_y, but when $A - 2R < y < -A + 2R$, neither II nor III is defined and E_y is given entirely by I.

We note that although ρ' has the dimensions of charge density it is actually the volume density of orbits multiplied by the charge associated with each orbit. To make comparisons meaningful we stipulate that the total charge per unit area in x and z be the same for any value of the radius R. This implies that

$$\rho' = \rho A/(A-R). \tag{B.15}$$

It also implies that at $y = A$ the electric field for any value of R is

$$E_A = \rho A.$$

Figure B.3 plots the relative electric field E_y/E_A as a function of y/A with R/A as a parameter.

Our principal interest is in the extent to which a nonzero value of R/A reduces the slip effect. The maximum slip velocity for any R is proportional to the electric field E_y at the outermost guiding center (at $y = A - R$) and the ratio of this velocity to the slip velocity at $y = A$, when $R = 0$, is just E_y/E_A $(y = A - R)$. Figure B.4 plots this ratio as a function of R/A. When the guiding center spread $2(A-R)$ is small compared to the beam width $2A$, we see that the

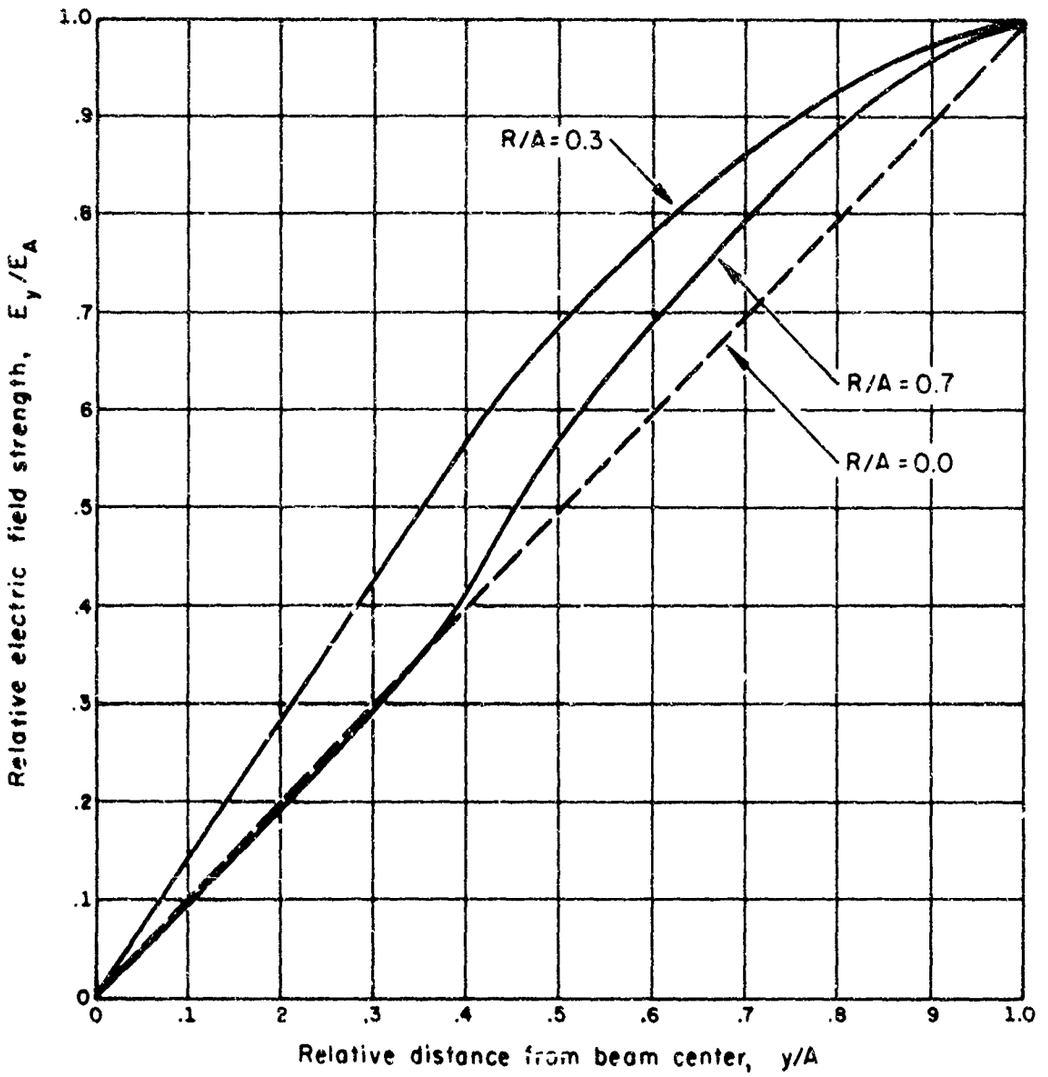

Figure B.3

Relative Electric Field vs. R/A

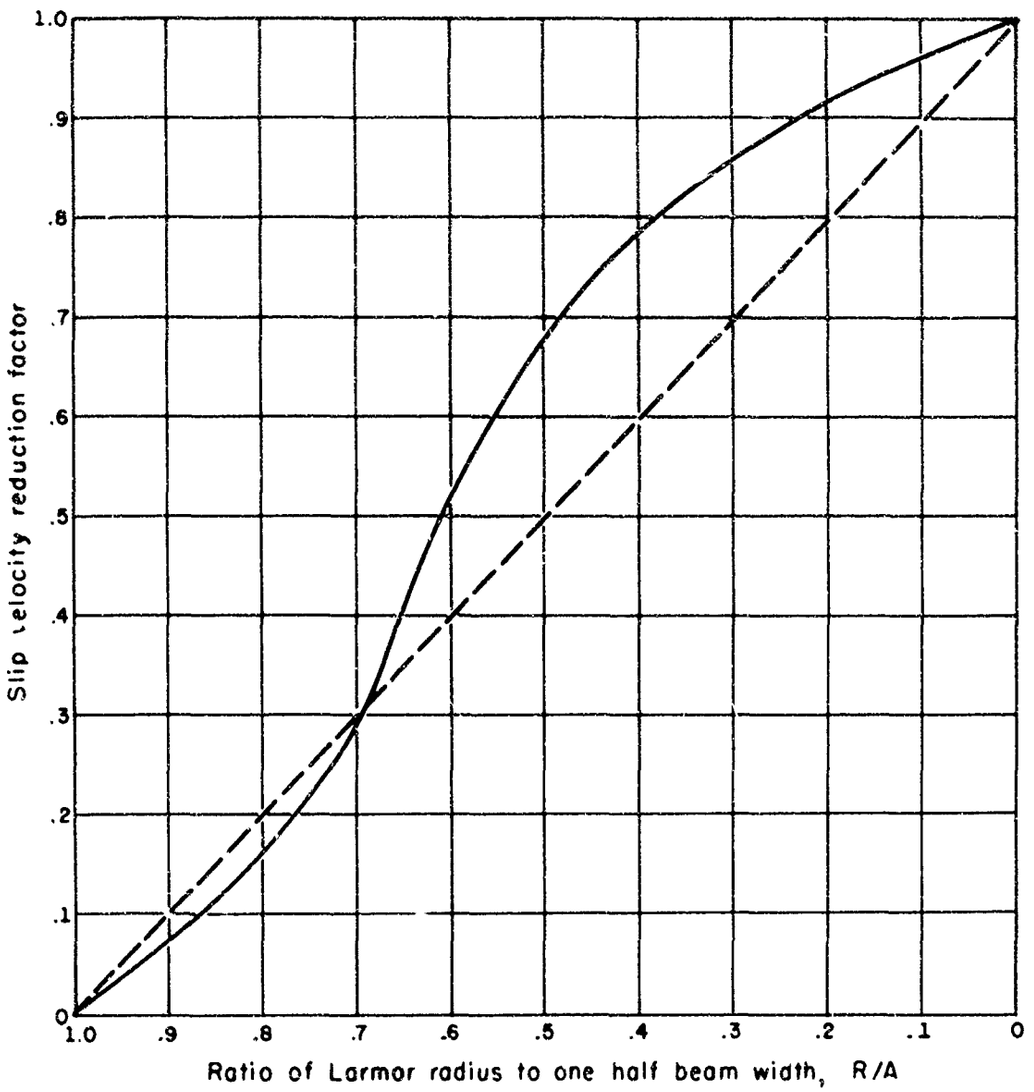

Figure B.4

Velocity Slip Reduction Factor

slip velocity is reduced to a value less than (A-R/A) times the maximum slip for R = 0.

We conclude that with a small spread of guiding centers in y, this method of reducing the slip velocity by partially averaging the space charge field is an effective one.

APPENDIX C

COMPUTER CALCULATION

We represent a thin electron pulse by n equal charges that, at $t = 0$, are equally spaced between $x = -a$ and $x = +a$, and that all are at $y = 0$. We calculate the trajectories of these charges in a reference frame in which there is no external electric field, and in which each charge q_i interacts with a uniform magnetic field $B = kB$ in the z direction and with the coulomb field $\vec{E}_i$, at $\vec{r}_i$, of the remaining charges. We assume, however, that the orbital motion is negligible, and that the trajectories are defined by the drift velocities

$$d\vec{r}_i/dt = (\vec{E}_i \times \vec{B})/B^2 \qquad (C.1)$$

We also assume that the charges are either concentrated at points, or that they are infinite line charges in the z direction. In the first case q_i is the value of the ith charge. In the second case q_i is the linear charge density. In either case the problem is two dimensional.

The field of the line charge q_j at $\vec{r}_i$ is

$$\vec{E}_{ij} = (q_j/2\pi\epsilon)(\vec{r}_{ij}/|\vec{r}_{ij}|^2) \qquad (C.2)$$

where $\vec{r}_{ij}$ is the vector difference in position between q_i and q_j. The velocity of the ith particle is then

$$d\vec{r}_i = \sum_{\substack{j=1 \\ i\neq j}}^{n} (q_j/2\pi\epsilon)(\vec{r}_{ij}/|\vec{r}_{ij}|^2), \qquad (C.3)$$

and with the dimensionless variables

$$\vec{R} = \vec{r}/\vec{r}_o$$
$$T = t/t_o \tag{C.4}$$

we obtain

$$d\vec{R}_i/dt = \frac{qt_o}{2\pi\epsilon r_o^2 B} \sum_{\substack{j=1 \\ i\neq j}}^{n} \frac{\vec{R}_{ij}}{\left|\vec{R}_{ij}\right|^2} \tag{C.5}$$

with

$$Q = (qt_o)/(2\pi\epsilon r_o^2 B) \tag{C.6}$$

we finally obtain for the dimensionless velocity of the ith particle,

$$d\vec{R}_i/dt = Q \sum_{\substack{j=1 \\ i\neq j}}^{n} \vec{R}_{ij}/\left|\vec{R}_{ij}\right|^2 \tag{C.7}$$

For point charges the equations are

$$Q = (qt_o)/(4\pi\epsilon r_o^3 B) \tag{C.8}$$

and

$$d\vec{R}_i/dt = Q \sum_{\substack{j=1 \\ i\neq j}}^{n} \vec{R}_{ij}/\left|\vec{R}_{ij}\right|^3 \tag{C.9}$$

We have prepared a program for the CDC 1604 digital computer that solves these equations. The curves of Figure 5.12 are plotted from a solution of Eq. (C.7) in which we chose n = 40. We neglected terms where $|n - i| > 20$.

We note that the choice of Q for the calculation is actually arbitrary. For example, we can interpret an increase in Q as a proportional increase in t_o. Thus the positions of the q_i at some real time t will correspond to an appropriately smaller value of T. Furthermore if the integration interval ΔT is reduced so that $Q\Delta T$ is a constant, the calculation, for any t, will proceed at the same rate and will give identical results.